Numerical Validation of Designed Aerostatic Bearing and Experimental Study with the Effect of Surface Roughness on its Performance

A Thesis Submitted in Partial Fulfillment of the Requirement for the Award of the Degree of

MASTER OF ENGINEERING

in

Production Engineering

Submitted By

KARAN SINGH JAMWAL

Roll No. 801685010

Under Supervision of

Dr. Anant Kumar Singh

Associate Professor

THAPAR INSTITUTE

OF ENGINEERING & TECHNOLOGY

(Deemed to be University)

MECHANICAL ENGINEERING DEPARTMENT

THAPAR INSTITUTE OF ENGINEERING & TECHNOLOGY
(A DEEMED TO BE UNIVERSITY), PATIALA, PUNJAB – 147004, INDIA

JULY, 2018

DECLARATION

I, **Karan Singh Jamwal** hereby declare that the work presented in this thesis entitled **"Numerical Validation of Designed Aerostatic Bearing and Experimental Study with the Effect of Surface Roughness on its Performance"** in fulfillment of the requirement for the award of degree of **Master of Engineering (Production Engineering)** submitted at Mechanical Engineering Department, Thapar Institute of Engineering & Technology (Deemed to be University), Patiala is an authentic record of work carried out under supervision of **Dr. Anant Kumar Singh** (Associate Professor, Mechanical Engineering Department, Thapar Institute of Engineering & Technology from August, 2017 to July, 2018. The matter presented in this has not been submitted either in part or full to any other university or institute for the award of any other degree.

Karan Singh Jamwal
(801685010)

Date: 09/08/2018

Dr. Anant Kumar Singh
(Associate Professor)
Mechanical Engineering Department,
Thapar Institute of Engineering & Technology
(A Deemed to be University), Patiala, Punjab.

Date: 09/08/2018

ACKNOWLEDGEMENT

I would first like to thank my thesis advisor **Dr. Anant Kumar Singh** (Associate Professor, Mechanical Engineering Department, Thapar Institute of Engineering & Technology). The door to his office was always open whenever I ran into a trouble spot or had a question about my research or writing. He steered me in the right the direction whenever he thought I needed it. His guidance helped me in all the time of research and writing of this thesis.

Secondly, I would like to thank **Mr. Om Prakash** (Senior Technical Assistant, Precision Tool Room), **Mr. Paramvir Singh** (Junior Technical Officer, Lab and Testing Section) and their colleagues for carrying out manufacturing and testing of this research project at R & D center for bicycle and sewing machine, Ludhiana. Their guidance regarding manufacturing errors and the problems related to assembling all the manufactured components helps in precise fabrication of various parts of aerostatic bearing.

I also place on record, my sense of gratitude to one and all, who directly or indirectly, have impart their hand in this venture.

TABLE OF CONTENTS

ABSTRACT

Aerostatic bearing is an ultra-precision component that uses spindle surrounded by a thin film of air. The advantage of air lubrication is that it is frictionless as the viscosity of air is less and it is easily available. Due to its high accuracy, the demand of these components is very high in electronic, instrumentation, healthcare and other manufacturing or processing industries. The development of aerostatic bearing is mainly focused on better design and optimization techniques which leads to improvements in performance. This study is focused on the experimental determination of the effect of roughness parameter on the performance of the aerostatic journal and thrust bearing. In order to achieve this target, the aerostatic bearing is designed based on theoretical analysis available in the literature review on the improvement in performance of the aerostatic bearing with the geometrical parameters. The design is numerically investigated by simulation of airflow in ANSYS Fluent with computational fluid dynamics (CFD) module. The model of aerostatic bearing for the journal and thrust bearings are analyzed based on boundary conditions of fluid flow within the orifice and clearance. The results from the simulation are validated by the results generated for pressure distribution in previous researches. After the validation of the model, the manufactured components are assembled to the analyze the variation in radial and axial loads acting on the spindle with the spindle displacement (1-5μm) in the direction of the load at supply pressures (3-6bar) in the clearance of 30μm. In order to analyse the effect of roughness parameter, the value of average surface roughness of bearing and spindle surfaces are improved with cylindrical grinding and MR fluid-based finishing method. For each roughness reduction technique, the variation in axial and radial load acting on the spindle are determined with variation in spindle displacement. The experimental results showed that for journal bearing at 5μm displacement in spindle, the average change in load capacity due to improvement in roughness values is found to be 0.68N. Similarly, the effect of roughness on thrust bearing at same parameters on the average change in load carrying capacity is evaluated as 2.0N. The results determined for the surface finish parameter gives the experimental proof for the effect of surface characterization on the load carrying capacity of the aerostatic journal and thrust bearing. The current study on the aerostatic bearing is effective for the applications such as drives in production machines where the friction and surface properties are the major parameters of performance and efficiency.

Keywords: Aerostatic bearing, pressure distribution, surface roughness, load carrying capacity.

LIST OF TABLES

LIST OF FIGURES

LIST OF SYMBOLS

τ_{ij}	j^{th} component of stress acting on fluid element perpendicular to i^{th} axis
μ	dynamic viscosity of fluid
v_i, v_j, v_k	velocity component in direction of i-, j- and k-axis
x_i, x_j, x_k	coordinate component of i-, j- and k-axis
λ	constant of proportionality with assumption that stress depends on strain
ρ	density of fluid
u, v, w	scaler valued function in x, y and z direction
j_x, j_y, j_z	momentum density in x, y and z direction
f_x, f_y, f_z	force density in x, y and z direction
c_p	specific heat at constant pressure
E_d	viscous dissipation energy
T	temperature
Q	rate of heat per unit mass
φ	thermal diffusivity
p	pressure of fluid
h	fluid film thickness
V_{inj}	velocity of fluid injection
d_o	outside diameter of bearing
$\dot{m}$	mass flow rate through an orifice restrictor
C_d	discharge coefficient
p_a, p_d, p_o	ambient pressure, pressure downstream of orifice, supply pressure
ε	eccentricity ratio
L, D	length and diameter of bearing

CHAPTER 1

INTRODUCTION

1.1 RESEARCH BACKGROUND

At early stages in the design of the rotating machine, the design engineer must decide the suitable type of bearing to achieve better performance. The two types of bearing which are always considered in the selection of bearing due to their wide applications and acceptance. They are rolling contact bearing and the hydrodynamic fluid type bearing. More recently, the new types of bearings have been introduced for some specialized applications. These include bearings with a thin film of gases, fluids, and solid lubricants.

The early developments on air lubricated bearings show a considerable improvement over other types which includes the spin axis bearing for high precision gyroscopes where low vibration and friction levels are required. The other development is gas circulators in nuclear reactors which were developed to be sealed inside the reactors for long-term purposes. From these specialized developments in air bearings, it has been developed for many applications such in several type hand tools, precision grinding machines and high-speed drilling machines of all types. In order to employ air bearing in a specific application, the designer must know the relative advantages and disadvantages of other bearing types. It can be understood by comparing air bearing with other types of bearing based on different parameters such as load capacity, stiffness, power consumption, axis definition and wear. However, it is necessary to understand the principle of different types of air bearings before considering them for a particular application.

The air bearing can be defined as two precisely machined surfaces are isolated by a thin film of air and positioned so that the change in air film pressure can resist the tendency to change in clearance due to external forces. Figure 1.1 shows the principle of working of different type of air bearings. The aerodynamic type is also known as self-acting because the pressure is generated in between surfaces by the mechanism of viscous shearing as shown in Figure 1.1(a). This process is similar to hydrodynamic oil bearings as pressure is generated due to the relative motion of one surface over other so that the fluid is dragged into two converging surfaces. The aerodynamic bearing is a simple concept as it is independent of the external pressure source and entirely self-contained within its system. The early developments on gyroscopes and nuclear applications were in connection with aerodynamic bearing, but there is no wide application of this kind because of its

high production cost as it requires very precise accuracy [1]. The other reason for wide exclusion is its load capacity which is proportional to the viscosity of a fluid. As the viscosity of air is very less than that of any liquid lubricant or oil, so the load carrying capacity of an aerodynamic bearing is not adequate for many applications. The working principle of squeeze film bearing is also similar to aerodynamic type as it also generated pressure within the bearing surface without any external source as shown in Figure 1.1(b). In squeeze film bearing, the pressure is generated by a vibratory movement which is normal to the surface of the bearing. But this kind of bearing is limited to laboratory applications because external mechanism such as vibration generator is used to generate load supporting pressure. In case of aerodynamic bearing, it is generated by the normal functioning of bearing i.e. by rotation of journal.

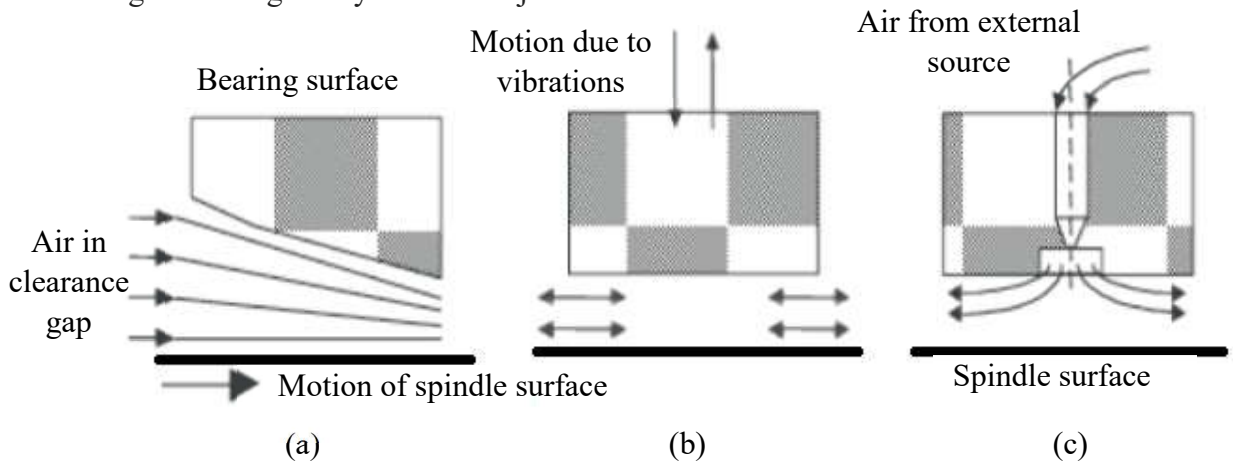

Figure 1.1 Various types of air bearing (a) aerodynamic, (b) squeeze film, and (c) aerostatic [1]

In aerostatic bearing, the pressure in clearance space is generated by an external source as shown in Figure 1.1(c). The pressurized air flow through the external source to flow restrictors of bearing, usually simple or annular orifices, slots, porous medium and capillary tubes. From these flow restrictors, air enters the clearance gap and exits via the end face of bearing surface. The load capacity in the aerostatic bearing is independent of the relative motion between the two surfaces. To maintain pressurized air within surfaces, the power is continuously required to run the external source.

Based on the functionality, the bearings are classified as the journal bearing and thrust bearing as shown in Figure 1.2(a) and (b) respectively. Journal bearing provide radial support a shaft and these have cylindrical geometry whereas thrust bearing provides supports for axial or thrust loads acting on axial location of the shaft. Thrust bearing has leveled horizontal surface and is circular

in shape from the top view. In aerostatic bearing, these two types of bearings can be used in the combined form to provide both axial and radial support.

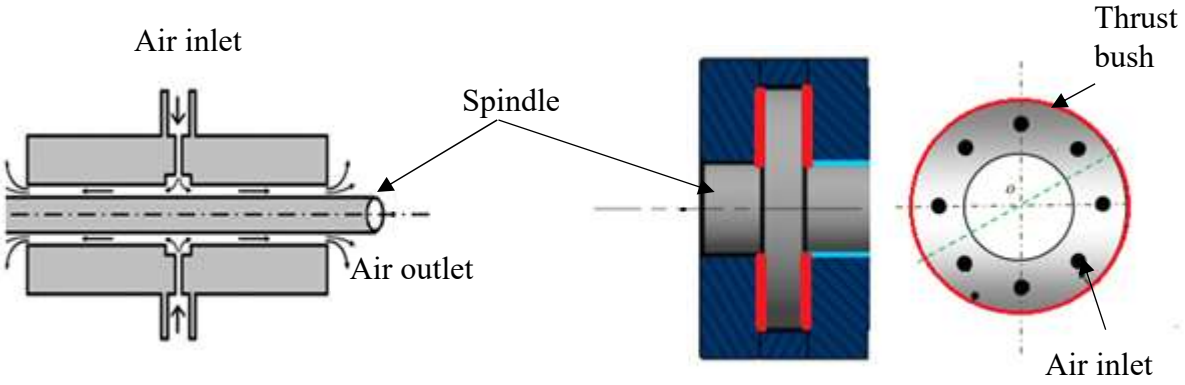

Figure 1.2 Bearing classification based on functionality (a) journal bearing, and (b) thrust bearing [1]

For more generalization, Powell [1] shows the comparison of bearing types to understand the advantages and difficulties to employ air bearing for a particular application. The comparison shows that for high-speed application (>20000 rpm), aerostatic bearing is preferred due to its load carrying capacity and nominal life of 10000 hours. In case of overall stiffness, the aerostatic bearing gains in relation to ball bearing because it can permit the use of a shaft of larger diameter and greater rigidity for the same deflection. It also exhibits the lowest power due to little heat generation and thermal distortion problems at high speed. In aerostatic bearing, the surface averaging effect of the air film can be reduced the run-out to below a quarter of roundness error produced on shaft surface. Due to this accuracy, aerostatic is widely used in precision spindle applications. Based on this comparison the advantages of the aerostatic bearing are summarised as follows:

- No friction in between surfaces that leads to zero wear rate. Hence, enhances the overall life of bearing.
- Low power loss losses due to its low temperature running conditions as air continuously flows through the system.
- Due to its accurate axis alignment, the noise and vibration levels are very low.
- Little or no maintenance required for the longer period of time.

As the compressed air is easily available due to its wide application in factories or other large-scale industries, the use of the air bearing with exiting availability compressed air at shop floors

seems to be a logical advancement in the field of bearing applications. The major consideration in the design of aerostatic bearing is its limited load carrying capacity. So, it's essential to estimate all the applied load acting on air bearing system due to many sources such as spindle weight, transmission forces by coupling, pressure forces by air supply on different components and applied loads on the shaft in axial and radial directions. These loads are accurately combined at each operating condition to evaluate the maximum load carrying capacity. The major aspect which is considered as a limitation in the air bearing system is the cleanliness of air supplied. The liquid or solid impurities in the supplied air can create a blockage to flow of air as the bearing clearances are very small in case of the air bearing. So, the design of clearance and feeding system demands the high quality for filtering of air and a higher degree of precision in manufacturing techniques for air bearing components.

1.2 NEED OF AEROSTATIC BEARING

There are various types of bearings available to work under different conditions. The two major types of bearings are non-contact bearings and contact bearings. By considering these bearings types, the advantages and the need of air bearing in particular application can be explained based on the number of properties such as speed limit, load carrying capacity, stiffness, power consumption, accurate axis definition, cost, and manufacturability.

1.2.1 Speed limit

The density of balls of the ceramic bearings is only 40% that of steel, substituting steel balls with ceramic ones greatly facilitates high-speed rotation. Under position preload in a machine tool spindle, the centrifugal force acting on the ceramic rolling elements is lower than steel rolling element which results in high-speed performance [2]. During the motion of the bearing, the fluid based and air-based bearings have only viscous friction associated with the sheared film layers. But they can experience hydrodynamic/aerodynamic effects due to which considerable amount of heat can be generated on high-speed condition whereas magnetic bearings do not limit the speed or acceleration of components they support [3]. The speed comparison of various bearing types is calculated by DN number which is the product of the bearing diameter (in mm) and the top speed (in rpm)

Table 1.1 Speed comparison of various bearing types [3]

Bearings	Approximately maximum speed (DN)*
Steel bearings	1,000,000
Hydrostatic/Hydrodynamic bearings	1,000,000
Ceramic bearings	2,000,000
Air bearings	4,400,000
Magnetic bearings	4,500,000

1.2.2 Load carrying capacity

The load carrying capacity of various bearings is shown in Table 1.2. It can be seen that the load carrying capacity of aerostatic bearing increased at higher speeds due to aerodynamic effects whereas in case of a ball bearing the load carrying capacity is decreasing under similar operating conditions. These two types of bearing become much closer if the speed is further increased.

Table 1.2 Load capacity of various bearing types [1]

Bearing Type	Maximum Radial Load (lbf)	
	At 3000 rpm	At 20,000 rpm
Aerostatic	95	120
Ball Bearing	1050	600
Hydrodynamic	5000 (40° C)	-
Hydrostatic	1900	-

1.2.3 Radial stiffness

The overall stiffness of machine tool spindle is dependent on the stiffness of spindle, bearing bushes and support structures i.e. the structures that are in contact with the spindle. In overall stiffness, the aerostatic bearing has more stiffness than ball bearings because the total deflection produced by all the components in ball bearing assembly is higher as they are in direct contact with the spindle. The values radial stiffness for hydrodynamic bearing for quill assemblies is in the region of 500000 to 1000000 lbf/in whereas, for aerostatic bearing, the stiffness is in the region of 250000 to 500000 lbf/in [1]. This permits the use of larger diameter shaft for greater rigidity.

1.2.4 Power consumption

The power consumption of various bearing types is given in Table 1.3. The aerostatic bearing consumes the lowest power caused due to the lowest frictional torque. It means that the aerostatic bearing provides the coolest running condition as compared to other bearing types. To evaluate total power consumption, it is necessary to include the power used by the external sources such as a compressor. This shows that the ball bearing consumes the less power at lower speed range. When it comes to higher speed ranges, the power loss due to frictional heat in ball bearing is increased. So, the ball bearing demands the compressor for lubrication and cooling. Hence, the total power consumption of the ball bearing is more at a higher speed as compared to the aerostatic bearing.

Table 1.3 Comparison of bearing types based on power consumption [1]

Bearing Type	Power Consumption (h. p.)			
	At 3000 rpm		At 20000 rpm	
	Friction	Total	Friction	Total
Aerostatic	0.001	0.101	0.045	0.145
Ball Bearing	0.07	0.07	0.164	0.164
Hydrodynamic	0.480	0.480	-	-
Hydrostatic	0.200	0.400	-	-

1.2.5 Axis definition

The major requirement of the bearing system is the ability to accurately defining the axis of the rotating spindle. Based on the manufacturing catalog, the ball races and hydrodynamic bearing gives the run-out in the region of 0.5μm whereas the spindle supported by the aerostatic bearing is capable of run-out less than 0.125μm. Due to this reason, the aerostatic bearing is equipped with precision spindle application.

1.2.6 Wear

Due to the rubbing contact in rolling contact bearings, the surfaces of the shaft and bearing subjects to wear. Hydrodynamic bearing subjects to small wear as compared with ball bearing as the fluid used in bearing provides boundary lubrication. But hydrodynamic bearing also has some wear during start and stop due to rubbing. The corrosion also may case wear in this type of bearing

due to oxidation of fluid or oil caused by temperature rise due to friction. So, the hydrodynamic bearing needs effective cooling to operate for many years.

Theoretically, the aerostatic bearing does not subject to wear as there is no rubbing contact between the surfaces and the most of gases does not cause corrosion and erosion over the surface. The gas supply needs to be filtered so that the solid impurity is not allowed within the clearance which can cause the damage to the surface of bearing and spindle.

1.3 RESEARCH CONTEXT

In 1886, Reynolds' discovery [5] expands the application of fluid film lubricated bearings in the field of high-speed turbochargers, machining equipment, hard disk drives, dental equipment and high precision stages. After these developments, the liquid and air are considered as a lubricant in thin film bearings due to its lower viscosity. The pressure is generated by the relative motion of bearing and spindle surfaces has named as aero-dynamic or is provided externally is named as aero-static.

1.3.1 Analysis of pressure distribution

The flow pattern of air and the pressure distribution is analyzed numerically by computational fluid dynamics (CFD). It provides both qualitative and quantitative prediction for the flow of air by mathematical modeling based on partial differential equations, discretization and solution techniques by numerical modeling. The results are generated based on these models by CFD tools by pre- and post-processing utilities. It helps the designer to perform computer simulations and numerical experiments in virtual flow environment. The simulations performed in CFD is not fully reliable as the accuracy of the results is totally dependent on the computing power of the system. Also, the processes based on input data involves guessing the behavior of the mathematical model. So, the solution may be inadequate or varies when compared with experimental analyses. The predictions are solved by the mathematical model based on momentum, energy and continuity equation by design cycle as follows:

- The designer defines the physical model for simulation.
- The flow models and solution methods are expressed in form of mathematical expressions.
- The computational code provided by the software analyses the mathematical model based on the number of iterations which is dependent computer hardware.

- The designer analyses the interpretations in form of results provided by simulating the mathematical model.

The fluid characteristics used in CFD simulation is based on macroscopic properties such as density, viscosity, temperature, velocity, and pressure. The steps involved in the analysis process by CFD simulations are as follows:

- *Problem definition:* Flow problem should be defined in form of physical phenomenon, geometry, operating conditions, type of flow pattern and the way to achieve the desired goal.
- *Mathematical modeling:* The computational domain for the flow model is defined based on governing equations and these equations are simplified in relation with boundary conditions.
- *Discretization model:* The system of partial differential equations based on the meshing model, space and time discretization model.
- *Iterative solution method:* The algebraic equations are then solved iteratively.
- *CFD simulation:* The model is computed based on a numerical algorithm, discretization parameters and assumptions in mathematical modeling.
- *Post-processing analysis:* The information of simulated results is extracted in form of visualization and effect shown by integral parameters and derived quantities by using the statistical tool. The analysis is performed to verify and validate the CFD model.
- *Uncertainty and error analysis:* The simulation results are verified by the cumulative effect of different errors and degree of uncertainty in flow model due to physical modeling and computational programming codes.
- *Verification and validation* of CFD model by adjusting and changing modeling definition based on experimental data and parametric study.

The results from CFD simulation validates the designed model based on experimental data in the literature. The experimental study focuses on the static performance of hybrid aerostatic bearings with the surface roughness effects. As the air bearings have some advantages over other bearing types, very low friction, no wear rate and accurate axis alignment, the manufacturing of precise bearing surface become the major priority. By eliminating the surface imperfections, the better performance of aerostatic bearing can be achieved.

1.3.2 Role of manufacturing techniques

In order to achieve a better smooth surface, the principal features for geometrical accuracy such as surface finish, roundness, flatness, taper, and other surface irregularities must be enhanced. This is possible by considering some of the manufacturing techniques that help in achieving the higher degree of accuracy. So, the components manufactured for this study are manufactured by the following processes which are explained below.

1.3.2.1 *CNC turning operations:* It is the initial process used for manufacturing the air bearing components. The material used for bearing surface is SS 316 because of its ability to resist almost all environmental condition. So, the industrial application of this type of steel is very wide. When machining this type of steel, several factors must be considered. During cutting operation, the tool absorbs more heat which may form build-up edges on the tool face. To provide resistance to the tool, the operator should use cermet coated drill bits with little increases the cutting speed or may choose positive insert geometry. The chips may tangle around the workpiece due to which the removal of chips becomes difficult. To avoid this problem, the tool with smaller nose radius, higher feed rates or chip-breaker geometry of inserts can be used. The feed rates can be maintained at the optimum range because if it too low then the machinability becomes difficult due to work-hardening of cut surfaces. To achieve better surface during turning operation of stainless steel, several parameters should be controlled.

- Reduction in feed rate
- Increase in top rake angle of the insert
- By using a chip breaker
- Larger nose radius
- Use different tools for roughing and finishing
- Calibrate the tool holder and work holder

1.3.2.2 *Grinding operations:* After CNC turning operation, air bearing components requires surface grinding operation to improve geometrical accuracy. There are a few considerations regarding surface grinding to ensure best possible results to be achieved by the equipment. The sideways must be in good mechanical condition and is properly lubricated because the roundness and surface finish is dependent on motion errors in sideways. The quality of these surface features also dependent on working condition of work and wheel head. So, before staring surface grinding on components, the operating condition of slides and machine is properly checked. It helps in

enhancing the surface features up to some extent. During the completion of the grinding cycle, the last depth of cut should be minimized to the lowest level less than 0.05 mm. This minimizes the temperature gradient effect on material due to machining which can avoid the material damage from degrading. Also, the grinding of components is performed in a clean environment as airborne and coolant borne particles can damage the surface finish generated by the process. So, the dry dressing of grinding tool, filtration of coolant and by covering entire grinding setup can avoid such type of damage. During grinding of shafts, the roundness is affected by the quality of the dead centers. It is also influenced by the accuracy level of wheel head bearings. For internal and external grinding, if the machine is in good working condition and is fitted with air bearing, it grinds external and internal surface up to 0.13μm because the axis definition of the aerostatic bearing is far better than ball bearings.

1.3.2.3 *Magnetorheological (MR) fluid-based finishing:* The permanent magnet tool is used in this study to finish the components made of stainless steel and aluminum. This process has greater flexibility used to achieve the roughness values lesser than 0.1μm. In this process, the MR polishing fluid is applied to the circumferential area of the rotating tool which is coupled with computer control. When the magnetic tool rotates within the gap, it results in high shear stress in the fluid contact zone. The shear stress in MR fluid is due to the presence of abrasive particles and that results in the removal of material. The magnetorheological polishing (MRP) fluid consist of very fine abrasives and iron particles which acquire magnetic dipole moment. This moment depends on field strength and inter-connected chain structure which is aligned in the direction of the magnetic field. The bonding strength of abrasives in presence of magnetic field and iron particles plays an important role in enhancing the rheological characteristics and MRF action. The composition of MR fluid is most crucial in the MRF process. It has a viscoelastic base such as paraffin oil, glycerol, water, silicone oil with some additives. The selection of the base depends on utilization of MR fluid in specific temperature ranges. Since, the magnetization of particles in the fluid is non-uniform as the particles are ferromagnetic in nature, the increase in the applied magnetic field increases the strength of MR fluid nonlinearly. So, the surface roughness is minimized up to nanometer scale without any damage to surface topography. After the completion of each surface enhancing technique, the load bearing capacity for each surface is analyzed experimentally.

1.4 INDUSTRIAL APPLICATIONS OF AEROSTATIC BEARING

1.4.1 Machine tool

The application of aerostatic spindle in machine tool have some principal advantages such as low friction (L.F.), precise axis definition (P.A.D.) and absence of wear (A.W.). The effect of these advantages during operation cycle is specified in Table 1.4.

1.4.2 Medical equipment

The medical equipment uses aerostatic bearing in high-speed applications such as

- High-speed dental drill
- Air turbine for the instrument of orthopedic surgery

1.4.3 Scientific instruments

The list of scientific instruments based on the low-speed and high-speed application of aerostatic bearing is given in Table 1.5.

Table 1.4 Advantages of aerostatic bearing in machine tool

Process	Function		Advantages
Grinding	Wheel head and work head spindle	L.F.	Eliminates thermal distortion and improves mechanical efficiency.
		P.A.D.	High order of roundness in work and helps the grinding wheel to hold its form longer.
		A.W.	Long bearing life and freedom from deterioration.
Drilling	Drill spindle	L.F.	High speed on lower power consumption.
		P.A.D.	Accurate hole size by minimizing burring and smearing.
		A.W.	Increase in cycle time by enhancing operational capability.
Milling	Mill spindle	L.F.	Less power loss due to low noise and vibrational level.
		P.A.D.	Minimize surface defects by improving surface accuracy.
		A.W.	Enables high speed to improve productivity.
Turning	Work head spindle	L.F.	Minimize thermal distortion.
		P.A.D	High order of roundness.
		A.W.	Avoid damage due to rubbing of surfaces during start and stop.

Table 1.5 List of scientific instruments with aerostatic spindle

Type	Advantage	Application
Low speed	L.F and P.A.D	Dynamometers Balances Friction pivots and pulleys Roundness and flatness testing instruments Roundness measurement
High speed	L.F, P.A.D., and less power consumption	High-speed cameras Prism and mirror spinners Optical and infrared scanner spindles

1.4.4 Other applications

a) Automotive technology
   - Air-guided knife drive
   - Air-guided trailer test stand
   - Air-guided turbocharger

b) Flat panel technology
   - 2-axis and 3-axis stage (x, y, z)
   - Precision chuck

c) Semiconductor technology
   - Air bearing for the inspection device
   - Air-guided chip packaging unit
   - Chuck with integrated lift drive
   - Air-guided x/y/z-drive for Bonders
   - Air-guided rotary/linear drive

d) Surface Mount Technology
   - Air-guided PCB support
   - Air-guided placement head

e) Linear drives
   - Precision measurement stage
   - High dynamic linear drive

- High-accelerated Doppler drive
- Air-guided positioning unit
- Drive for a production machine

f) Medical technology
- Air-guided Computed Tomography

g) Pick & place
- Pick & place module with a rotary drive
- Air-guided z/theta unit

h) Production technology
- Air bearing for the adjustment of components
- Adjustment slider for optics production
- The cylindrical air bearing for small tubes

i) Space technology
- Air-magnetic slip system

j) Textile technology
- Air-guided rotor spinning
- Air Guided ring spinning

CHAPTER 2

LITERATURE REVIEW

2.1 HISTORY OF AIR BEARING

In 1883, N.P. Petrov published the first article on the theory of gas lubrication and gas dynamics in the Journal of the Engineering [4]. In this study, the expression for the cylindrical shaft is formulated to calculate the rotational resistance moment within the coaxial race, with fluid as a medium for pressure distribution. However, the behavior of the incompressible fluid in sleeve bearings along with a shaft was first fully examined in the study of O. Reynolds [5]. In 1886 Reynolds published the article in Tower's experiments" with a title "The hydrodynamic theory of lubrication and its application". After the completion of Reynold's study, the various hypothesis on the approximation of Reynolds equation, boundary layer flow, turbulent length characteristics, velocity scales and transport equations were published. In 1894, the first patent on an air bearing was granted in U.S. Zhukovsky and Chaplygin [6] published an article "On the pressure exerted by a plane-parallel flow of air on an obstructing body, which gave the lift on a wing section". This study is based on the aerodynamic principle to calculate the pressure along with the flow of the stream on the body. The use of the air as a lubricant in the bearing was tested by Kingsberry [7] and Harrison [8].

2.2 AIR FLOW THEORY

The air flow and air-film forces are dependent on the pressure distribution within the bearing and spindle surfaces. The study of pressure and flow velocity is governed by the fluid properties such as viscosity, density, and compressibility.

The fluid i.e. air flowing through aerostatic bearing is considered as a Newtonian fluid which is defined as the fluid which causes viscous stresses and they are linear and proportional to local strain rate. In general, stress in fluid (τ_{ij}) for incompressible and constant viscosity across the fluid is given by the equation (2.1)

$$\tau_{ij} = \mu\left(\frac{\partial v_i}{\partial x_j} + \frac{\partial v_j}{\partial x_i}\right) + \lambda\frac{\partial v_k}{\partial x_k} \tag{2.1}$$

where μ is the dynamic viscosity of the fluid, λ is a constant of proportionality with the assumption that stress depends on strain, v_i, v_j and v_k are the velocity component in direction of coordinate components x_i, x_j, and x_k respectively.

The air lubrication is better understood by the physical behavior of air by varying flow parameters. The flow of air in aerostatic bearing in different regions is governed by Naiver-Stocks equation, Reynold's equations and Darcy's law. The solution for this equation for air is given in literature in order to simplify the numerical calculation of air flow. The motion of fluid follows three basic laws which are represented by Navier-Stocks equations [9].

The Law of conservation of mass (Continuity Equation) is given by equation (2.2).

$$\frac{\partial \rho}{\partial t} + \frac{\partial(\rho u)}{\partial x} + \frac{\partial(\rho v)}{\partial y} + \frac{\partial(\rho w)}{\partial z} = 0 \tag{2.2}$$

where, ρ is the density of fluid and u, v, and w are the scalar valued function in x, y and z-direction.

The law of conservation of momentum based on Newton's second law in x, y, and z-direction is expressed as in equations (2.3)-(2.5)

$$\frac{\partial(j_x)}{\partial t} + \nabla.(j_x \vec{u}) = -\frac{dp}{dx} + \frac{\partial \tau_{xx}}{\partial x} + \frac{\partial \tau_{yx}}{\partial y} + \frac{\partial \tau_{zx}}{\partial z} + f_x \tag{2.3}$$

$$\frac{\partial(j_y)}{\partial t} + \nabla.(j_y \vec{u}) = -\frac{dp}{dy} + \frac{\partial \tau_{xy}}{\partial x} + \frac{\partial \tau_{yy}}{\partial y} + \frac{\partial \tau_{zy}}{\partial z} + f_y \tag{2.4}$$

$$\frac{\partial(j_z)}{\partial t} + \nabla.(j_z \vec{u}) = -\frac{dp}{dz} + \frac{\partial \tau_{xz}}{\partial x} + \frac{\partial \tau_{yz}}{\partial y} + \frac{\partial \tau_{zz}}{\partial z} + f_z \tag{2.5}$$

where, j_x, j_y, j_z are the momentum density in x, y, and z-direction, f_x, f_y, f_z are the force density in x, y, and z-direction, and $\vec{u}$ is the velocity vector.

The law of conservation of energy based on the 1st law of thermodynamics is given by equation (2.6)

$$\frac{\partial(\rho T)}{\partial t} + \nabla(\rho \vec{u} T) = \nabla(\varphi \, grad \, T) + E_d \tag{2.6}$$

where T is temperature and E_d is viscous dissipation energy.

These equations are derived using the Lagrangian approach [9] and the Eulerian method [10]. These methods help in generalizing the velocity of the boundary layer for rotating fluid system. It was shown in the literature that there were some fictitious effects added in the energy equation but in a recent study [11], it proved that there are no fictitious effects present in the energy equation.

The Reynold's equation shows the effect of pressure distribution along two surfaces with varying film thickness [5]. In recent literature, the study is focused on modified Reynold's equation which introduces velocity profiles based on external air injection for finite length bearing [12, 13]. The general form of continuity is expressed as equation (2.7).

$$\int_0^h \left(\frac{\partial \rho}{\partial t} + \frac{\partial(\rho u)}{\partial x} + \frac{\partial(\rho v)}{\partial y} + \frac{\partial(\rho w)}{\partial z}\right) = 0 \tag{2.7}$$

where h is the fluid film thickness.

For this relation, the profile of lubrication film becomes continuous which follows the ideal gas law for an isothermal condition. The pressure distribution follows a general form of modified Reynold's equation as given in equation (2.8).

$$\frac{\partial}{\partial y}\left(\rho h^3 \frac{\partial p}{\partial y}\right) + \frac{\partial}{\partial z}\left(\rho h^3 \frac{\partial p}{\partial z}\right) = 6\mu U \frac{\partial(\rho h)}{\partial y} + 12\mu \frac{\partial(\rho h)}{\partial t} + 12\rho V_{inj} \tag{2.8}$$

where V_{inj} is simplified by Naiver-Stocks equation and expressed in cylindrical coordinates [14] and U is the spindle surface velocity.

$$V_{inj}(y,z,t) = -\frac{1}{4\mu}\frac{\partial p}{\partial x}\left[\frac{d_o^2}{4} - (y-y_i)^2 - (z-z_i)^2\right] \tag{2.9}$$

where d_o is the outside diameter of bearing

This equation can be used for thrust bearing system where the shaft and bearing surfaces are very small distance. In the case of a journal bearing, the flow velocity is evaluated in radial and circumferential direction. For this purpose, the modified Reynold's in term of radial polar coordinates can be written as equation (2.10).

$$\frac{\partial}{\partial r}\left(prh^3 \frac{\partial p}{\partial y}\right) + \frac{1}{r}\frac{\partial}{\partial \theta}\left(ph^3 \frac{\partial p}{\partial \theta}\right) = 12\mu\left[v_r \frac{\partial(prh)}{\partial r} + v_\theta \frac{\partial(\rho h)}{\partial \theta}\right] + \frac{\partial(ph)}{\partial t} \tag{2.10}$$

where, r and θ are the radial and circumferential components, and v_r and v_θ are the velocity in radial and circumferential direction.

2.2.1 Air flow through an orifice

For the analysis of air flow behavior, the recent researches pointed out finite element method which helps in analyzing pressure distribution within the bearing surface and spindle [15,16]. The use of pocketed type orifice rather than inherent orifice shows the enhancement in load carrying capacity, inertial forces, whirl ratio and stiffness by minimizing instability induced in an aerostatic bearing

system [17]. The design of restrictor is dependent on the geometrical parameters of an orifice such as recess shape, supply hole diameter, and orifice length.

The recess shapes or pressure equalizing grooves used in gas-lubricated bearing are spherical and rectangular in shape which shows its effect on load capacity, mass flow rate and stability of bearing. At same supply pressure, recess width and outer diameter, the load carrying capacity increases in the sequence of non-recessed bearing, spherical recessed bearing, rectangularly recessed bearing. Also, the sequence is the same for an increase in mass flow rate [18]. The recessed shape also leads to vortex formation at the outlet of orifice restrictor due to change in the air which is caused by the increase in flow rate and the decrease in pressure. This may cause instability in bearing due to vibrations in bearing and by increasing the temperature in the recessed region. This vortex formation in a thrust bearing can be minimized by making rounded corners at the outlet of orifice restrictor and the vibrations are suppressed by using film thickness smaller than 10μm [19]. To avoid the instability phenomenon in journal bearing, the depth of the pressure equalizing grooves should be approximately two or three times of bearing clearance and to attain maximum load capacity in circumferential and axial directions, these groves should be placed where the film thickness of air is minimum [20].

The pressure distribution is also affected by the increase in orifice diameter to bearing outer length ratio (dimensionless supply hole diameter). As this ratio increases, both the load carrying capacity and the mass flow rate increases on decreasing the film thickness and increasing the supply pressure [21]. So, to ensure better performance of the gas lubricated bearings, the area of the air chamber should be large and the film thickness and orifice diameter should be small [22]. The influence of orifice length cannot be ignored as it produces large errors in the evaluation of performance. The numerical calculations for small orifices of diameter less than 0.05mm show that the bearing with small feed holes could have better performance in term of damping coefficient and stiffness than bearing with compound restrictor [23]. The pressure drop within the orifice is based on dynamic effect which depends on the mass flow rate through orifice restrictor. The generalized equation for mass flow rate ($\dot{m}$) through an orifice restrictor can be defined as equation (2.11) and (2.12) [24].

$$\dot{m} = C\rho p_1 \sqrt{\frac{T_2}{T_1}\left\{1 - \left(\frac{p_2/p_1 - b}{1 - b}\right)^2\right\}} \qquad \text{for } \frac{p_2}{p_1} > b \qquad (2.11)$$

$$\dot{m} = C\rho p_1 \sqrt{\frac{T_2}{T_1}} \qquad \text{for } \frac{p_2}{p_1} \leq b \tag{2.12}$$

where C is the conductive value, p_1 and T_1 are pressure and temperature at the inlet, p_2 and T_2 are pressure and temperature at outlet and b is the critical pressure ratio.

For generalized equations, the conductive value is defined as

$$C = \frac{AC_d}{g\rho_2} \sqrt{\frac{2gk}{(k-1)RT_2}\left(\frac{2}{k+1}\right)^{\frac{2}{k-1}}} \tag{2.13}$$

where, C_d is discharge coefficient.

For an ideal nozzle, critical pressure ratio is given by equation (2.14)

$$b = \left(\frac{2}{k+1}\right)^{\frac{k}{k-1}} \tag{2.14}$$

where k is the specific heat ratio.

For modeling and simulation of mass flow rate in aerostatic bearing with orifice restrictor, the equation given in literature are described as equation (2.15) - (2.17) [24]

$$\dot{m} = AC_d\vartheta \frac{p_1}{g\sqrt{RT_1}} \tag{2.15}$$

$$\vartheta = \sqrt{2g\frac{k}{k-1}\left\{\left(\frac{p_2}{p_1}\right)^{\frac{2}{k}} - \left(\frac{p_2}{p_1}\right)^{\frac{k+1}{k}}\right\}} \qquad \text{for } \frac{p_2}{p_1} > b \tag{2.16}$$

$$\vartheta = \sqrt{2g\frac{k}{k-1}\left(\frac{2}{k+1}\right)^{\frac{2}{k-1}}} \qquad \text{for } \frac{P_2}{P_1} \leq b \tag{2.17}$$

where, A is the area of orifice, R is gas constant, and g is adiabatic index.

For plain orifice, $A = \pi dh$ and for pocketed orifice type, $A = \frac{\pi}{4}d^2$

where d is the diameter of the orifice.

Based on these equations, the recommended values for the discharge coefficient and critical pressure ratio are derived from simulation model are $0.8 < C_d < 0.85$ and $0.35 < b < 0.4$ respectively [25]. When load capacity and mass flow are considered as a function of discharge coefficient, it is found that the load carrying capacity of the bearing is 0.5% lower and the mass

flow rate is 7.4% higher at eccentricity ratio of 0.5 [26]. CFD simulations based on FDM (Finite Difference Method) calculations show that the discharge coefficient is decreased with increase in orifice diameter and increased with increase in film thickness [27].

2.3 LITERATURE RELATED TO PERFORMANCE PARAMETERS

2.3.1 Effect of flow parameters

The load capacity is estimated by comparing the geometrical conditions with flow velocity from the graphical presentation of the general performance of aerostatic bearing as shown in Figure 2.1 and Figure 2.2. This performance evaluation provides the static load capacity of a bearing of up to 150 mm in diameter and 150 mm in length supplied at 0.7 MPa. This relation is suitable for bearing with two-row orifices and the load given in graph can be achieved by a bearing manufactured at eccentricity ratio of 0.5 for journal bearing and clearance of 0.025 mm for the thrust bearing.

For orifice fed bearings, the value of load capacity and stiffness is dependent on the gauge pressure ratio (K_g). The optimum value for gauge pressure ratio is defined in the work of Taufik and Stout as equation (2.17) [28].

$$K_g = \frac{p_d - p_a}{p_o - p_a} \tag{2.17}$$

where, p_a, p_d, and p_o are the ambient pressure, pressure downstream of the orifice, and supply pressure respectively.

In case of journal bearings, the optimum value of K_g provides the maximum stiffness during unloaded condition (i.e. concentric position) [29] whereas, in case of thrust bearings, there is an opposed pad system due to which flat pad bearings doesn't have any concentric position. Therefore, the optimum value for K_g is more complex to define in the flat pad system and should be approached with care. Also, the thrust bearings may have varying pressures at the inlet of orifices. A study on orifice type bearing [30] shows that there is significant variation in pressure along the grooves for flat pad bearings in concentric state and for journal bearing, each orifice pressure can be equal. This proves that there may be some variation in pressure at downstream of orifice due to multiple entry points. This would introduce some inexactness in the definition of K_g. Figure 2.3 shows the variation of the gauge pressure ratio with the load coefficient and it can be seen that the variation of K_g with respect to eccentricity ratio is expressed in Table 2.1

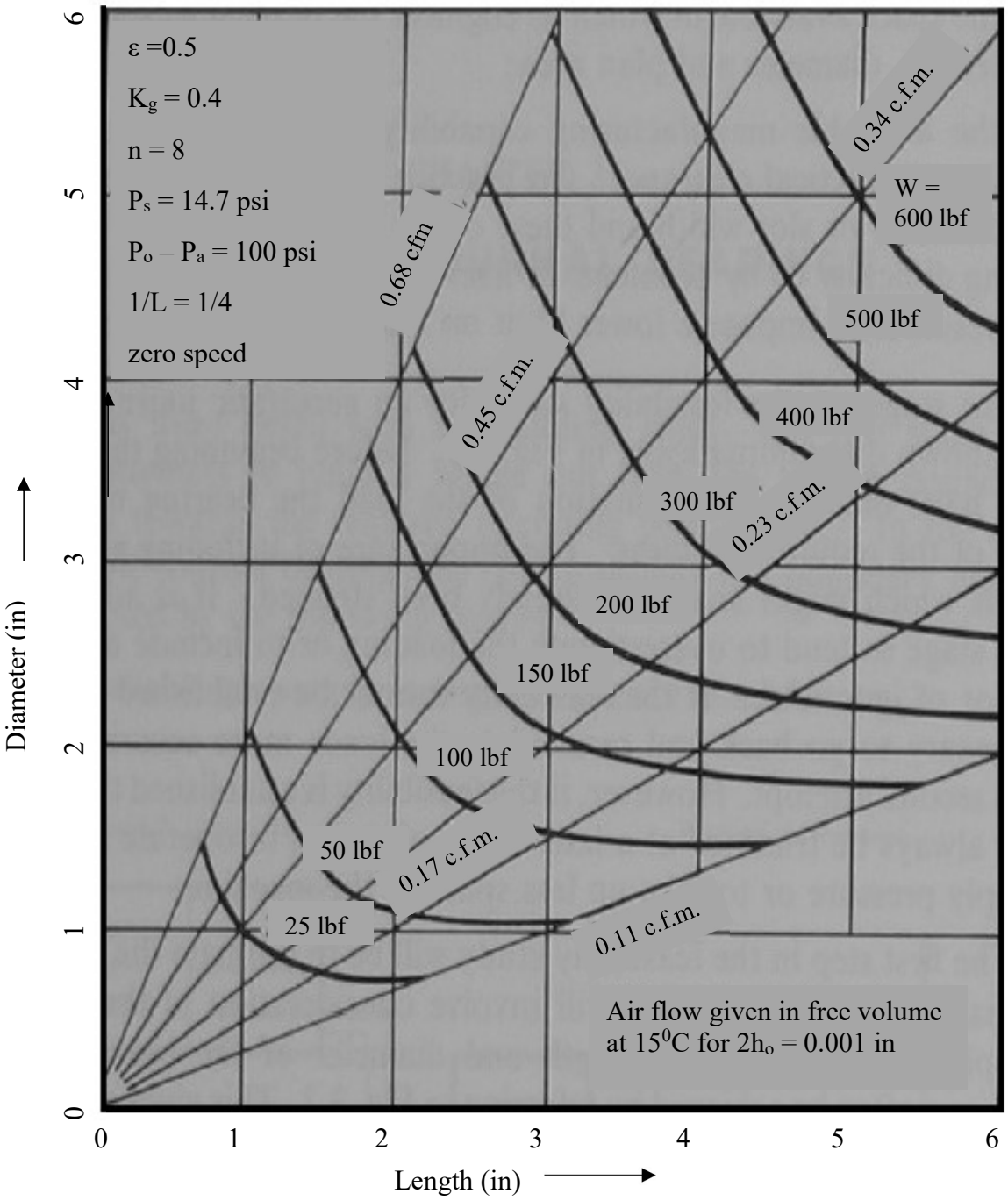

Figure 2.1 General performance characteristics of journal bearing [1]

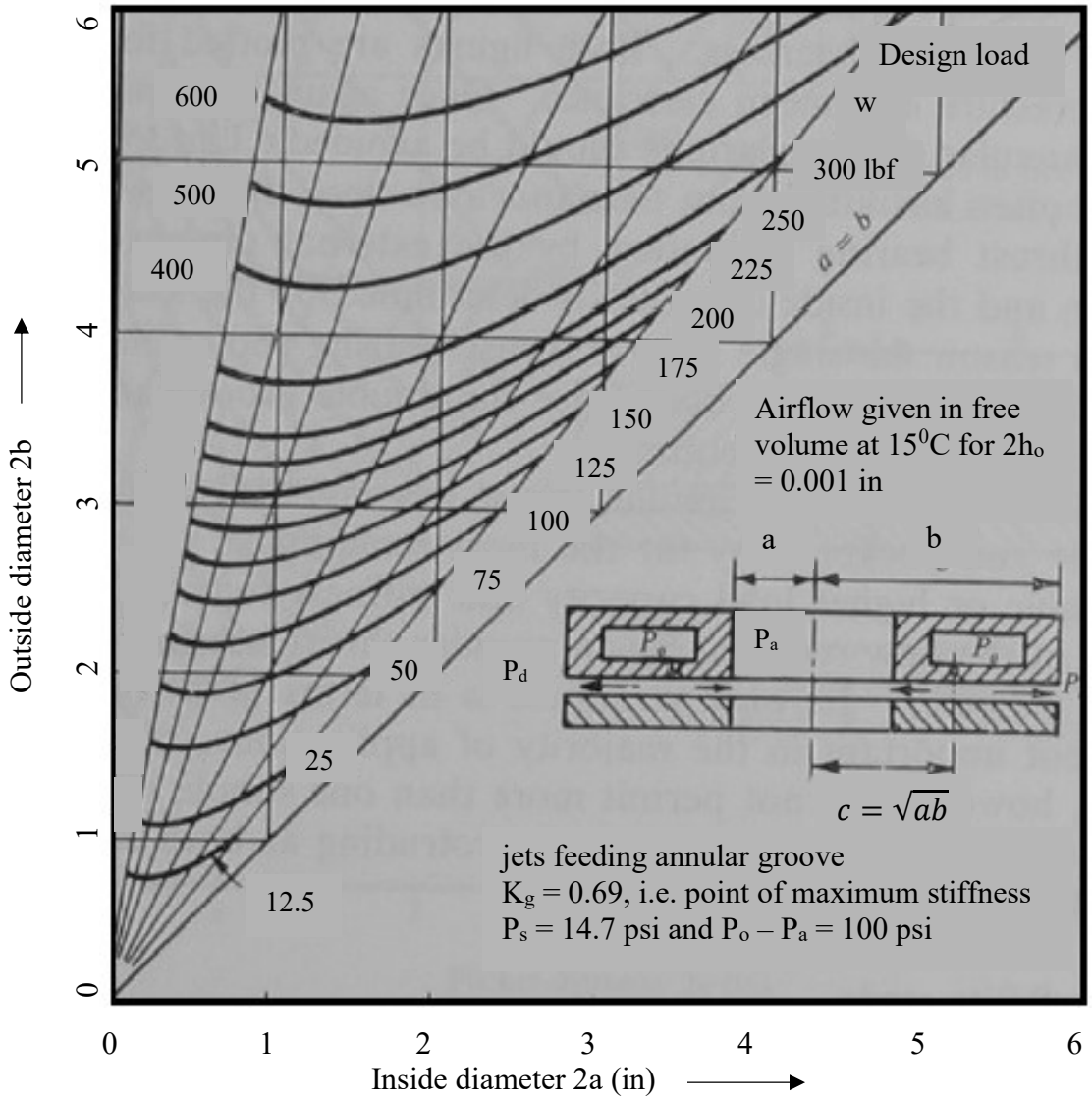

Figure 2.2 General performance characteristics of thrust bearing [1]

Table 2.1 Optimum value of K_g from presented graphs [1]

Eccentricity; ε	Optimum value of K_g
0.1	0.6
0.5	0.4
0.9	0.35

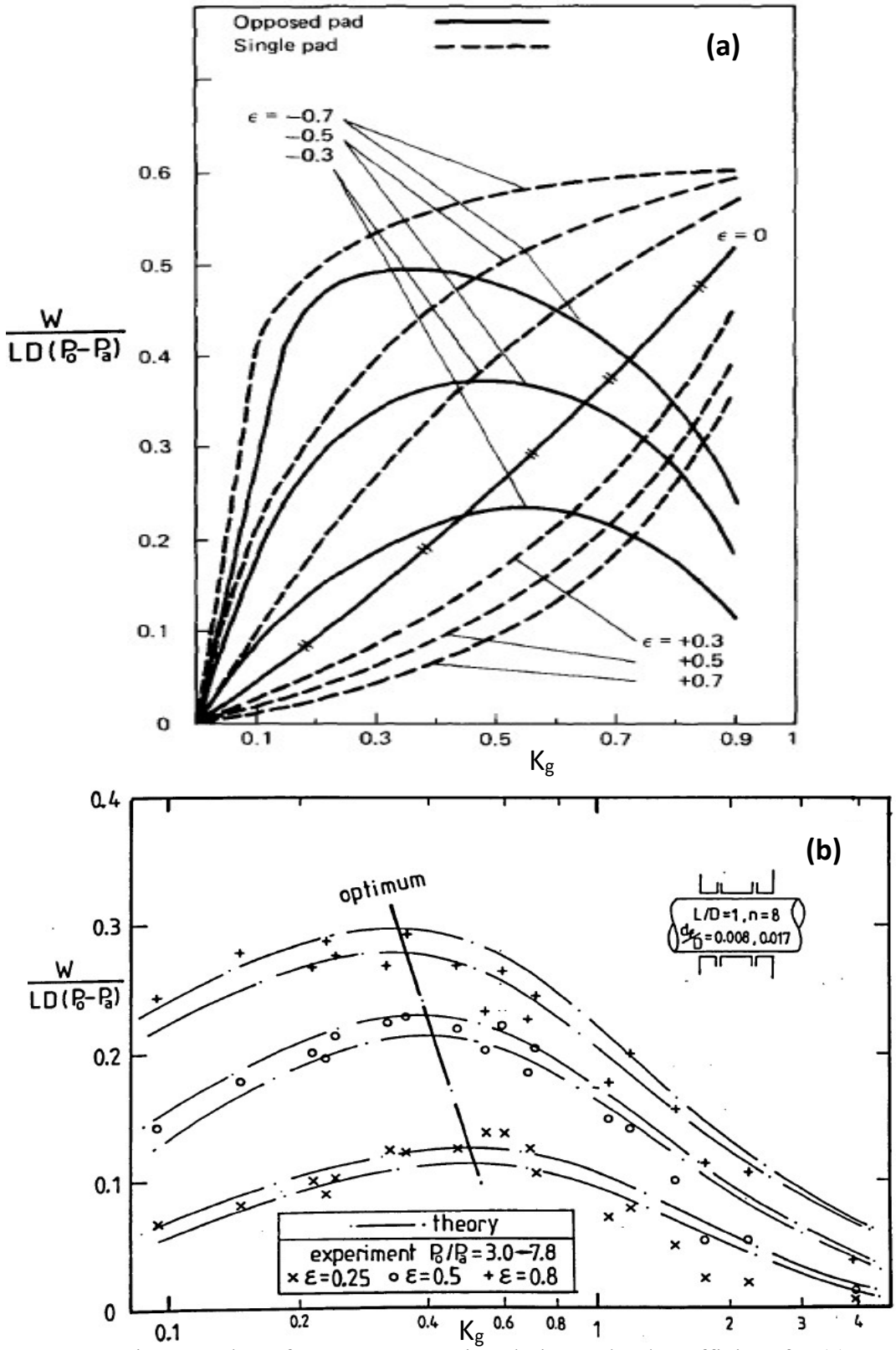

Figure 2.3 Optimum value of gauge pressure in relation to load coefficient for (a) aerostatic thrust bearing [28], and (b) aerostatic journal bearing [29]

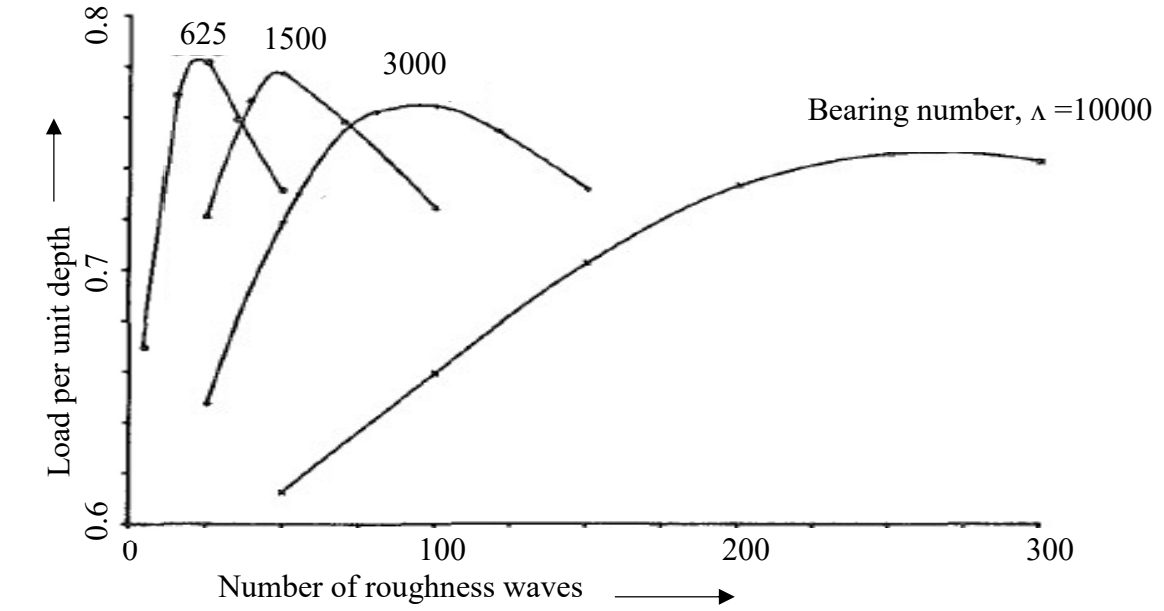

(a)

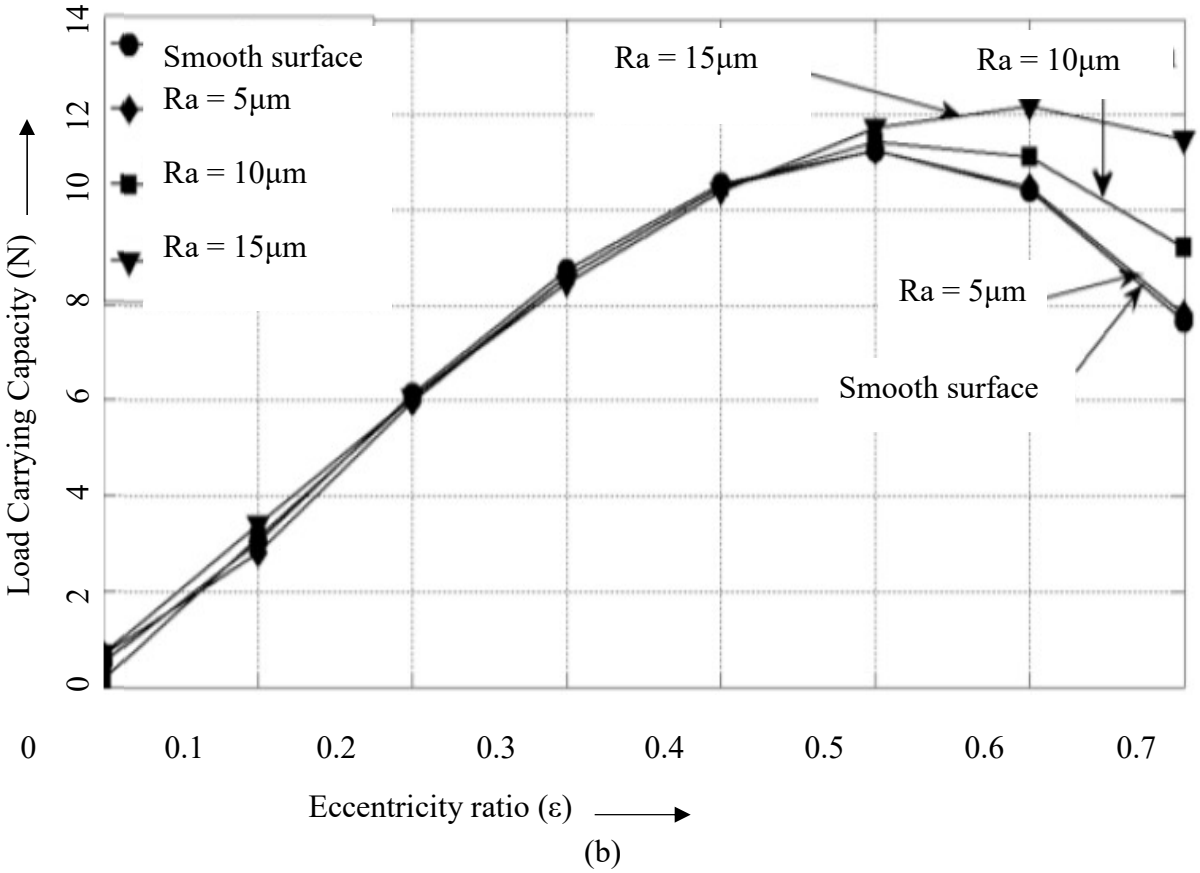

(b)

Figure 2.4 (a) Effect of number of roughness waves on load per unit depth with respect to bearing number [31], and (b) effect of surface roughness on load carrying capacity with respect to eccentricity ratio [32]

2.3.2 Effect of roughness parameters

Numerical analysis of surface roughness also shows that for a similar magnitude of Couette effect for fluid film and pressure distribution, the value of load capacity gives maximum peak. According to this criterion, for the high value of film height, the bearing number comes out to be minimum which shows the decrease in load capacity for both rough and smooth surfaces [31]. To analyze surface roughness, Reynold's equation model is used with clearance function that it has a direct relation with bearing and spindle surfaces. This model is solved to obtain air film forces and then simulated with different values of surface roughness and spindle mass. This model shows us that for the lower value of surface roughness, the load capacity is higher and system vibrations are lower. Also, for the weighty spindle, the eccentricity is higher. So, spindle oscillates around the bearing center for the higher value of surface roughness [32]. The results are shown in Figure 2.4. The comparison between the rough and smooth surface of bearing showed that the consideration of roughness on bearing surface affects the load carrying capacity. The loading forces generated in air bearing increases quadratically with an increase in static roughness amplitude. The results shown concludes that the amplitude of the surface roughness affects the performance of aerostatic bearing by affecting its load carrying capacity. In literature, the studies carried out to analyze the effect of bearing design parameters are based on the assumption that the surface of bearing and the spindle are smooth. But the actual surface contains higher roughness amplitude which affects the results of experimental analyses. So, the effect of surface roughness on the performance of aerostatic bearing is analyzed in the present study.

2.4 RESEARCH GAPS

- The pressure equalizing groove has to be employed in aerostatic bearing after the orifice section in order to improve the pressure distribution within the clearance gap.
- The major researches on the effect of surface finish on bearing performance are mostly determined by mathematical simulation models. In the present research, the effect of finishing parameters will be determined experimentally.
- The performance of aerostatic bearing given in previous research is evaluated by the numerical model by considering the average surface roughness larger than 1μm. The present research shows the effect of enhanced roughness values up to the nanometer scale.

2.5 RESEARCH OBJECTIVES

- The theoretical analysis of bearing has to be performed to evaluate the design parameters of the aerostatic bearing.
- The bearing components to be designed based on the theoretical analysis.
- The designed aerostatic bearing is to be validated by CFD (Computational Fluid Dynamics) analysis for fluid flow.
- After validation of the designed model of aerostatic bearing, the components of bearing assembly are fabricated using selected manufacturing techniques.
- The load carrying capacity of the designed aerostatic bearing is evaluated on various surfaces of journal and thrust which are achieved by processes used in the manufacturing of components.

2.6 METHODOLOGY FOLLOWED FOR THE PRESENT RESEARCH

This research project starts with the analysis of the design parameters based on the theoretical modeling based on previous literature. This analysis gives a brief idea for the selection of geometrical parameters of the aerostatic journal and thrust bearing and with these parameters, the bearing model is designed by using 3d modeling software. Further, the numerical analysis is carried out using CFD Fluent in ANSYS to analyze the behavior of air flow through the orifice and clearance sections of the bearing. This analysis helps in validating the designed model by comparing the model with previous analysis based on convergence criteria and the results obtained in studies carried out in literature.

After the validation of the designed model, the components of the aerostatic bearing are fabricated with various manufacturing techniques. To analyze the effect of surface roughness on the load carrying capacity of aerostatic bearing, the surface characteristics of the bearing and spindle surfaces are enhanced by manufacturing techniques. The test setup for the aerostatic bearing is built on which the results are carried out for various surfaces.

CHAPTER 3

DESIGN AND NUMERICAL ANALYSIS OF MODIFIED AEROSTATIC BEARING

3.1 DESIGN STEPS

The primary target of aerostatic bearing design is to develop an experimental setup to evaluate the performance of designed aerostatic bearing. The major challenge of any design of aerostatic bearing is to improve the load carrying capacity at various operating conditions. In the present study, the effect of surface roughness of bearing and spindle surface is analyzed to improve the load carrying capacity of the designed aerostatic bearing. The flow chart in Figure 3.1 explains the basic steps involved in the aerostatic bearing design.

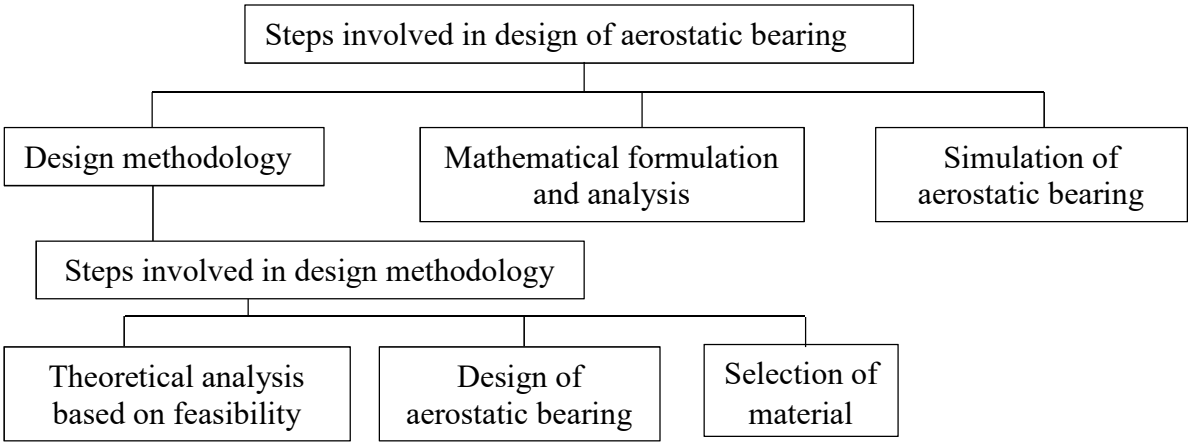

Figure 3.1 Steps involved in a design of the aerostatic bearing

3.1.1 Theoretical analysis of bearing design

The design of aerostatic bearing starts with the feasibility study as shown in Figure 3.2. In this stage, the designer attempts to figure out the boundary limitations of a particular design to achieve optimum performance which is affected by the following factors:

- Availability of air supply in form of pressure and flow velocity.
- Geometrical parameters of bearing.
- Manufacturing capability to attain minimum clearance.
- Fluid properties.

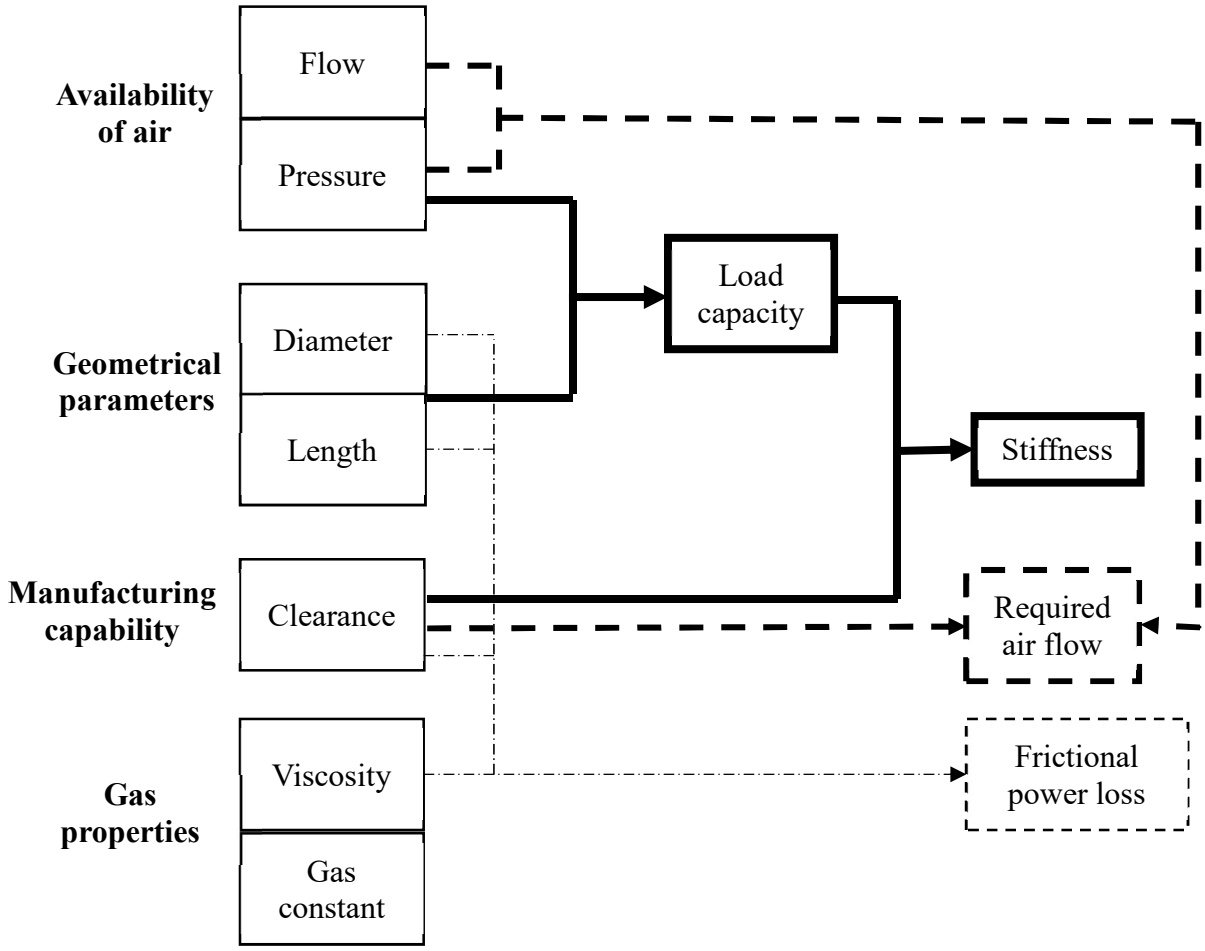

Figure 3.2 Feasibility study for a design of the aerostatic bearing

Based on these factors, the first stage of the feasibility study is to estimate maximum radial and axial load capacity in journal and thrust bearing respectively from the general representation of performance. This estimation involves the geometrical parameters such as diameter and length of bearing. The radial load capacity of the bearing can be defined in form of load coefficient (C_L) as equation (3.1) [1]

$$C_L = \frac{W_r}{(P_o - P_a)LD} \tag{3.1}$$

where W_r is radial load acting on the spindle, L is the length of the bearing, D is the diameter of the bearing, P_o is supply pressure, and P_a is ambient pressure.

The axial load capacity (W_a) of the bearing is given by equation (3.2) [1]

$$W_a = (P_o - P_a)\pi \frac{[b^2 - a^2(2log_e(b/a) + 1)]}{2log_e(b/a)} \tag{3.2}$$

where a and b are the radius of internal pocket and bearing respectively.

The second stage of the feasibility study to estimate the stiffness which includes the maximum load-bearing capacity and clearance between the bearing and spindle surface. As most of the bearing operates linearly up to the eccentricity ratio of 0.5, therefore, the eccentricity ratio ranging from 0 to 0.5, the radial stiffness (K_r) can be calculated by the equation (3.3) [1]

$$K_r = \frac{W_r}{\varepsilon h_o} \tag{3.3}$$

For axial stiffness, the relation can be written as equation (3.4)

$$K_a = 2.88\frac{W_r}{h_t} \tag{3.4}$$

where, h_o and h_t are the clearance gaps in journal and thrust bearing respectively.

The comparison with other types of bearings, the air bearing has very low friction. So, the frictional power loss is neglected in the feasibility study. But the power loss due to friction becomes an important aspect of output given by the machine. Theoretically, the dissipation of power (P_L) in term of heat due to friction in journal bearing is given by equation (3.5) [1]

$$P_L = \frac{\pi \mu D^3 L \omega^2}{4h_o} \tag{3.5}$$

where h_o is the clearance gap, and ω is the thermal conductivity of the bearing material

The final stage of the feasibility study involves the estimation of the airflow required in bearing based on the supplied pressure and the chosen clearance. Then the comparison of the calculated value with the value available at supply is analyzed the actual mass flow rate from the inlet to exit of the bearing. The stages of the feasibility are repeated several times at various flow conditions for the evolution of optimum design. The final stage of feasibility is achieved by approximation of different boundary values but the prior knowledge of performance factors such as load capacity, stiffness, clearance, mass flow rate and frictions should be useful in the estimation of performance.

3.1.2 Example of the theoretical design procedure

3.1.2.1 *Journal bearing*

For example, an aerostatic journal bearing must be designed with geometrical parameters of L/D=1.5 which carries the maximum permissible radial load of 5N at eccentricity ratio of 0.5. The radial stiffness should be higher than 100N/mm. The initial pressure for the design is considered to be 3bar. The flow rate in bearing should not exceed 0.0003m^3/s. The errors considered in the

manufacturing process are 0.001mm in clearance and holes which should be drilled with a diameter of 0.5mm. The design limits of the bearing are diameter 25mm; hole pattern is 2 row and 3 column orifices. The length of the bearing is considered based on the feasibility study. The solution for the design procedure of the given example can be performed to evaluate the design parameters of the aerostatic bearing. A study showed in Figure 2.1 of the previous chapter, for 8 number of rows (n) at a supply pressure of 6.9bar, bearing diameter of 25mm and length of 40mm, the load carrying capacity is about 100N. So, the load capacity at a supply pressure of 3bar is calculated to be 14.49N.

So, based on the flow rate of 2-row orifices, the load carrying capacity would be 3.62N. The clearance of 0.01 mm is required for the flow rate less than 0.0003m^3/s at 6.9bar pressure. (From figure 2.1). So, the initial mass flow rate for the initial design would be about 0.0001m^3/s. To achieve this flow rate, the clearance in bearing should be four to five times greater than manufacturing error. To calculate the optimum clearance, the stiffness is calculated based on designed clearance as given in Equation (3.3).

$$K_r = \frac{W_r}{\varepsilon h_o} = \frac{3.62}{0.5 \times 0.04} = 181 N/mm$$

From these calculations, it can be concluded that the suitable dimension for aerostatic journal bearing are diameter 25mm, length 40mm, and clearance 0.04mm.

Further, the various design parameters for orifice fed bearings are the number of orifices per row and length-to-diameter ratio. For six or eight holes feeding system at the quarter station with 1.0 length-to-diameter ratio and supply pressure of 6.9bar requires the hole diameter of 0.25mm, 0.5mm and 0.7mm at gauge pressure ratio of 0.4, 0.6 and 0.8 respectively [1]. For L/D ratio of 1.5 and the initial supply of 3bar, the dimensions of orifice diameter are corrected by the relation between L/D ratio and the orifice of the bearing which is given as $d = d^* \sqrt{1/(L/D)}$

$0.25 \times \sqrt{1/(40/25)}$= 0.197 mm at K_g = 0.4

$0.5 \times \sqrt{1/(40/25)}$= 0.395 mm at K_g = 0.6

$0.7 \times \sqrt{1/(40/25)}$ = 0.553 mm at K_g = 0.8

It can be seen that at K_g = 0.4 is not possible because of the variation in inlet pressure and an exit pressure of the orifice is not large. It may cause due to leakage of gases within the system. So, the alternatives of K_g between 0.6 and 0.8 is considered for practical design. Hence, the final design

parameters are specified in Table 3.1. Also, the performance o the supply pressure of 6.9bar at ε = 0.5 is reported in Table 3.2.

Table 3.1 Final design parameters for journal bearing

Parameter	Value
Diameter	25 mm
Length	40 mm
Clearance	0.04 mm
Feeding	6 simple orifices: 2 rows of one-third station
Feed hole diameter	0.5 mm

Table 3.2 Performance on the supply of 6.9 bar at ε = 0.5

Radial load capacity	3.62 N
Stiffness	181 N/mm
Airflow	0.0003 m^3/s

3.1.2.2 *Thrust bearing*

For example, the combination of two aerostatic thrust bearings is used to carry the axial load of 50N in both directions. The air supply pressure used in practical experimentation is 5bar. The inside and outside diameters are limited to 25mm and 75mm respectively. For better design, the axial stiffness should not increase as 5000N/mm for small axial loads and air flow should be about 0.0003m^3/s.

The design procedure of the thrust bearing for the given example can be performed as follows: The Figure 2.2 shows that the dimensional parameter for the 100N load carried at a 6.9bar pressure within the design criteria will be: Inside diameter is 25mm and outside diameter should be greater than 50mm but less than 75mm. In case of two thrust bearing, the ultimate load is 1.25 times greater than the design load. So, the equivalent load at 5bar pressure is given by 55N.

The air flow at a gauge pressure of 6.9 bar and clearance of 0.02 mm is 0.0003 m^3/s (From Figure 2.2). So, at 5 bar pressure it would be $0.0005 \times 0.69 = 0.0002$ m^3/s. It shows the reduction in flow rate within the system. To improve the reduction in order to maintain proper air film distribution annular thrust bearing along with simple orifice bearing is used. Hence axial stiffness is evaluated by using equation (3.4).

$$K_a = 2.88\frac{W_r}{h_t} = 1.25 \times 2.88 \times \frac{55}{2 \times 0.02} = 4950\ N/mm$$

This value of stiffness is calculated for the combination of two thrust bearings with equal clearance on both sides. However, the use of two thrust bearings increases the air flow rate up to 0.0006 m^3/s which is the excess airflow in the bearing design. In order to avoid this excess flow, the other combination is the use of the exit flow of air from the journal bearing as shown in Figure 3.3. It can reduce the consumption of air up to 0.00035m^3/s.

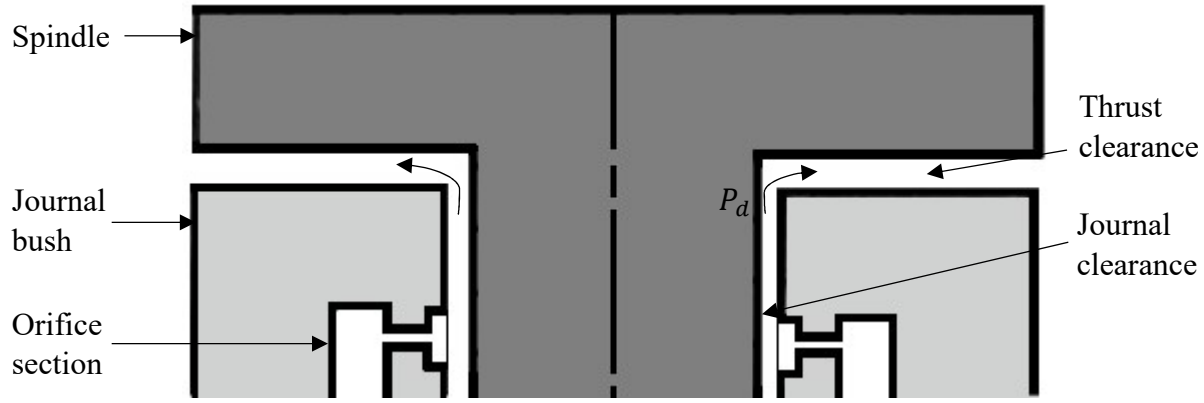

Figure 3.3 Air supply from the journal bearing to thrust pad

The ratio of outside (b) and inside diameter (a) of the thrust bearing is 70/25 = 2.8. Based on this ratio, the diameter of each orifice can be determined by the relation of designed clearance and jet diameter given by Figure 2.2 of the previous chapter. The graph shows that for designed clearance of 0.02mm and b/a ratio of 3, the orifice diameter for thrust bearing should be 0.5mm. The operating parameter for this study is calculated as outlet pressure 1.01bar; inlet pressure 3.5bar at 15°C and K_g of 0.6. The practical choice of a number of feed holes is dependent on manufacturing capabilities. In this case, the diameter is a little larger so the one row with 6 orifices is considered to maintain the air flow rate of 0.0003 m^3/s. Hence, the final design parameters are specified in Table 3.3

Table 3.3 Final design parameters for the thrust bearing

Parameter	Value
Outside diameter	70 mm
Inside diameter	25 mm
Clearance	0.02 mm each side
Ultimate load	55 N
Air flow	0.0003 – 0.0004 m^3/s

3.2 SELECTION OF MATERIAL

The need to select a suitable combination of materials for bearing surfaces becomes important when the parts have to function for a longer lifespan and with reliability. The aerostatic bearing works at very high as well as at very low rotational speeds. So, in case of failure which may cause due to rubbing of surfaces during the occurrence of starting and stopping or due to a gradual decrease in pressure, it is assumed that the contact between two surfaces will cause a seizure. To avoid such failures, the designer must use a material with anti-seizure properties or that can be easily repaired several times without replacing the part. This property tends to focus attention on suitable material selection for bearing and shaft surfaces. So, the following factors that can be considered in the selection of material.

- Corrosion resistance
- Thermal expansion
- Thermal conductivity
- Material stability
- Machinability

Table 3.4 reports the list of material along with their properties that can be used for various surfaces of the aerostatic bearing. Based on these properties, the material for each component of the aerostatic bearing can be selected as per requirement. The major components which can be considered for material selection.

- Journal and thrust housing
- Spindle
- Thrust plates
- Bearing bush

3.2.1 Journal and thrust housing material

This structural member contains passage for air supply through drilled holes and also acts as an outer casing for the shaft. So, the most advantageous properties for this member are corrosion resistance, stability and high modulus of elasticity. For this purpose, austenitic steel grades are considered which are hardened by cold working rather than heat treatment processes. They have two sub-groups that are used for air bearing, 200 series, and 300 series:

- 200 series of steel are the alloys of nickel, chromium, and manganese in which the use of manganese is maximized and the content of nickel is minimized by adding some amount

of nitrogen. Due to the addition of nitrogen, the yield strength of 200 series is up to 50% better than the yield strength of 300 series stainless steel. But due to increase in manganese content and decrease in nickel content makes it less resistant to corrosion.

Table 3.4 List of material for bearing components along with their properties [1]

Material	Density (kg/m^3)	Thermal conductivity (W/m-K)	Coefficient of thermal expansion (0-100ºC) (x 10^{-6} /K)	Modulus of elasticity (GPa)	Electrode potential (V)
Magnesium	1720	159	14.39	44.13	-1.60
Magnesium alloys	1740-1860	79.5-154.9	14.2-15.3	44.13	-1.60
Aluminum	2712	238.49	13.1	68.9	-0.75
Aluminum alloys	2630-2830	146.44	11.2-13.7	68.3-72.3	-0.90 to -0.65
Titanium alloys	4370-4900	6.7-17.2	4.2-5.5	103.5-124.2	-0.09 to +0.06
Grey cast iron	680-7340	54.4	6.5	62.1-162	-0.70
Stainless steel (Martensitic)	7695	25.1	5.6	210.3	-0.35
Mild steel	7834	50.21	5.6	206.9	-0.75
Stainless steel (Austenitic)	7917	15.07	9.5	200	-0.20
Brass	8471	121.4	11.2	103.5	-0.30
Annealed Nickel	8886	87.9	7.3	206.9	-0.15
Annealed Copper	8913	393.3	9.5	117.3	-0.20
Bronze (Phosphor)	8858	83.7	9.5-10	110.4	-0.20
Bronze (Lead)	8940-9275	58.2	9.7-10.2	100	-0.20

- 300 series are alloys of nickel and chromium, which have a wide range of application. The two most common grades used in 300 series are type 304 and type 316. The commonly used type 304 has 18% chromium and 8% nickel. The major difference between type 304 and type 316 is the addition of molybdenum up to 2-3% in type 316 which enhances the corrosion resistance from saline, chlorides and other acids present in the environment. In order to avoid corrosion problems due to heat treatment processes such as welding, the type 304 or type 316 also has low- carbon versions denoted by 'L' with carbon content less than 0.03% which prevents material from sensitization.

The martensite steels are less preferred because of their corrosion resistance as they are hardened by heat treatment. But due to its coefficient of thermal expansion, it can be preferred in some application with high-temperature conditions. The stainless steel in various applications is not used as the gas is supplied to the shaft without exposing it to the outer surface of bearing. This may achieve by inserting tubes for gas flow or by treating the material to avoid the effect of gas on the bearing surface. Some applications also use the mild steel or cast iron for bearing surface but the designer must know the consequences of the corrosion in bearing clearance or in orifices that may lead to failure of the machine by blockage of flow gaps.

3.2.2 Spindle material

The density and modulus of elasticity are two major properties which are necessary to consider for the selection of spindle material. The shaft used in high-speed rotors are made of light alloys to avoid the rubbing contact between bearing surfaces. So, for aerostatic bearing, the selection of spindle material is based on lower density and higher values of E/ρ (young modulus of elasticity/ density) ratio. E/ρ for the various material used for bearing surfaces are reported in Table 3.5.

Table 3.5 E/ρ ratio of bearing and spindle materials [1]

Material	Magnesium	Magnesium alloy	Aluminum	Aluminum alloy	Mild steel	Stainless steel	Titanium alloy
E/ρ ratio (kgf.m/kg)	26.2	24.2-26	26	26.2	27	25.7	23.9-28.8

3.2.3 Material for thrust plates

The thrust plates are used for passage of air flow in thrust bearing which contains a number of orifices and pockets. The material properties required for thrust plates are corrosion resistance, hardness, and stability to provide better handling during surface finishing processes and during assembly. So, the material for thrust plate is high chromium tool steel or hardened stainless steel. The holes in thrust plates are drilled before hardening or by inserting brass plugs with a hole drilled in it because the drilling of fine holes in stainless steel would be difficult than in brass and also the hardening may affect the dimension of already drilled holes. But brass air plugs are undesirable in small machines and in high-temperature conditions, so it is necessary to use a material with higher seizure resistance on the thrust plate face. The other materials such as mild steel and cast iron could be used if they are protected with plating or some other surface treatment processes to avoid corrosion formation.

3.2.4 Bearing bush material

The aerostatic bearing bushes are commonly made of bronze and brass. Lead bronze has a wide range of applications in bearing bushes as it can be easily machined and are corrosion resistant. These two materials are the suitable combination to use with stainless steel material for the journal and thrust housing as the coefficient of thermal expansion of both materials are almost similar which avoids the problems due to thermal stresses. In a combination of both journal and thrust bearing, these bushes are used as spacers to separate components which makes the stable and rigid assembly to prevent the structure from vibrations and failure conditions.

3.2.5 Material selection for the current model of aerostatic bearing

Table 3.6 Material selection for modified aerostatic bearing

Component	Material
Journal and thrust bush	Stainless steel
Spindle	Aluminum alloy
Thrust plate	Mild steel
Bearing bush	Stainless steel and brass

3.3 DESIGN OF MODIFIED AEROSTATIC BEARING

The analysis of parameters carried out in feasibility study gives a basic approach for exact dimensions of various components of aerostatic bearing such as length-to-diameter ratio for journal bearing and inside and outside diameter of the thrust bearing along with orifice size approximation. The various design parameters of the internal geometry can be analyzed such that it can fulfill the required design requirements of aerostatic bearing

- Reduction in weight and size.
- Reduction in friction on bearing and spindle surface.
- High radial and axial stiffness
- Support high axial and radial loads

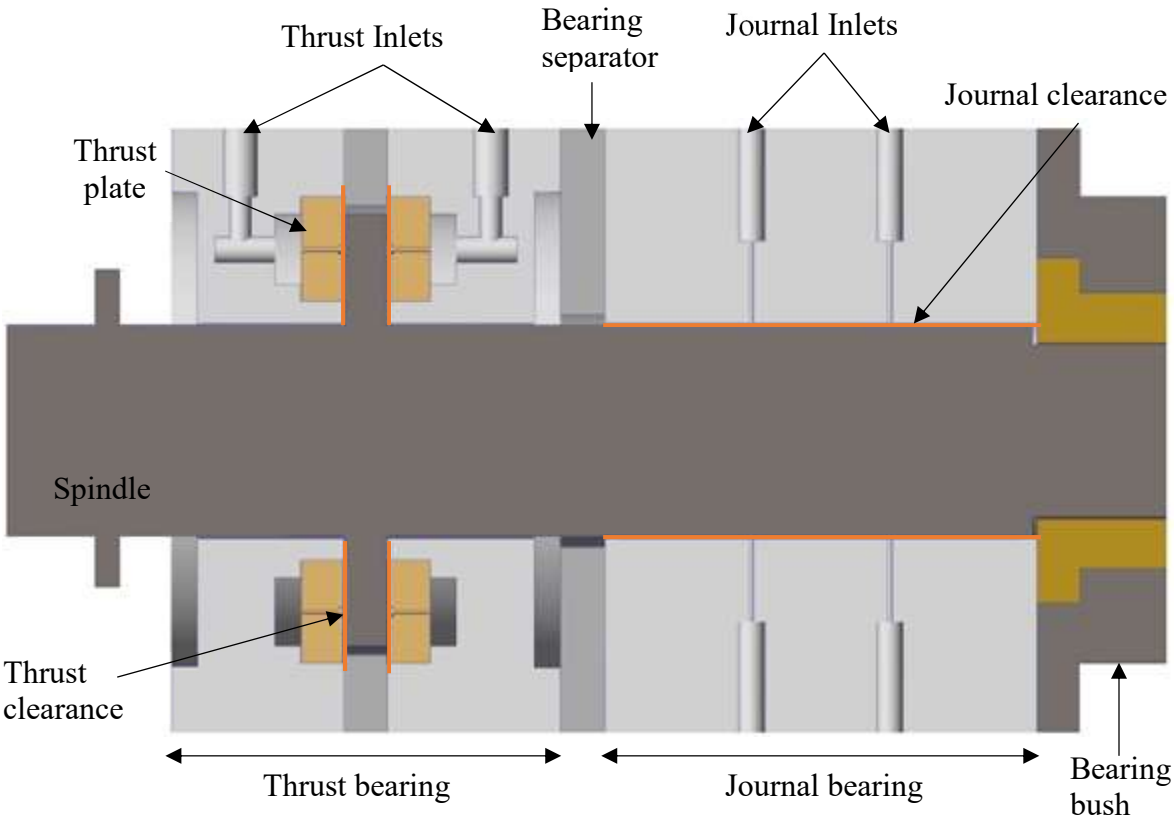

Figure 3.4 3D CAD model of the modified aerostatic bearing

3.3.1 CAD modeling of an aerostatic bearing

Based on the feasibility study and theoretical design parameters, the aerostatic bearing is modeled in Creo parametric 3.0. Figure 3.4 shows the design of aerostatic bearing in the 3D CAD model.

Figure 3.5 shows the 2D sectional view of the bearing surface, the thrust plate surface, and the shaft surface.

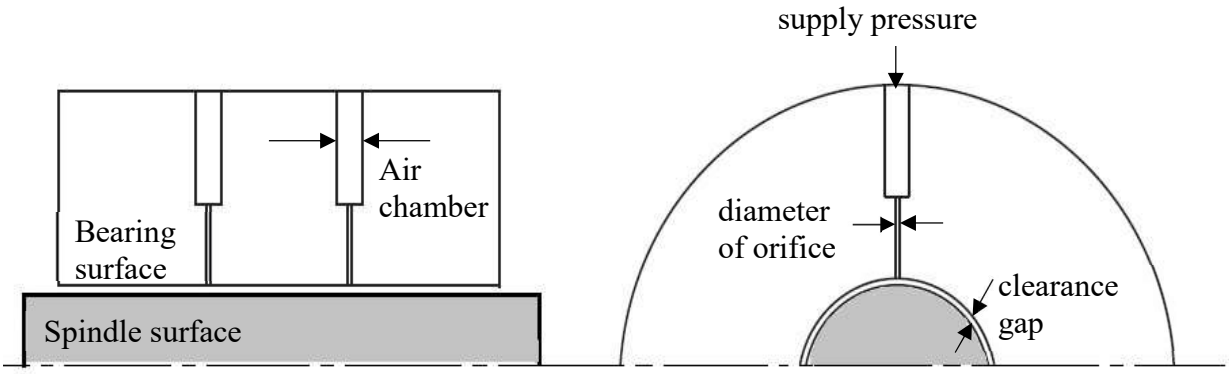

(a)

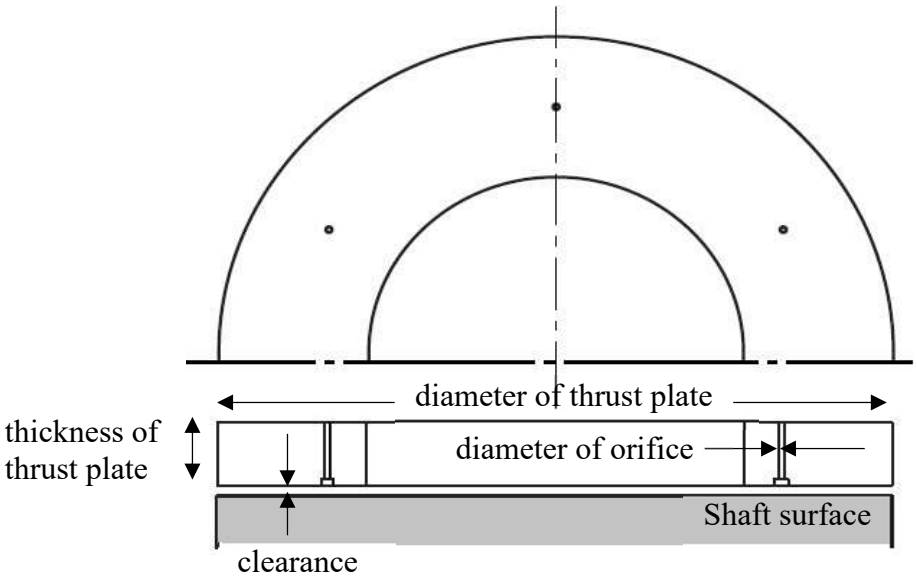

(b)

Figure 3.5 2D Sectional view of (a) journal bearing, and (b) thrust plate with shaft surface

3.3.2 Design of components

Figure 3.6 and Figure 3.7 shows the drawings of the aerostatic bearing components.

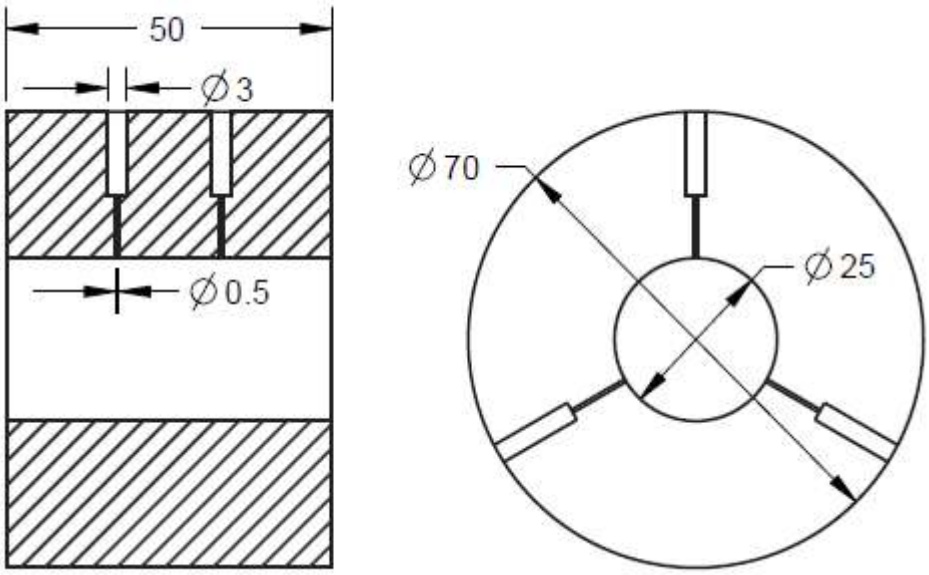

(a)

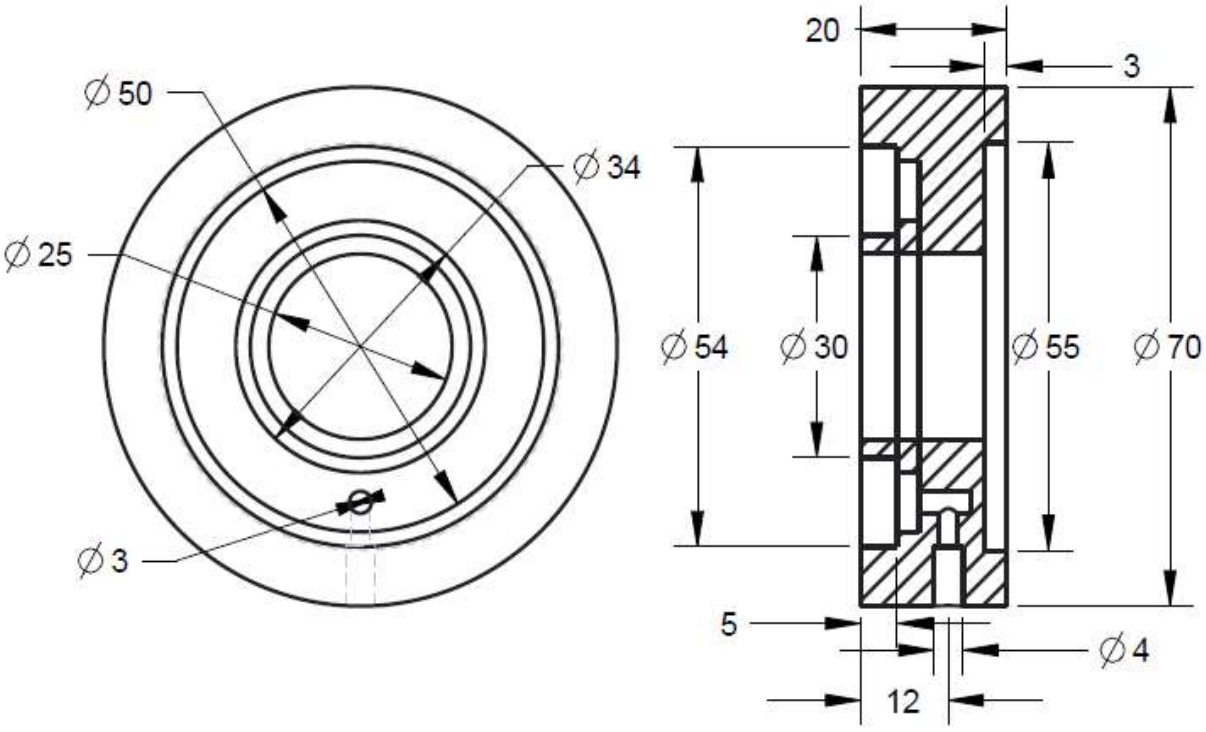

(b)

Figure 3.6 Components of aerostatic bearing (a) journal bush, and (b) thrust bush

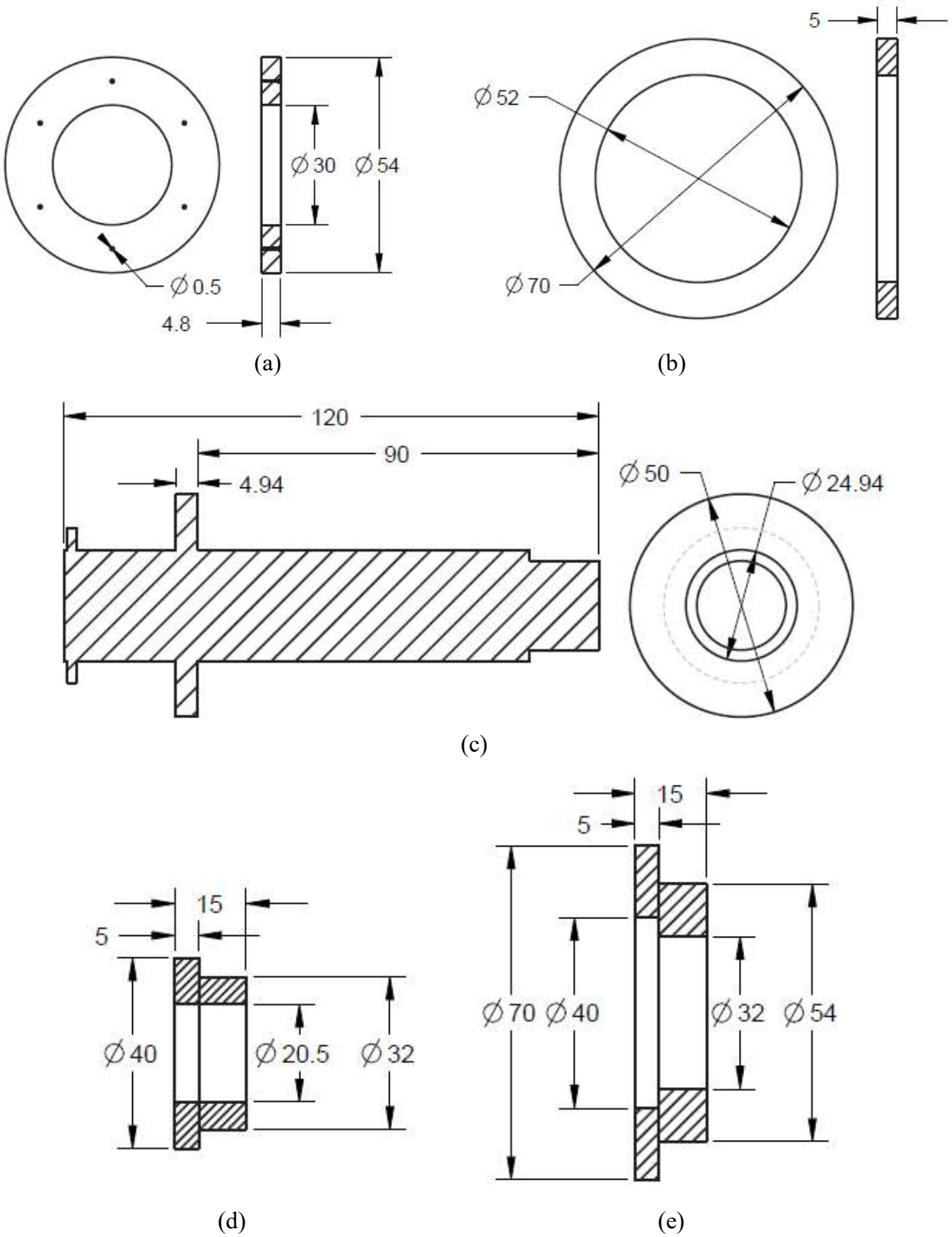

Figure 3.7 Components of bearing assembly (a) thrust plate, (b) bearing separator, (c) spindle, (d) bearing bush, and (e) bush cover

The manufacturing of these components should be precise in term of flatness, cylindricity, and roundness because if there is any presence of these errors then it arises problems during assembly due to mismatching of axis alignment of all the component. If axis alignment is precise then the clearance of both sides of journal and thrust bearing can be properly maintained.

3.4 NUMERICAL ANALYSIS OF MODIFIED AEROSTATIC BEARING

3.4.1 Fluid flow model

The Reynolds model for pressure distribution in thin film lubrication is the commonly used as fluid flow model that describes the flow of fluid in gas lubricated bearings based on its pressure and velocity profile. The equation that governs the thin-film lubrication is derived from Navier-stokes equations i.e. continuity equation, momentum equation and energy equation under the assumption of thin-film, Newtonian, laminar, isothermal and inertia-less flows. For a thrust bearing, Reynolds equation is defined in cartesian coordinates (x, y, and z), presented in Equation 3.6 and in case of a journal bearing, polar coordinates are used, presented in Equation 3.8. The modified Reynold's equation for pressure distribution is expressed in the general form of as Equation (3.6) [12, 13].

$$\frac{\partial}{\partial y}\left(\rho h^3 \frac{\partial p}{\partial y}\right) + \frac{\partial}{\partial z}\left(\rho h^3 \frac{\partial p}{\partial z}\right) = 6\mu U \frac{\partial(\rho h)}{\partial y} + 12\mu \frac{\partial(\rho h)}{\partial t} + 12\rho V_{inj} \tag{3.6}$$

where U is surface velocity, ρ is the ensity of a fluid, h is air film thickness, μ is the dynamic viscosity of a fluid, and V_{inj} is expressed in cylindrical coordinates which is known as the Hagen-Poiseuille formula and is simplified using Naiver-Stocks equation [12] as Equation (3.7).

$$V_{inj}(y, z, t) = -\frac{1}{4\mu}\frac{\partial p}{\partial x}\left[\frac{d_o^2}{4} - (y - y_i)^2 - (z - z_i)^2\right] \tag{3.7}$$

where d_o is the outside diameter of bearing

The Equation 3.6 is used for thrust bearing whereas, for journal bearing, the velocity of air is evaluated in radial and circumferential direction. So, the modified Reynold's equation can be expressed in term of radial polar coordinates as Equation (3.8) [12].

$$\frac{\partial}{\partial r}\left(prh^3 \frac{\partial p}{\partial y}\right) + \frac{1}{r}\frac{\partial}{\partial \theta}\left(ph^3 \frac{\partial p}{\partial \theta}\right) = 12\mu\left[v_r \frac{\partial(prh)}{\partial r} + v_\theta \frac{\partial(\rho h)}{\partial \theta}\right] + \frac{\partial(ph)}{\partial t} \tag{3.8}$$

where, r and θ are the radial and circumferential components, and v_r and v_θ are the velocity in radial and circumferential direction.

This formula implies for laminar flow of incompressible fluids through a cylindrical pipe where viscosity is defined as Equation (3.9).

$$\tau = \mu \frac{du}{dy} \tag{3.9}$$

where, τ = shear stress in the fluid, μ = dynamic viscosity of the fluid, du/dy is a derivative of velocity with respect to displacement in the perpendicular direction

For turbulent flow model, the viscosity (μ_T) is evaluated by using the standard k-epsilon model [31] as Equation (3.10).

$$\mu_T = \rho C_\mu \frac{k^2}{\epsilon} \tag{3.10}$$

where k is turbulence kinetic energy, ϵ is dissipation rate of turbulence kinetic energy, and C_μ is model constant.

This turbulent model is derived from the momentum equation and is expressed in form of transport equations. These factors k and ϵ are derived in form of transport equations [31] as given in Equations (3.11) and (3.12).

$$\frac{\partial k}{\partial t} + \frac{\partial (k u_i)}{\partial x_i} = \frac{\partial}{\partial x_i}\left(\frac{\mu_T}{\sigma_k}\frac{\partial k}{\partial x_i}\right) + \frac{\partial u_i}{\partial x_j}\left(\frac{\partial u_j}{\partial x_i} + \frac{\partial u_i}{\partial x_j}\right)\mu_T - \epsilon \tag{3.11}$$

$$\frac{\partial \epsilon}{\partial t} + \frac{\partial (\epsilon u_i)}{\partial x_i} = \frac{\partial}{\partial x_i}\left(\frac{\mu_T}{\sigma_\epsilon}\frac{\partial \epsilon}{\partial x_i}\right) + \frac{\partial u_i}{\partial x_j}\left(\frac{\partial u_j}{\partial x_i} + \frac{\partial u_i}{\partial x_j}\right)\mu_T \frac{\epsilon}{k} C_{1\epsilon} - \frac{\epsilon^2}{k} C_{2\epsilon} \tag{3.12}$$

where, u_i and u_j are velocity components, and C_μ, $C_{1\epsilon}$, $C_{2\epsilon}$, σ_k and σ_ϵ are model constant with values 0.09, 1.44, 1.92, 1.0 and 1.3 respectively. These values are derived from experiments and analytical optimization with assumption of fluid as air.

In the modified Reynolds equation (3.6), the effect of inertia is considered in fluid flow by introducing the factor known as the coefficient of discharge (C_d). This coefficient is evaluated from the comparison of mass flow rate predicted by simulation models such as computational fluid dynamics (CFD) and theoretical model of the modified Reynolds equation. The results evaluated in simulation performed by CFD are very close to the experimental results of the actual model.

3.4.2 Simulation of airflow using ANSYS Fluent

The air bearing model is simulated in ANSYS Fluent to evaluate the pressure distribution in a journal and thrust parts of aerostatic bearing along with the velocity and pressure profiles to

analyze the behavior of air within the clearance gap. The CFD model is developed to understand the behavior of pressure distribution due to fluid flow within the orifice and bearing clearance. The main assumptions for air in air bearing model are given as follows.

- Ideal gas
- No-slip boundary condition
- Thin-film flow
- Isothermal flow
- Newtonian flow
- Inertia-less flow

3.4.3 Model geometry

The hypothetical surfaces for bearing, shaft and air gap with actual dimensions are modeled in CREO Parametric. These surfaces are updated to the geometry section of ANSYS Fluent. The geometry is generated in design modular and then it is ready for next step. Figure 3.8 shows the geometry used in the simulation with various boundary conditions.

3.4.4 Meshing

Meshing is a robust and flexible grid generation program that consists of tetrahedral, prismatic, hexahedral or pyramidal cells to generate smaller domains or elements on which fluid equations are solved. The use of sizing functions influences the mesh distribution by various parameters such as growth rate, minimum and maximum face size, maximum tet size and relevance center. Based on these parameters the presence of obsolete and failed meshes can be reduced. In order to produce an unstructured mesh is by defining mesh boundary layers by inserting inflation function on meshing. It helps in capturing the boundary region accurately for turbulent flows near the wall faces. The boundary meshes can be modified by improving its quality of smoothening or by creating surface meshes of various primitive shapes. After applying all sizing functions, the nodes and elements generated by meshing should be checked. More the number of elements, the more accurately FLUENT helps in defining each domain for flow conditions. The elements on which the boundary conditions have to apply in later steps, they must be given some specific names so that they could be identified directly. Figure 3.9 shows the meshed objects by meshing tool in FLUENT.

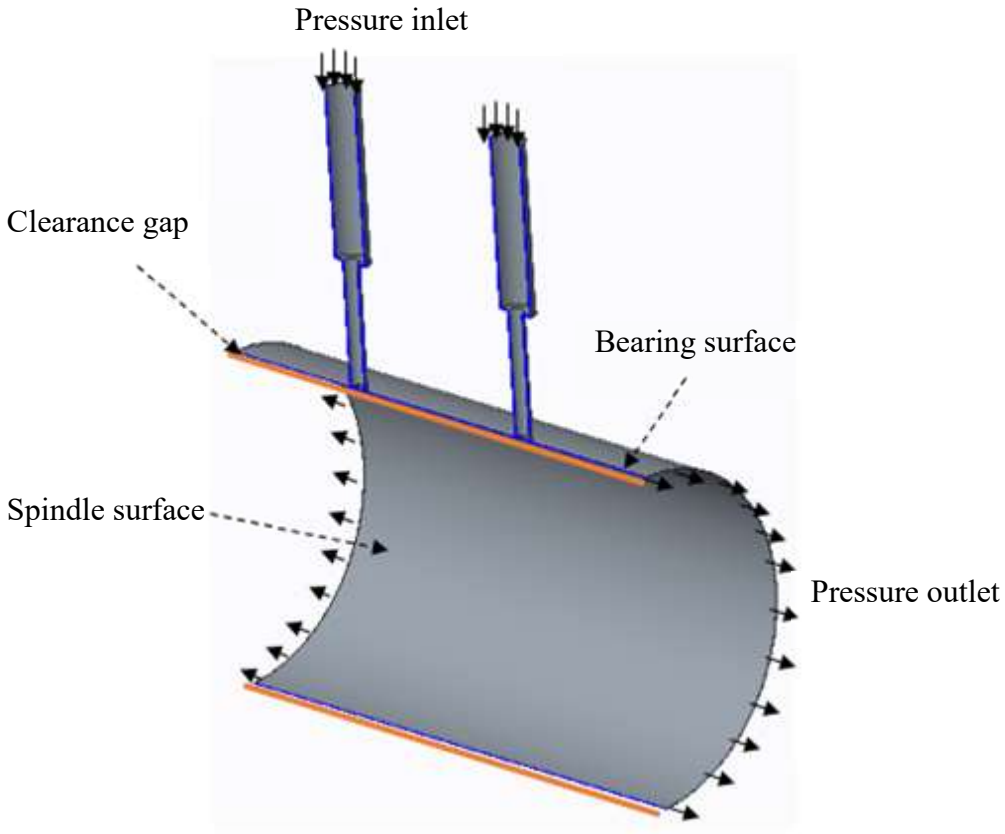

(a)

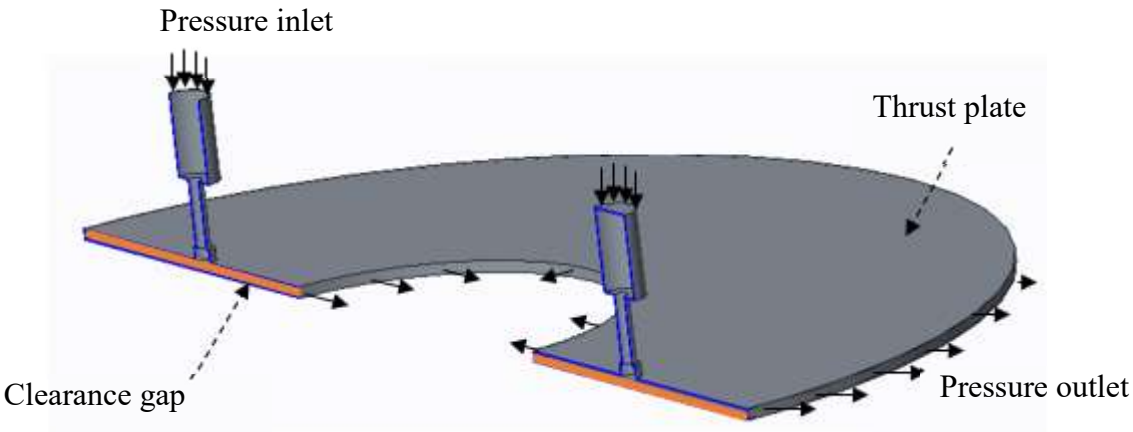

(b)

Figure 3.8 Bearing geometry used in the CFD model (a) journal bearing, and (b) thrust bearing

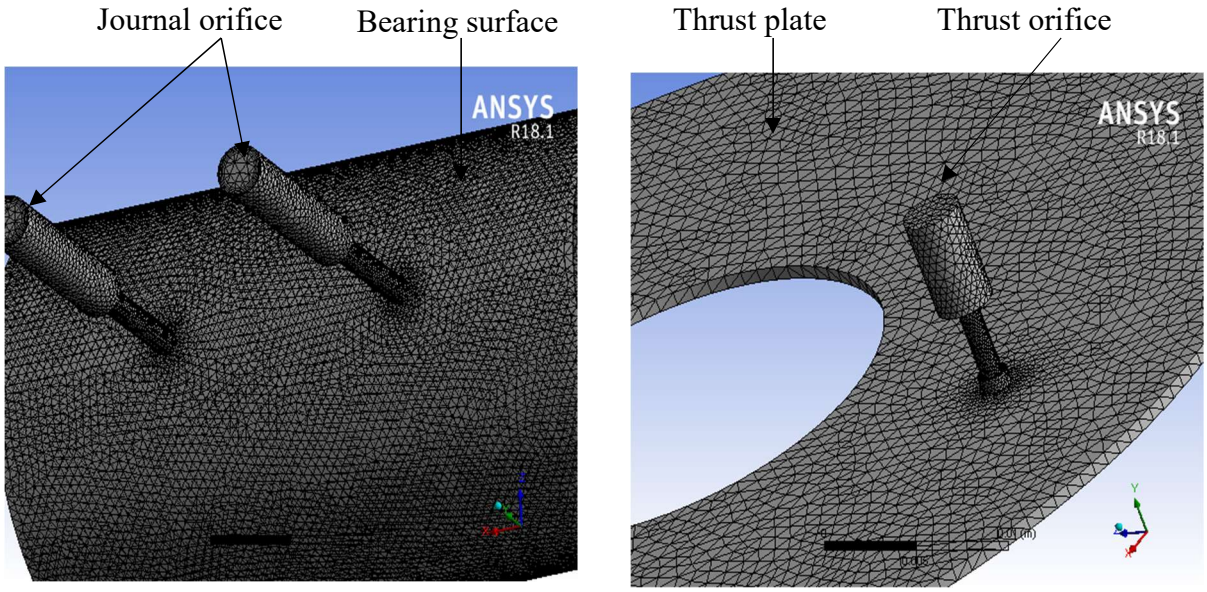

(a) (b)

Figure 3.9 Meshed surface of bearing model (a) journal bearing, and (b) thrust bearing

3.4.5 Setup and solution controls

The setup and solution are performed with series processing option with the double precision mode. The solver used for CFD model is pressure based with absolute velocity formulations in steady state characteristics. The parameters used for the model setup in CFD are as follows.

- Enable energy transfer equation.
- Enable the viscous model.
    - For turbulent flow, the standard k-epsilon model with standard wall function for near-wall treatment is used. Then define the model constants for transport equations as per model conditions.
- The air is selected as fluid and stainless steel is selected for solids in material selection.
- In cell zone condition, the air is selected as fluid.
- Boundary conditions are selected for operating conditions for the type of inlet and outlet as pressure inlet and pressure outlet respectively under normal atmospheric pressure i.e. 1.01 bar.
    - The initial and total gauge pressure values are selected based on the gauge pressure ratio and initial pressure value given to the bearing model.

- For turbulence model, k-epsilon specification method is used with the turbulent kinetic energy of $0.02 m^2/s^2$ and turbulent dissipation rate of $1 m^2/s^3$.
- Similarly, for pressure outlet, the specification method for turbulence is selected.
- The thermal characteristic of air is set at 300 K.

The solution for setup is performed with calculation tasks for specified geometrical and theoretical model. The set-up of solution parameters for CFD simulation of fluid flow is run by performing the following steps.

- Specify the solution methods for iterative calculations.
  - The scheme for velocity-pressure coupling is selected as coupled because this algorithm is efficient and flexible for single-phase analysis of steady-state flow.
  - The spatial discretization for momentum, energy and turbulence parameters are selected as QUICK because it has better accuracy than first order upwind in case of viscous models. The gradient is selected as Green-gauss node based because it is considered to be more accurate than cell-based. For pressure, the PRESTO! is considered as a discretization method as the model includes flow domains which have rotational flows and involves body forces due to pressure distribution.
- Specify the values of relaxation factors for variables and equation.
  - The default values for relaxation factors of variables is 0.75. But, the values of these factors up to 0.95 helps in accelerating the iteration of the turbulence flow and it helps in making the calculation more robust.
  - For the relaxation factors for the equation, the values are set up as default values for density, energy and turbulence parameters.
- Select the values of convergence criteria for equation under the residual monitors.
  - The value for convergence criteria for equations such as velocity, continuity, energy, k, and epsilon are selected as 1e-06.
- Initialize the solution by standard initialization method. The solution must be computed from the inlet with an absolute frame of reference.
- Run calculations for each value of total gauge pressure.

3.5 SIMULATION RESULTS

The results generated from the flow model helps to visualize the contour velocity and pressure profiles of air flow on a designated plane from initial point i.e. orifice to the edge of the bearing. Based on pressure and velocity profile, the pressure distribution plots for journal and thrust bearing can be generated. The streamline data of air flow can also be analyzed to understand the behavior of airflow within the bearing clearance. The results are calculated in the term of radial distance (r) which starts from the central axis of orifice towards the edge of bearing as shown in Figure 3.10. This radial distance helps in analyzing the pressure distribution at each point towards the edge of bearing.

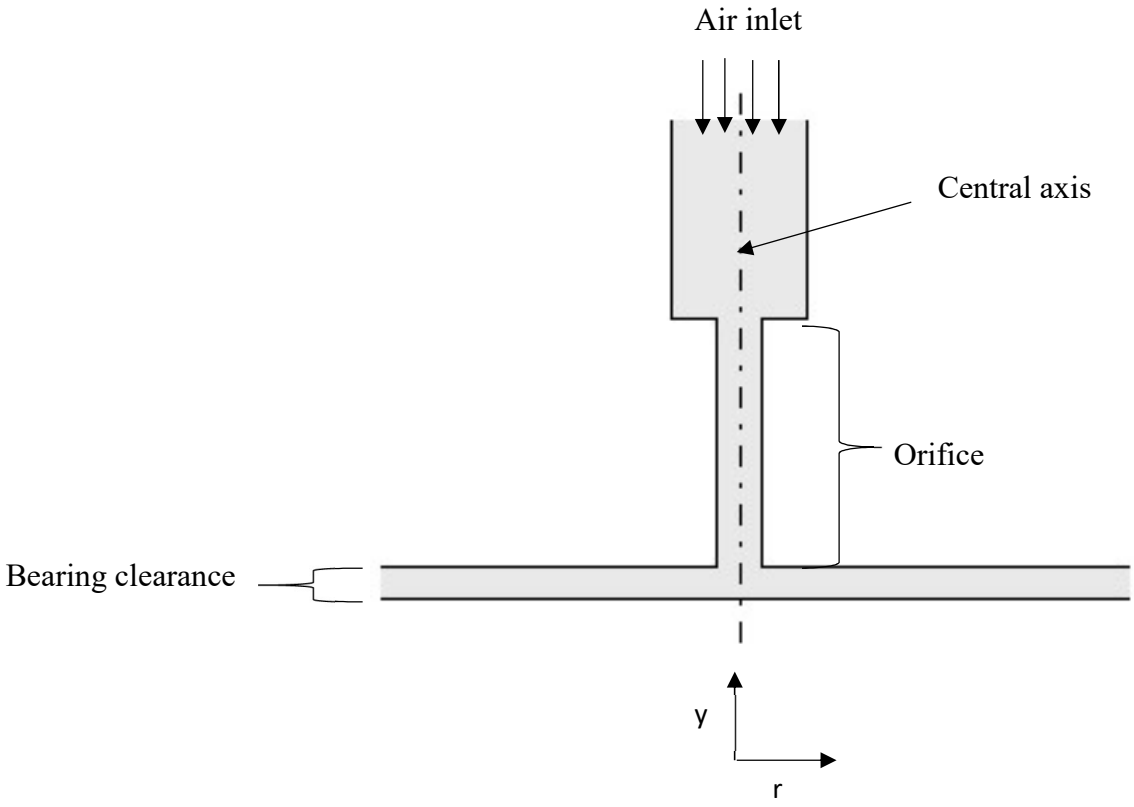

Figure 3.10 Bearing parameters used in the simulation

3.5.1 Velocity and pressure profiles for bearing model

The variation in velocity and pressure within the clearance for the journal and thrust bearing are given in Table 3.7 and Table 3.8 respectively. As air enters the bearing clearance through the orifice, the rapid change in flow direction and area of cross-section forms a small separation bubble at the wall of spindle surface. Due to this bubble formation, the area of the cross-section for the air flow decreases and velocity keeps increasing which cause the air to cross sound velocity barrier

up to r = 0.06mm which may form shock waves in the sonic region. After air passes through the axial distance of 0.06mm, the area of the cross-section of the flow region starts to increase, thereby velocity decreases to the sub-sonic region. The formation of the sonic region in a journal bearing at a supply pressure of 3bar and 4bar has flow velocity less than sound velocity. So, there is no shock wave formation in the flow region. The further increase in supply pressure produces the shock waves due to high compression of air which increases the pressure in the clearance region.

Table 3.7 Variation in velocity and pressure in the journal bearing

Orifice		Bearing clearance			
Supply pressure (bar)	Inlet velocity (m/s)	Velocity (m/s) at r = 0.06 mm	Velocity (m/s) at r = 0.5 mm	Pressure (bar) at r = 0.06 mm	Pressure (bar) at r = 0.5 mm
3	188	232	122	1.4	2
4		242	140	1.3	2.2
5		254	161	1.2	2.5
6		270	183	1.1	2.8

Table 3.8 Variation in velocity and pressure in the thrust bearing

Orifice		Bearing clearance			
Supply pressure (bar)	Inlet velocity (m/s)	Velocity (m/s) at r = 0.06 mm	Velocity (m/s) at r = 0.5 mm	Pressure (bar) at r = 0.06 mm	Pressure (bar) at r = 0.5 mm
3	188	244	115	1.35	1.6
4		274	124	1.3	2.1
5		299	136	1.25	2.6
6		328	155	1.2	3.1

The velocity and pressure profiles for journal bearing and thrust bearing are shown in Figure 3.11 and Figure 3.12 respectively. The velocity and pressure profile of journal bearing shows that the pressure decreases and velocity increase at the edge of orifice i.e. at the entry of orifice through air chamber up to clearance space due to a decrease in the area of cross-section. Due to the divergence in air flow in the clearance gap, the pressure is maximum and velocity is minimum at

r = 0. As air flows in the direction towards the edge of bearing, velocity keeps on decreasing while pressure is normally distributed within the clearance gap. The variation in velocity and pressure profiles in thrust bearing is similar to journal bearing in the orifice section. But due to flat clearance gap and recess shape in the thrust bearing, the pressure is maintained up to a larger value of radial distance (r) which also increases the load carrying capacity.

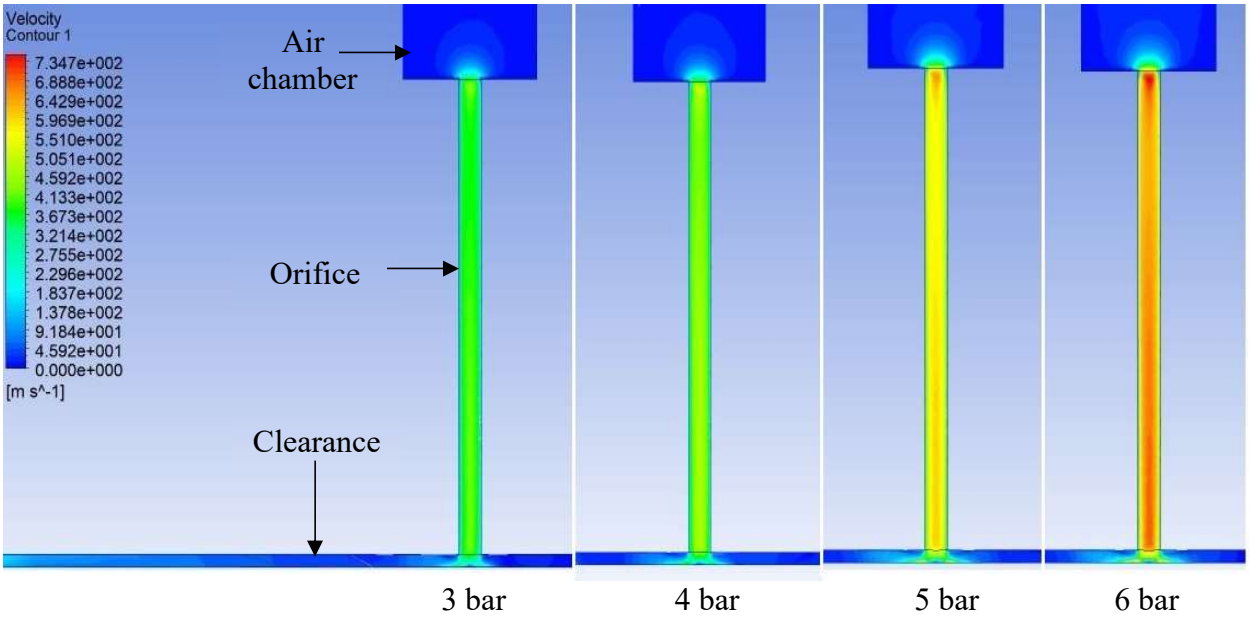

(a)

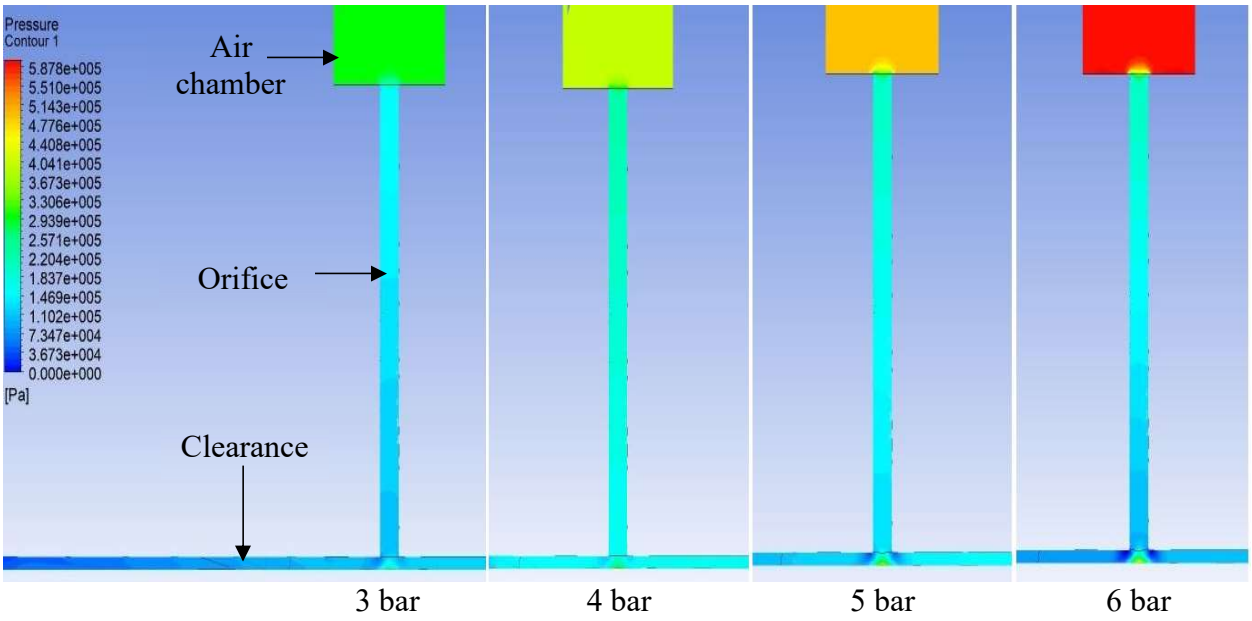

(b)

Figure 3.11 (a) Velocity profiles, and (b) pressure profiles for the journal bearing

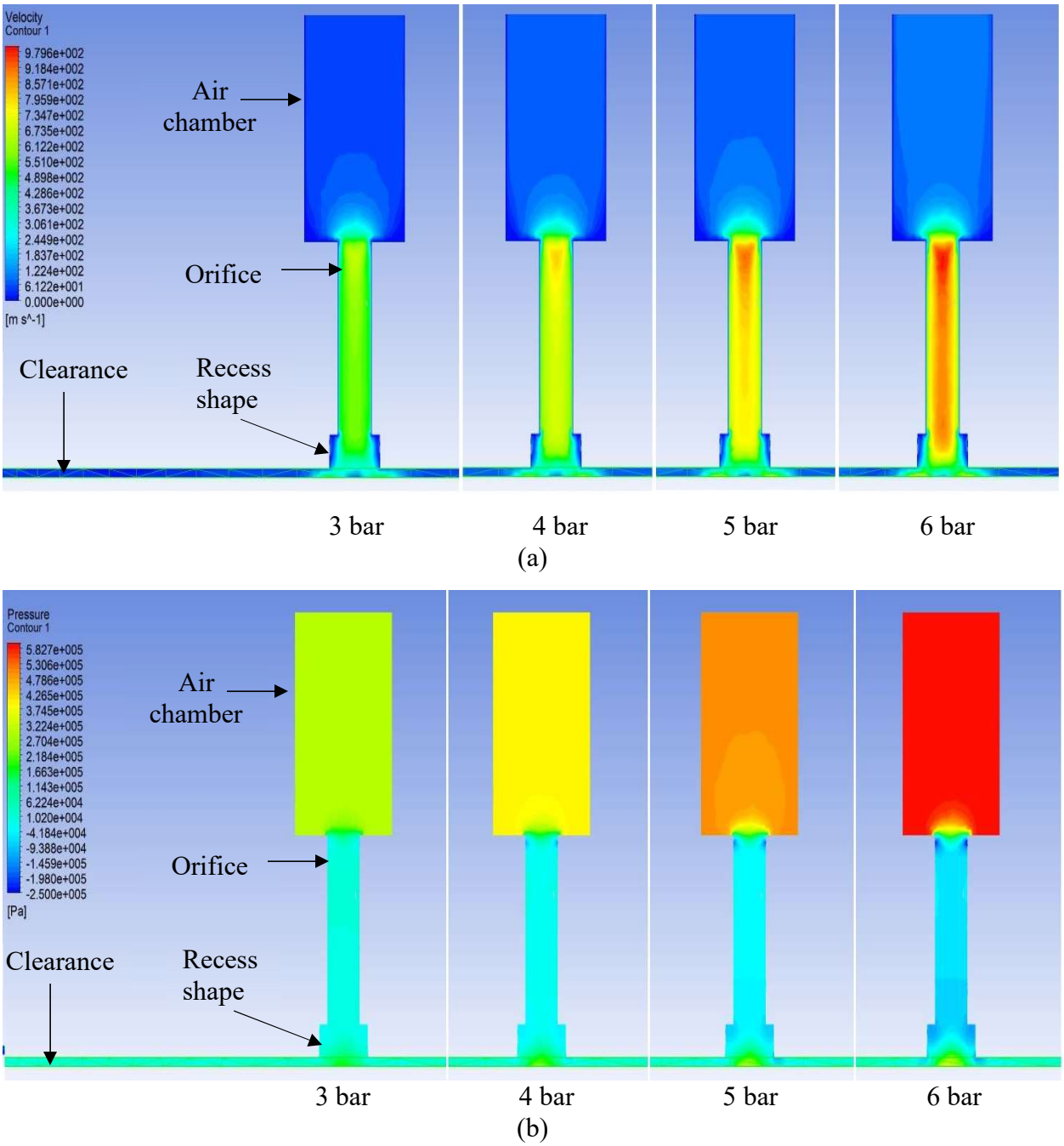

Figure 3.12 (a) Velocity profiles, and (b) pressure profiles for the thrust bearing

3.5.2 Pressure distribution profile for bearing model

3.5.2.1 *Journal bearing*

The pressure distribution in journal bearing is dependent on the compensation system. This mechanism holds the loads acting on the shaft by creating the pressure difference within the bearing system. Figure 3.13 shows the pressure distribution of air film in a journal bearing in axial

and circumferential direction with two double orifices at one-third station. The location of the orifice is shown by pressure peaks. The pressure between two orifices is almost the same as the average pressure value due to pressure drop by the divergent flow of air.

The pressure distribution profiles in Figure 3.13 show that the pressure within the bearing clearance decays towards the edge of the bearing as shown by axial profile. Along the axial direction, the presence of orifices creates the pressure spikes which shows the position of high-pressure ratios. In the circumferential direction, the value of pressure ratio at $\theta = \pi/3$ is higher than pressure ratio at $\theta = \pi$ and $\theta = 5\pi/3$ because the maximum airflow comes out through the one side of bearing clearance and remaining flow creates higher pressure on another side of the journal bearing. These values of high-pressure ratios have a direct impact on the load carrying capacity of the aerostatic bearing. The value of the critical pressure ratio depends on the inlet velocity and discharge coefficient of the orifice. In order to ensure the normal pressure distribution, the higher values of pressure ratio due to the location of orifices should be close to the average pressure ratio in the air gap region.

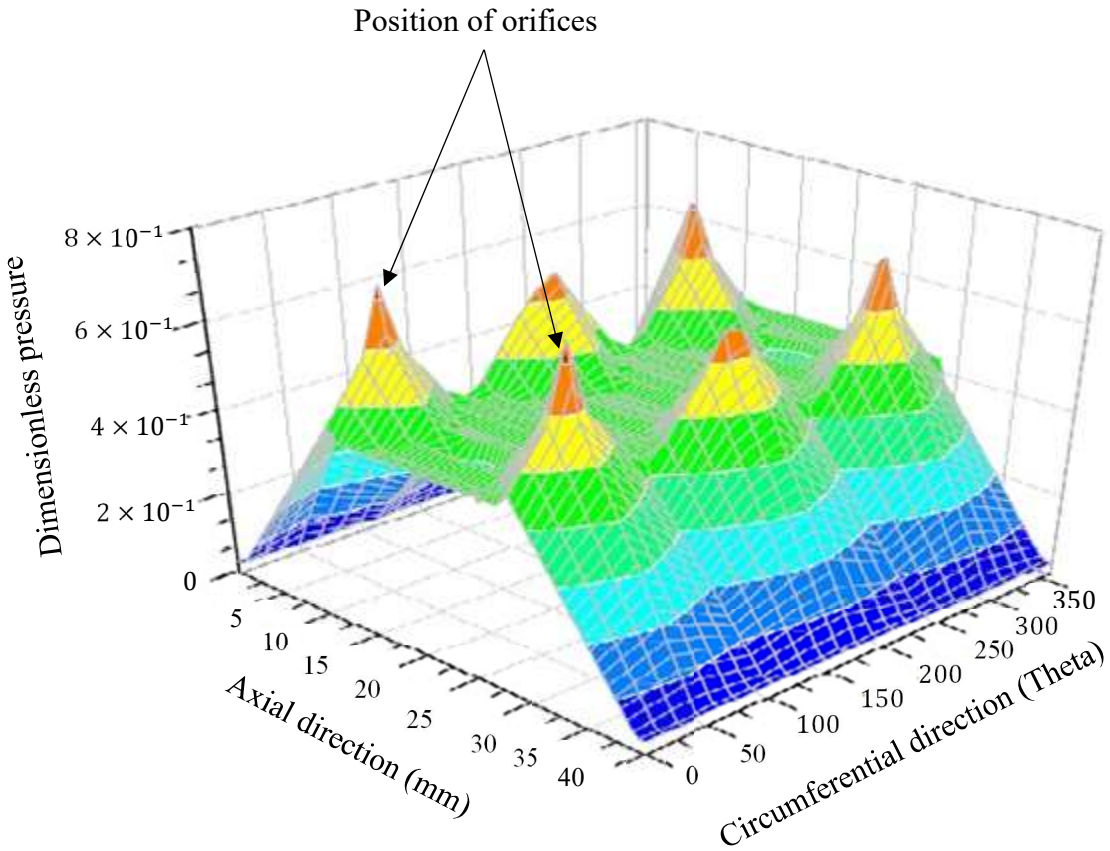

Figure 3.13 Pressure distribution of air film pressure in a journal bearing

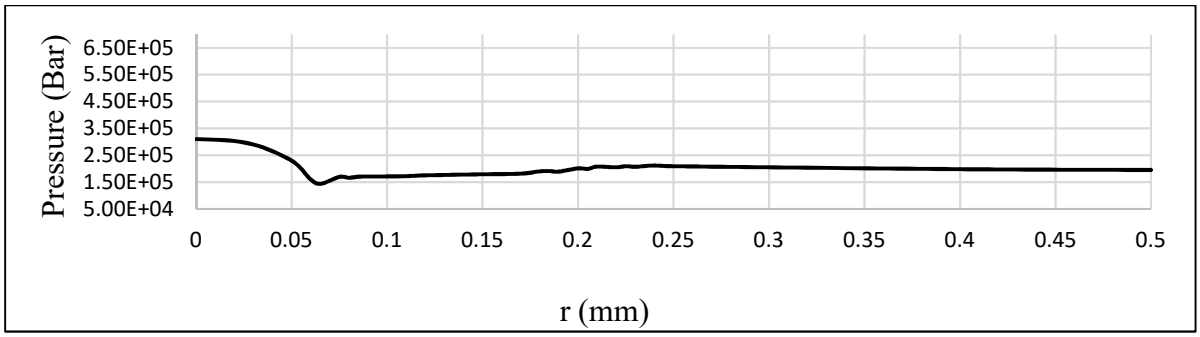

(a)

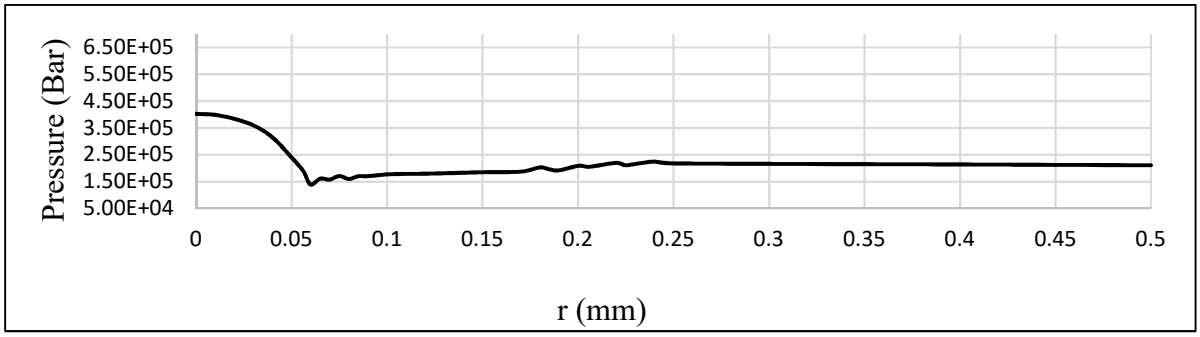

(b)

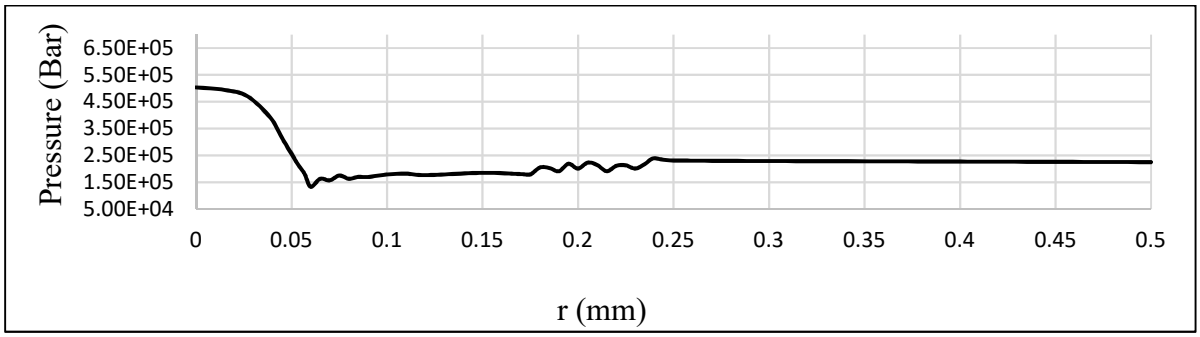

(c)

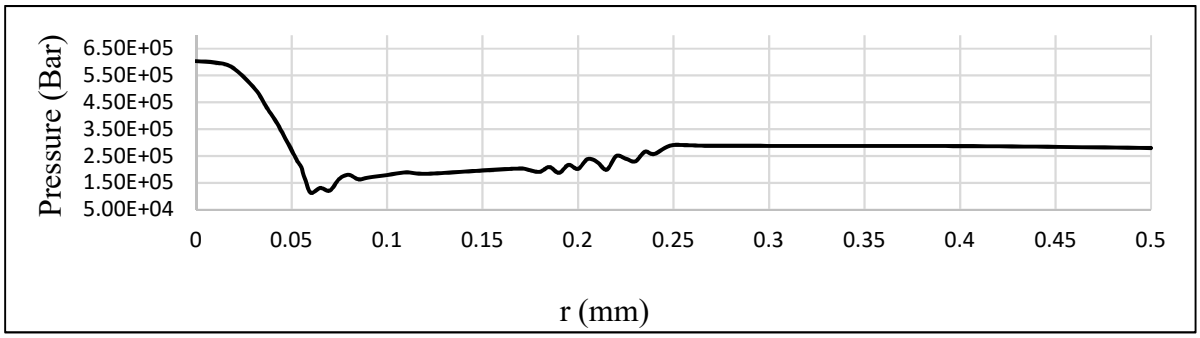

(d)

Figure 3.14 Pressure distribution curves in the thrust bearing at a supply pressure of (a) 3bar, (b) 4bar, (c) 5bar, and (d) 6bar

3.5.2.2 *Thrust bearing*

The pressure distribution in aerostatic thrust bearing is due to the small clearance gap which is selected as 30μm for this study. The pressure variations in thrust bearing are mainly due to the vortex flows at the edge of the orifice which decreases the pressure of air film. To minimize this effect, the geometric corrections in shape and size of the orifice should be analyzed. In this study, the recess shape at the outlet of the orifice is designed to minimize the effect of the vortex flow. So, the numerical study shows that the pressure distribution for thrust bearing is enhanced by using recess shape as outlet compensation. Figure 3.14 shows the pressure distribution curves at various supply pressure along the radial distance.

The results from numerical simulation show that the pressure decreases on flow through the orifice and also in bearing clearance up to a radial distance of 0.06mm due to changes in the cross-section of flow. After 0.06mm the velocity of the fluid decreases, thereby the pressure increases. Due to the continuous generation of compressive forces within the air, the pressure keeps on increasing until 0.25mm and starts to distribute normally along the axial direction. The abrupt changes in pressure before 0.25mm is due to the pressure forces generated by the compressive flow of air along the complete bearing surface. With the increase in pressure, these compressive forces increase which also increases the final pressure within the bearing gap.

3.6 COMPARISON OF THE PRESENT NUMERICAL STUDY

The present numerical study is compared with literature to validate the present design of the aerostatic journal and thrust bearing. The pressure distribution graphs and velocity profile of the current study are compared with the existing studies performed by the researchers as shown in Figure 3.15 and Figure 3.16 respectively.

The comparison between Figure 3.13 and Figure 3.15(a) shows the similar pressure curves are obtained in both the studies. But the behavior of pressure distribution for journal bearing in the present study is improved as the value of dimensionless pressure or gauge pressure ratio varies from 0.3 to 0.6 whereas in previous studies this value is larger than 0.6. These values are compared with the optimum value of the gauge pressure ratio given in Table 2.1 of Chapter 2 which shows the optimum range of gauge pressure ratio. These variations validate the present model of pressure distribution for journal bearing.

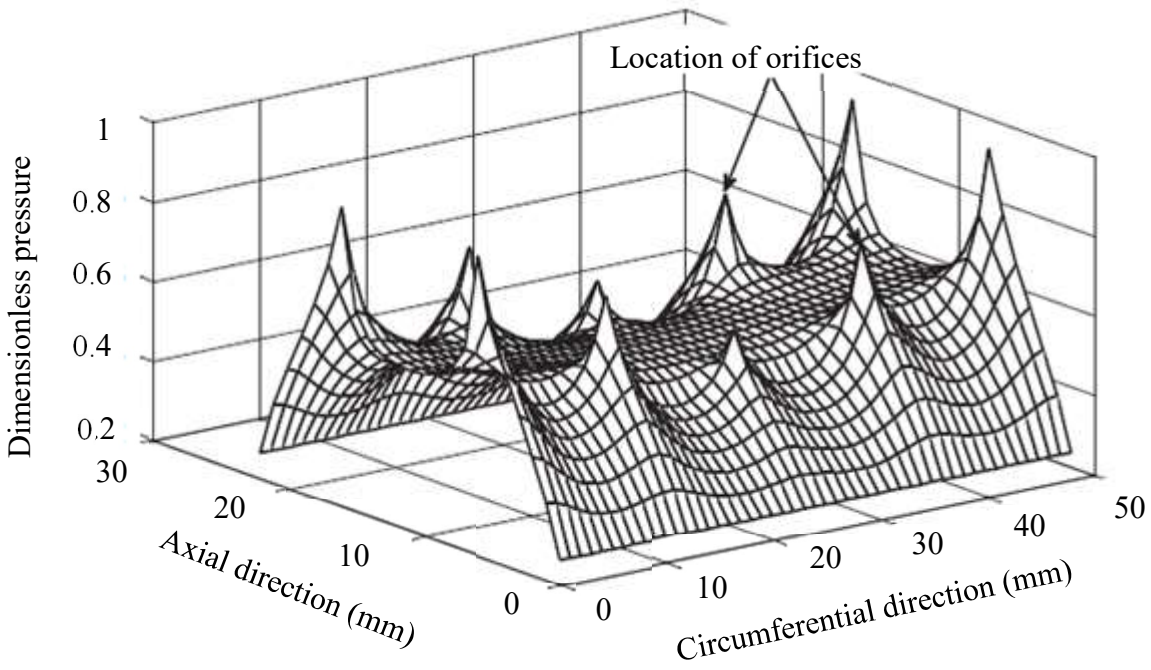

(a)

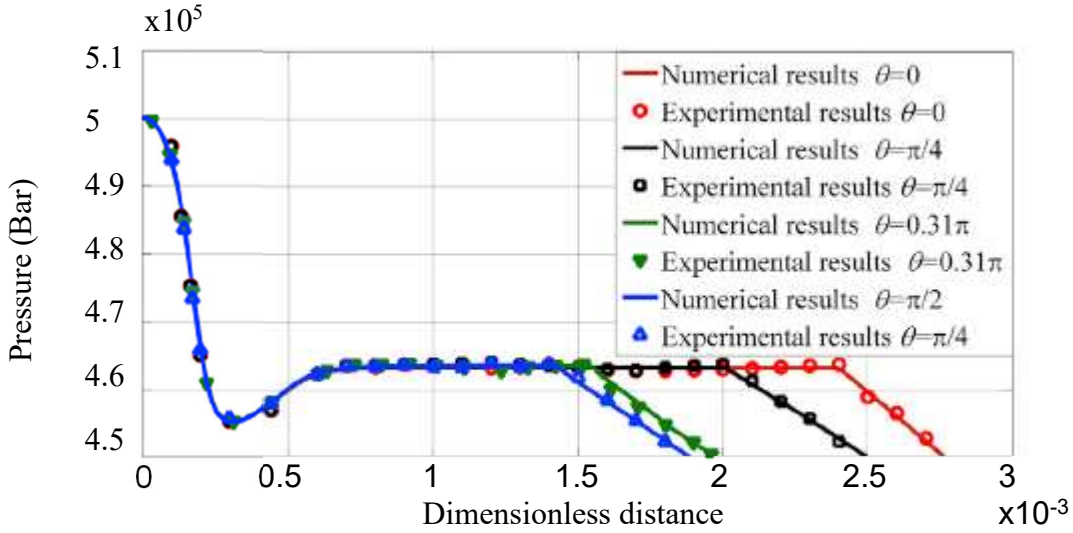

(b)

Figure 3.15 Pressure distribution profile of air film for (a) journal bearing [20], and (b) thrust bearing [34]

For thrust bearing, the comparison between Figure 3.14 and Figure 3.15(b) also shows the exact relationship but there is variation in pressure distribution in both the studies. The previous study shows the high-pressure region as compared to the current study within the clearance gap. It also

shows the abrupt decrement in pressure before the radial distance of 0.05mm which is improved in the present study by using a recess shape at the end of the orifice section. This allows the decrement in pressure after the radial distance of 0.05mm which means that the pressure is maintained up to larger radial distance towards the edge of the bearing.

The comparison between velocity profiles presented in Figure 3.12 and Figure 3.16 shows the similar velocity patterns in the orifice section for both journal and thrust bearing. But due to recess shape in the present study, velocity is minimized in the clearance gap by some extent which thereby increases the pressure up to a radial distance of 0.5mm. The formation of the sonic region in previous studies due to the convergence of flow of air by an abrupt change in flow direction is also minimized due to recess shape. The flow of air in the present study retrieves back to the recess region which minimizes the air velocity thereby creating a high-pressure region within the clearance gap. It means that the pressure distribution due to the velocity profile obtained in the present study enhances the pressure distribution in the modified aerostatic bearing.

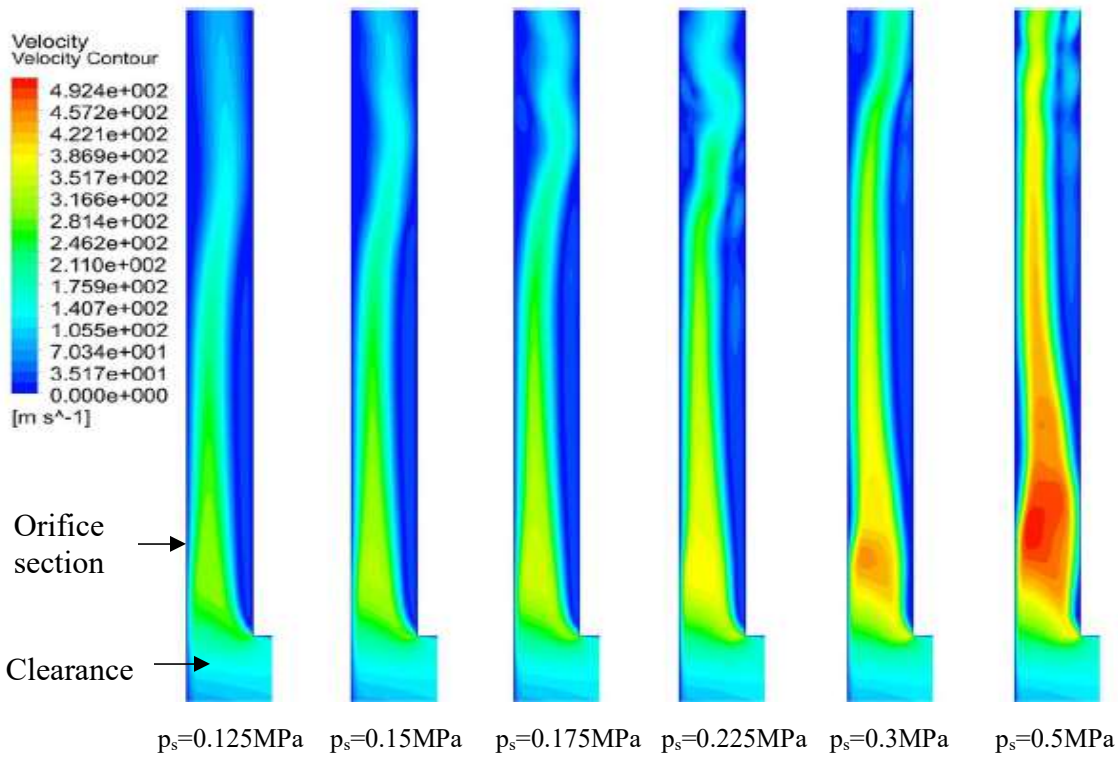

Figure 3.16 Airflow simulation in orifice-fed aerostatic bearing [36]

3.7 CONCLUSIONS

The comparison between the geometrical parameters of the present designed aerostatic bearing with previous studies showed the following points which validate the current design study.

- For journal bearing, the pressure ratios in both axial and circumferential directions are found almost similar variations in the orifice and air film gap. The current studies showed the improvement in pressure ratios i.e. from 0.4 to 0.6 which are closest to the required optimum value of pressure ratio i.e. from 0.35 to 0.6.
- For thrust bearing, the pressure distribution curve in the present study showed the improvement in pressure ratios generated in numerical simulation as compared to previous studies. The pressure curve evaluated in the present study showed that the pressure distribution was enhanced along the radial direction due to the recess region at the end of the orifice section.
- In the present study, the region of pressure distribution at each domain in clearance gap was extended up to 0.06mm which showed the improvement in pressure distribution which minimized the high-velocity and maximizes the low-pressure within the region. But, the numerical simulation given in previous studies showed the bubble formation at the wall of spindle surface due to high velocity and low-pressure regions when the radial distance is less than 0.05mm.

CHAPTER 4

EXPERIMENTAL ANALYSIS OF MODIFIED AEROSTATIC BEARING

4.1 EXPERIMENTATION METHODOLOGY

The procedure involved in experimental analysis are shown in Figure 4.1.

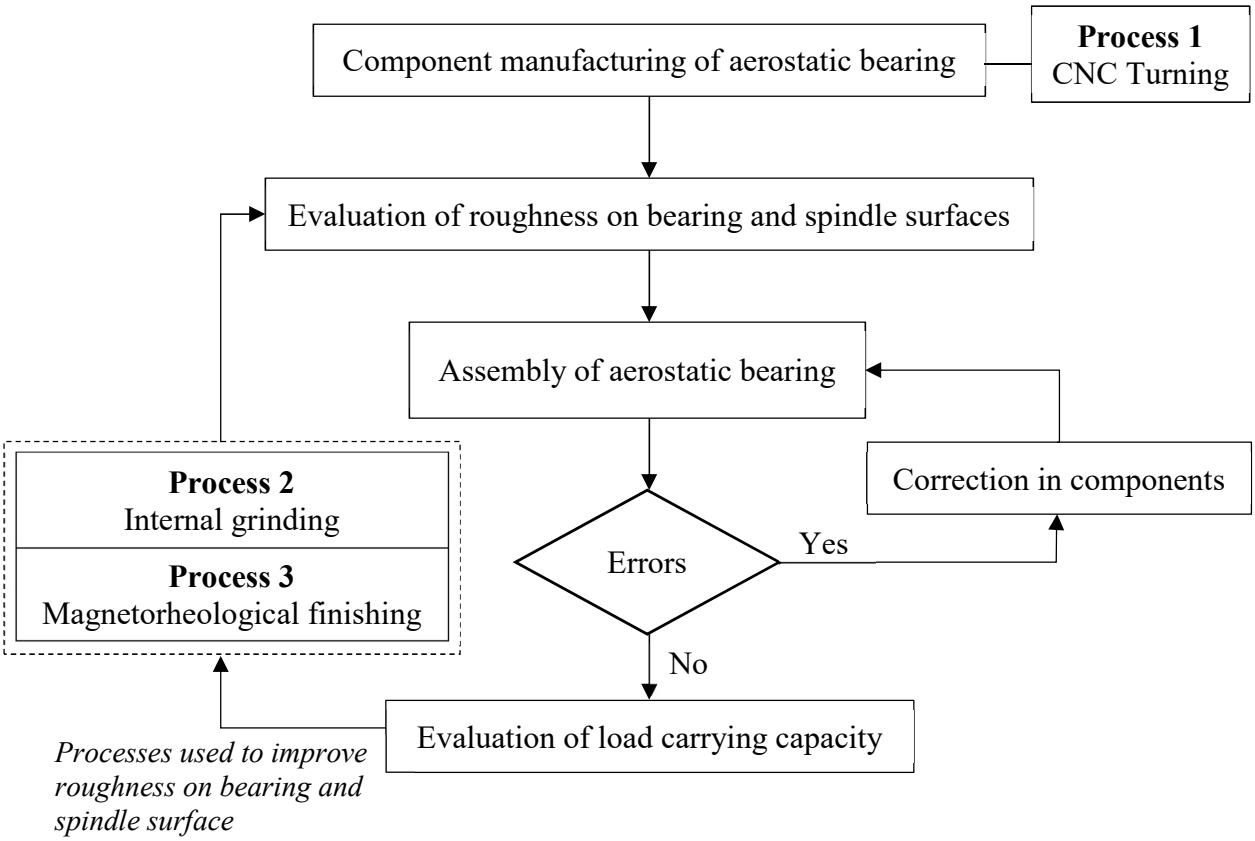

Figure 4.1 Flow chart of steps involved in the experimental analysis

Aerostatic bearings have a very precise axis of definition. So, the presence of manufacturing errors during the assembly causes the problem in axis alignment of all the components of the aerostatic bearing. Due to these errors, it is difficult to maintain a constant clearance gap in journal and thrust bearing. The common errors encountered due to manufacturing processes are as follows.

- Flatness
- Irregular roundness
- Concentricity
- Taper

Before proceeding to assembly, the presence of these errors must be checked on bearing and spindle surfaces. These errors are eliminated by improving the geometrical accuracy of components by surface finishing techniques.

4.2 COMPARISON STUDY OF SURFACE FINISHING TECHNIQUES

4.2.1 CNC Turning

The surface of the spindle and bearing shell is machined by CNC-Turno mill center. The material used for bearing shell is SS 316 and the spindle is of Al 2024. The machined components are shown in Fig 4.2. The initial machined surface gives the roughness values (Ra) of 1.1 µm and 0.54 µm for bearing and spindle respectively. The roughness profiles of these surfaces are shown in Figure 4.3(a) and Figure 4.3(b). Based on these values of surface roughness, the total load capacity of thrust and journal bearing is evaluated with respect to pressure and eccentricity. In order to improve current performance, the surfaces are finished with the cylindrical grinding process.

Figure 4.2 Machined components of the aerostatic bearing

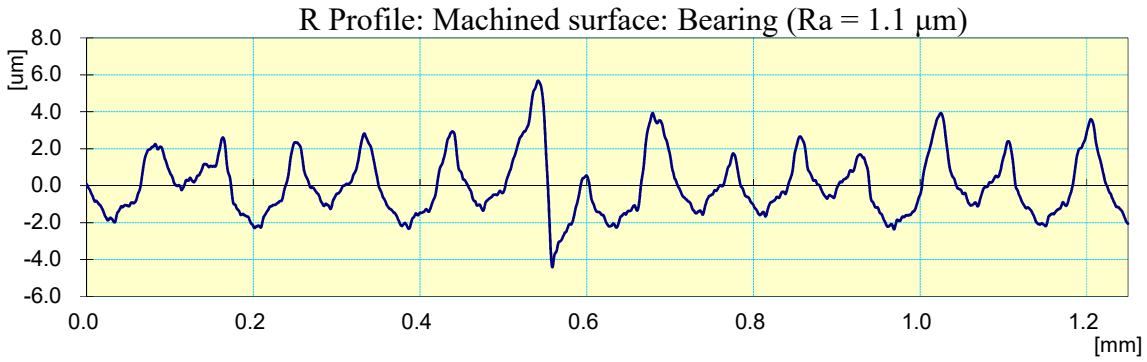

(a)

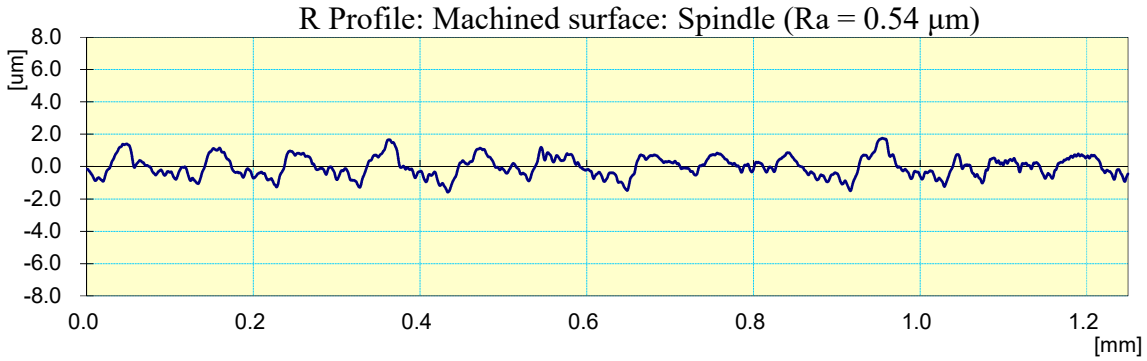

(b)

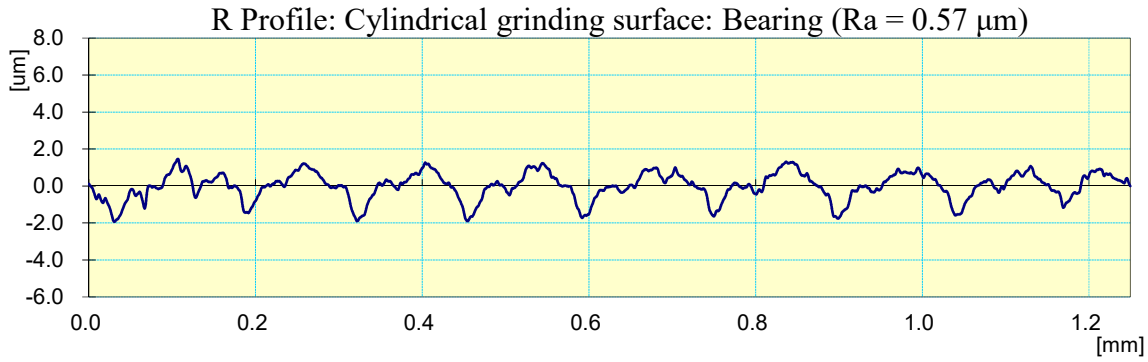

(c)

Figure 4.3 Roughness profiles of (a) bearing surface after machining, (b) spindle surface after machining, and (c) bearing surface after internal cylindrical grinding

4.2.2 Internal cylindrical grinding

The major parameters in cylindrical grinding that minimize surface roughness are hardness, depth of cut and speed. So, based on the hardness of SS 316 (bearing bush), the cutting conditions are workpiece speed is set at 120 rpm, grinding wheel speed is 10000 rpm, the longitudinal feed is 10 mm/s and infeed is set at 0.0125 mm/cycle. For removal of chips and to avoid local temperature

gradients due to grinding tool, the coolant is constantly supplied. The surface roughness achieved by these working parameters is 0.57 μm on bearing surface shown in Figure 4.3(b).

4.2.3 Magnetorheological fluid-based finishing (MRF)

The MRF process is used in this study to finish the non-ferromagnetic materials such as stainless steel and aluminum workpieces. The roughness of the surface of both the material is further improved by rotational and reciprocation motion of magnetic tool and rotational motion of the workpiece. The capability of the MRF process is to finish the surface of the workpiece up to nanometers level. In order to achieve this level, the magnetorheological honing tool is used that was developed in previous studies [37, 38]. The permanent magnet tool is used to finish the internal cylindrical surface of stainless steel while for the external surface of the aluminum spindle, the electromagnet tool is used. The MR polishing fluid sticks to the surface of the magnetic tool which remains in the gap between tool and workpiece. With the effect of the magnetic field, the abrasive particles align along with iron particles chain. Due to this mechanism, the removal of material in gap takes place and roughness peaks decrease to some extent. The composition of MR polishing fluid used for this process is given in Table 4.1.

Table 4.1 Composition of MR polishing fluid for finishing of stainless steel and aluminum

Process	**Components**	**Specification**	
MR polishing fluid for stainless steel	Iron particles	800 mesh (18μm)	20 vol. %
	Abrasives: Sic particles	700 mesh (20μm)	20 vol. %
	Carrier fluid	Paraffin oil: 80%	60 vol. %
		AP3 grease: 20%	
MR polishing fluid for aluminum	Iron particles	800 mesh (18μm)	20 vol. %
	Abrasives: Al_2O_3	1000 mesh (15μm)	20 vol. %
	Carrier fluid	Deionized water	57.7 vol. %
		Na_2CO_3	2 vol. %
		Glycerin	0.03 vol. %

The MRF process is carried out based on the finishing parameters which are selected as based on the available literature on improved results of MR finishing. For the bearing surface, the developed tool is rotating at a speed of 200 rpm with a reciprocation motion of 70cm/min within the clearance

gap of 0.6 mm between the magnetic tool and non-ferromagnetic workpiece. In case of spindle surface, the developed tool with flat tip is used for finishing the experiment. The rotational speed of tool used in finishing operation is 400 rpm with the feed rate of 25 mm/min. The workpiece is rotating at 100mm/min with the clearance gap of 0.6 mm maintained between the surface of the tool and workpiece. The current used for magnetization of the electromagnetic tool is 2A. The processing time for each finishing cycle for both bearing and spindle surfaces is selected as 30 min and roughness is evaluated after each finishing cycle. Also, the total finishing time for bearing and spindle surfaces is 90 min each.

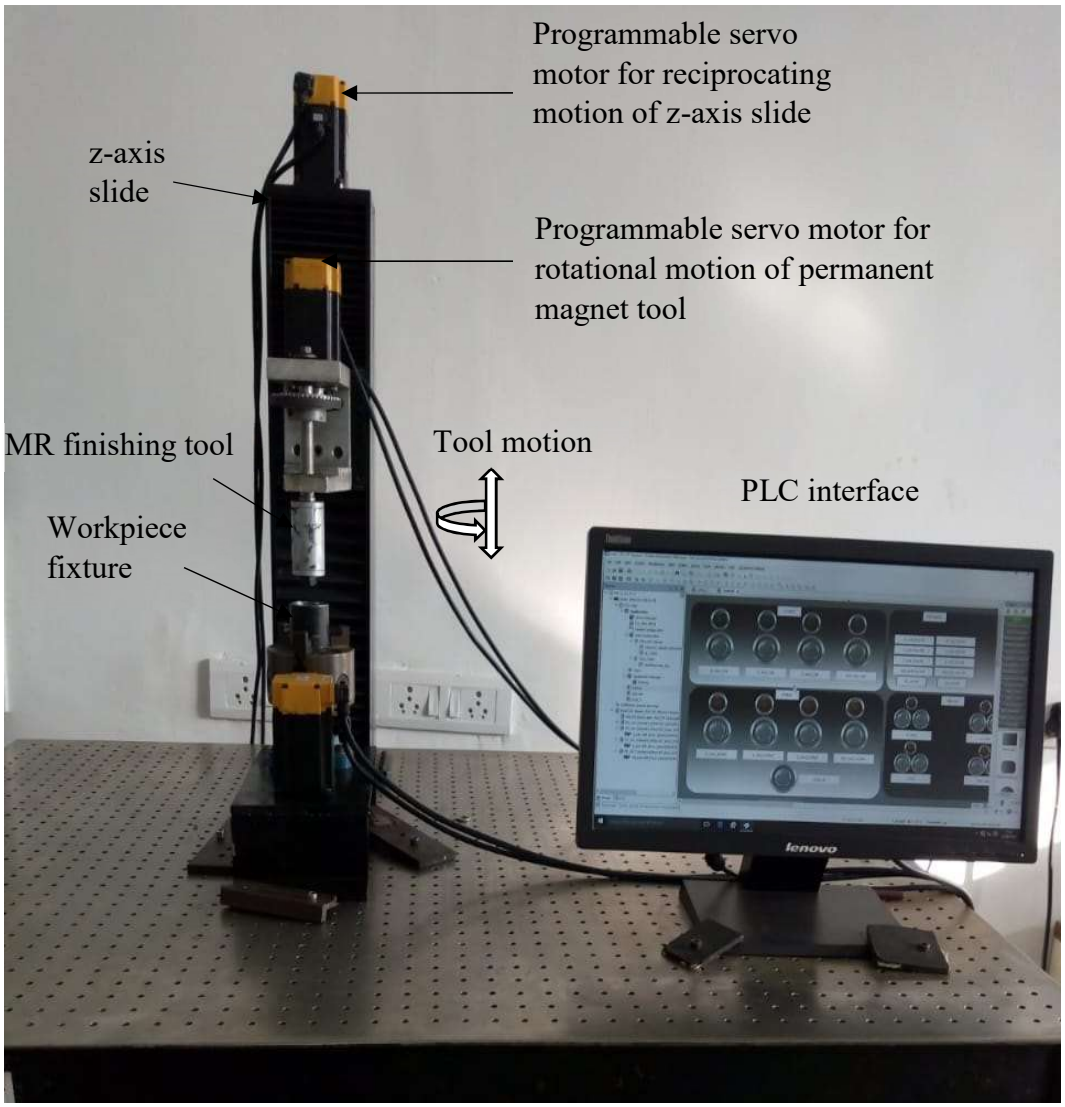

Figure 4.4 Experimental setup of magnetorheological fluid-based finishing for bearing surface

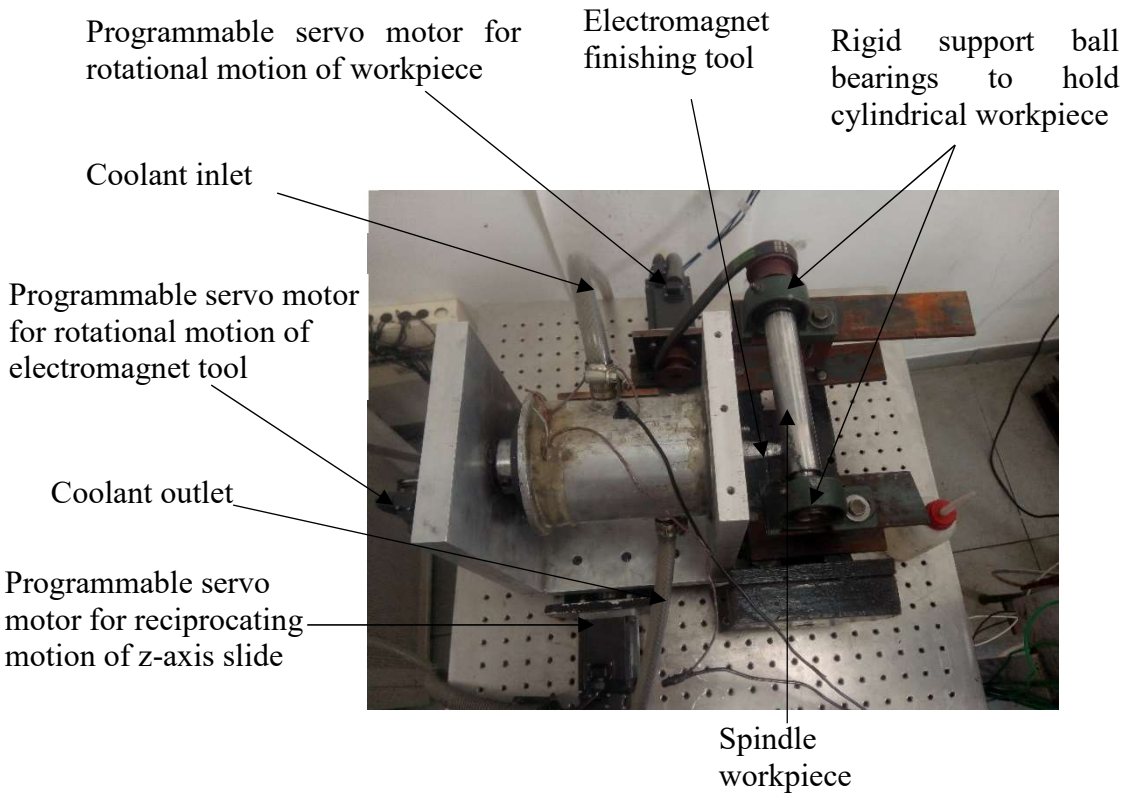

(b)

Figure 4.5 Experimental setup of magnetorheological fluid finishing for spindle surface

The experimental setup for MR finishing process for bearing and spindle surface are shown in Figure 4.4 and Figure 4.5. The MR fluid finishing removes the roughness peaks which are left after internal grinding of a cylindrical workpiece. The change in average roughness values for bearing and spindle surfaces after being processed for each MR finishing cycle of 30min is achieved as 59.64% (from 570 nm to 230 nm) and 55.55% (from 540 nm to 240 nm) respectively. This reduction shows that this process has the ability to perform surface finishing on the non-ferromagnetic cylindrical workpiece. In next 30 min of finishing the cycle, the reduction in roughness observed on both surfaces is 50.00% (from 230 nm to 85 nm) and 45.83% (from 240 nm to 130 nm). After each finishing cycle, the MR polishing fluid is changed and fresh fluid is applied over the surface of the magnetic tool. The percentage reduction in average roughness values is minimized after 60min as removal rate becomes slow. This is due to the higher surface area of roughness peaks at the flat base surface than at the top layer of the workpiece. So, the roughness peaks are left out on the surface of the workpiece. The minimum average roughness values achieved after 90min of finishing time on bearing and spindle surface is 0.045μm and 0.08 μm respectively. The roughness profiles and images of finished surfaces are shown in Figure 4.6.

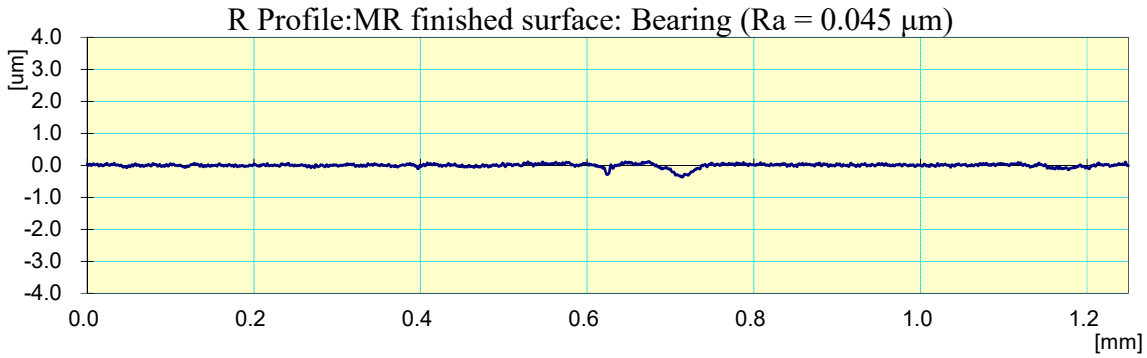

(a)

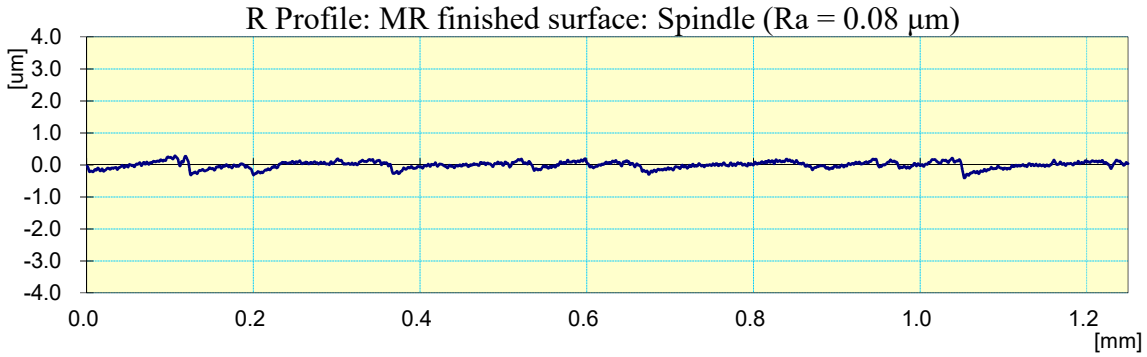

(b)

(c)

Figure 4.6 (a) Roughness profile of the bearing surface, (b) roughness profile of the spindle surface, and (c) bearing components after MR finishing

The comparison of surface finishing techniques for bearing and spindle surface is studied by evaluating the load carrying capacity experimentally at various supply pressures and axis

displacements. The values of maximum load carrying capacity for the journal and thrust bearings are determined for each surface finishing technique.

4.3 EXPERIMENTAL SETUP TO STUDY THE LOAD CARRYING CAPACITY ON AN AEROSTATIC BEARING

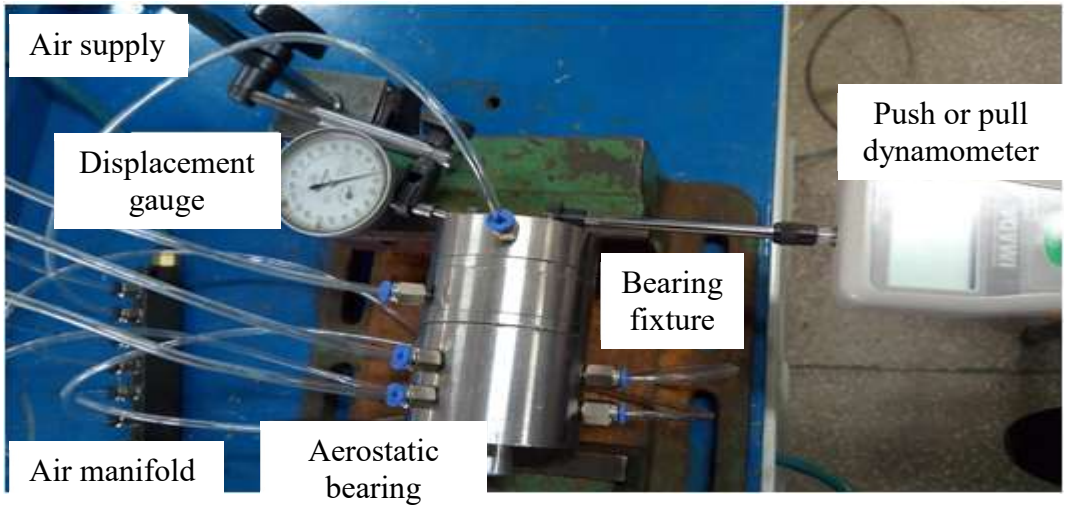

Figure 4.7 Experimental setup for evaluating load carrying capacity of an aerostatic bearing

The experimental setup includes the air supply components and the testing equipment such as displacement gauge and dynamometer. The radial and axial loads are applied by dynamometer and the corresponding value of the displacement in the spindle is calculated. In order to calculate the load carrying capacity, the positions for placing the dynamometer and displacement gauge are different for the journal and thrust bearing as shown in Figure 4.7. The components used in the air supply unit are as follows.

- Compressor
- Air filter
- Pressure reducing valve
- Pressure gauge
- Air manifold

Figure 4.8 shows the experimental setup along with measurement instruments and air supply circuit.

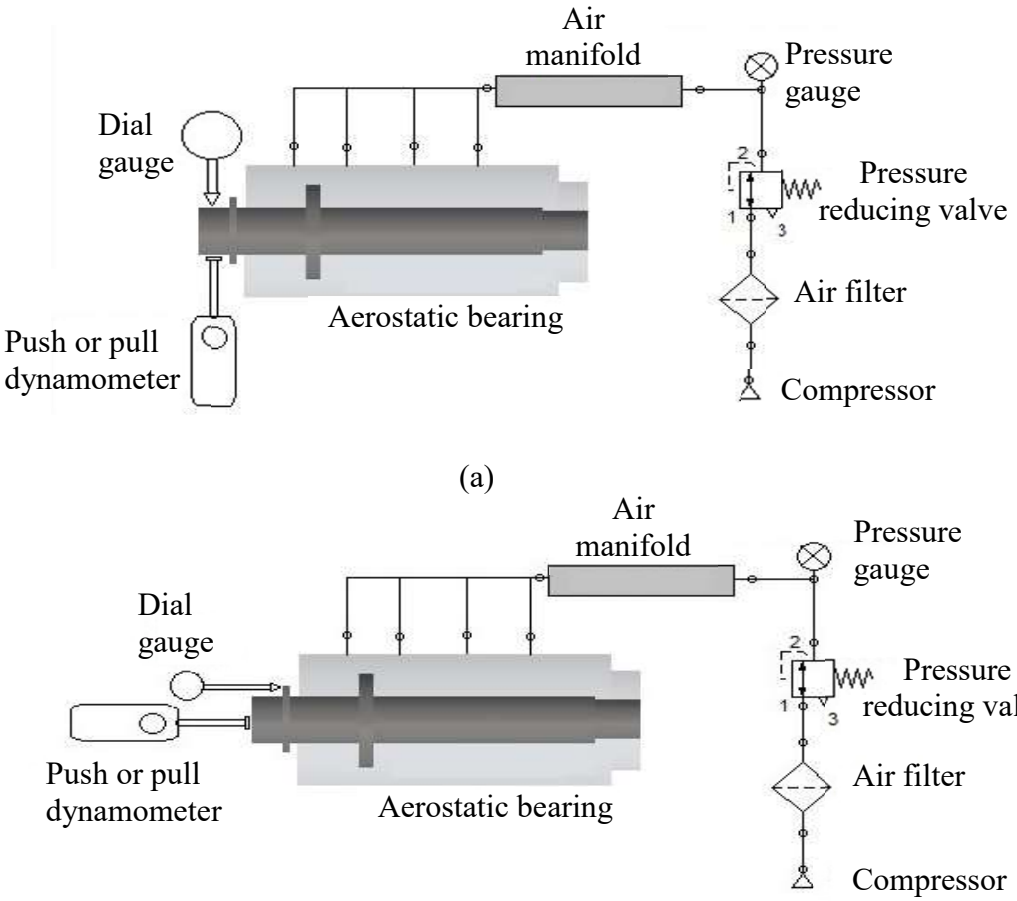

Figure 4.8 Experimental setup, measurement instruments and air supply circuit for (a) journal bearing, and (b) thrust bearing

4.4 RESULTS AND DISCUSSION

The effect of surface roughness on the load carrying capacity of the aerostatic journal and thrust bearing is analyzed by comparison of load carrying capacity at various finished surfaces. At first, the machined surfaces of bearing (R_a = 1.1µm) and spindle (R_a = 0.54µm) are assembled to evaluate the load carrying capacity at the various supply pressure. After the calculation of load data on the machined surface, the internal grinding surface of bearing (R_a = 0.57µm) is assembled to calculate the same results as calculated for the machined surface. Finally, the last finished surface which is processed by MR fluid-based finishing technique (R_a = 0.045µm for bearing surface and R_a = 0.09µm for spindle surface) is used in the calculation of same data as calculated

before. These results are compared to validate the effect of surface roughness on the load carrying capacity of the aerostatic bearing. The average increase in load carrying capacity (ΔL_{avg}) due to the effect of surface roughness for a specific amount of spindle displacement is calculated using Equation 4.1.

$$\Delta L_{\text{avg}} = \frac{\sum_{i=3ba \quad to\ 6\ bar}\left[(L_{improved})_i - (L_{initial})_i\right]}{Number\ of variations\ in\ pressure} \tag{4.1}$$

where $L_{improved}$ is the final value of average surface roughness achieved by MR fluid finishing process and $L_{initial}$ is the average surface roughness value of machined surface. The variation in the pressure is from 3bar to 6bar (i.e. 4 variations). This solution from Equation (4.1) is first evaluated for the comparison of grinding surface with the initial machined surface based on the average increase in load capacity for grinding surface. Then the solution from Equation (4.1) is analyzed for MR fluid finished surface to show the change in load capacity on further improvement in average roughness value. These comparisons provide the total effect of surface roughness on both journal and thrust bearings.

4.4.1 Effect of surface roughness on journal bearing

The test is performed for journal bearing at initial supply pressure of 3bar with the bearing clearance of 30µm. The supply pressure is maintained until the maximum radial load achieved at 1µm to 5µm displacement of the spindle is being evaluated. Similarly, the load capacity at each value of displacement is evaluated at a supply pressure of 4bar, 5bar, and 6bar. This data on load carrying capacity generates the load-displacement relation at various supply pressure as shown in Figure 4.9 and Figure 4.10. The experimental data is evaluated for three surfaces namely machined surface, internal grinding surface and MR fluid finished surface. The first comparison is made between machined and internal grinding surface using the Equation (4.1). The load-deflection data at various pressures show the variation in the value of radial load on machined and internal grinding surface at a radial deflection of 5µm for a supply pressure of 3bar varies from 0.15N to 0.3N. The increase in supply pressure from 3bar to 4bar, the variation becomes 0.75N to 0.86N. Similarly, when pressure is increased to 5bar and 6bar, the variation in load capacity is evaluated as 1.25N to 1.45N and 2.1N to 2.2N respectively. Hence, the approximate value of the average increase in load carrying capacity for 5µm is found to be 0.14N. This value shows the effect of surface roughness on maximum load carrying capacity at 5µm displacement in spindle achieved

by internal cylindrical grinding. Similarly, the average increase in load carrying capacity for spindle displacement of 1µm to 4µm is calculated as 0.075N, 0.096N, 0.11N and 0.12N respectively. These variations show the effect of surface roughness on load carrying capacity when the surface roughness is improved by internal grinding technique. Further, the comparison between the machined surface and MR fluid finished surface is made to evaluate total variation in load carrying capacity. Based on Equation (4.1), the values of ΔL_{avg} at various spindle displacement from 1µm to 5µm are found to be 0.163N, 0.198N, 0.218N, 0.233N and 0.268N respectively.

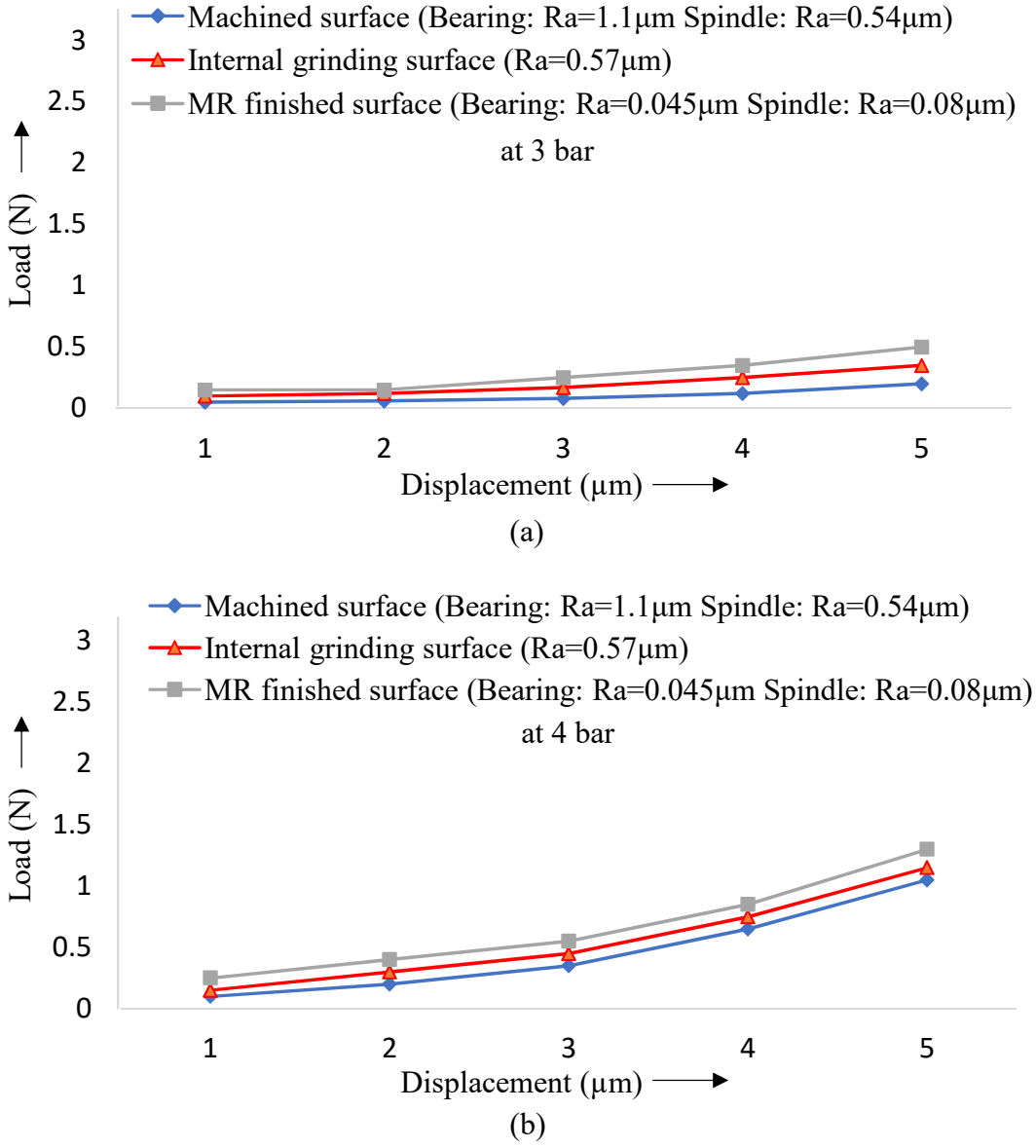

Figure 4.9 Load-displacement analysis of journal bearing at various surfaces with a supply pressure of (a) 3bar, and (b) 4bar

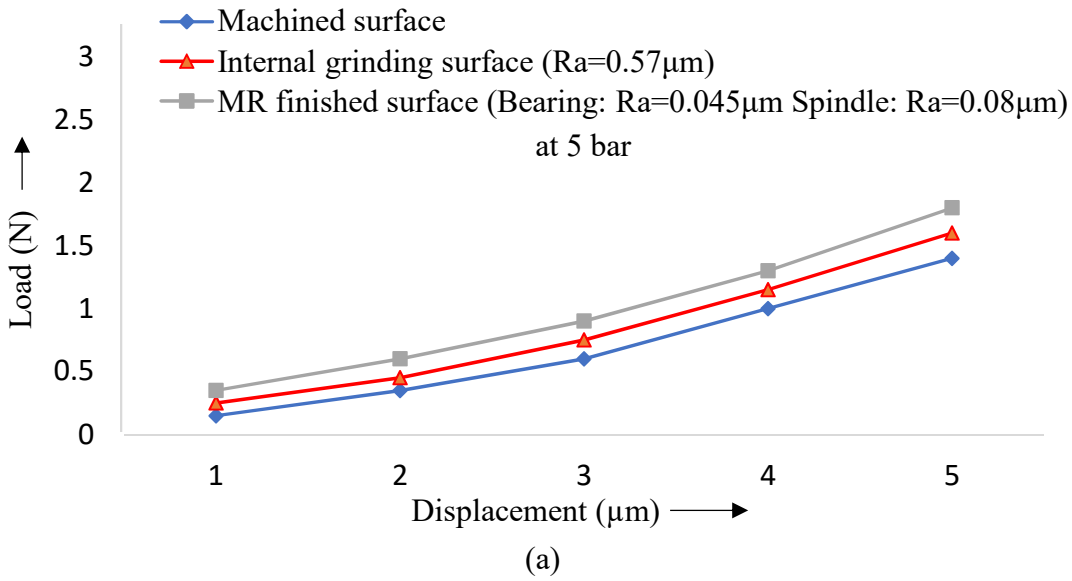

(a)

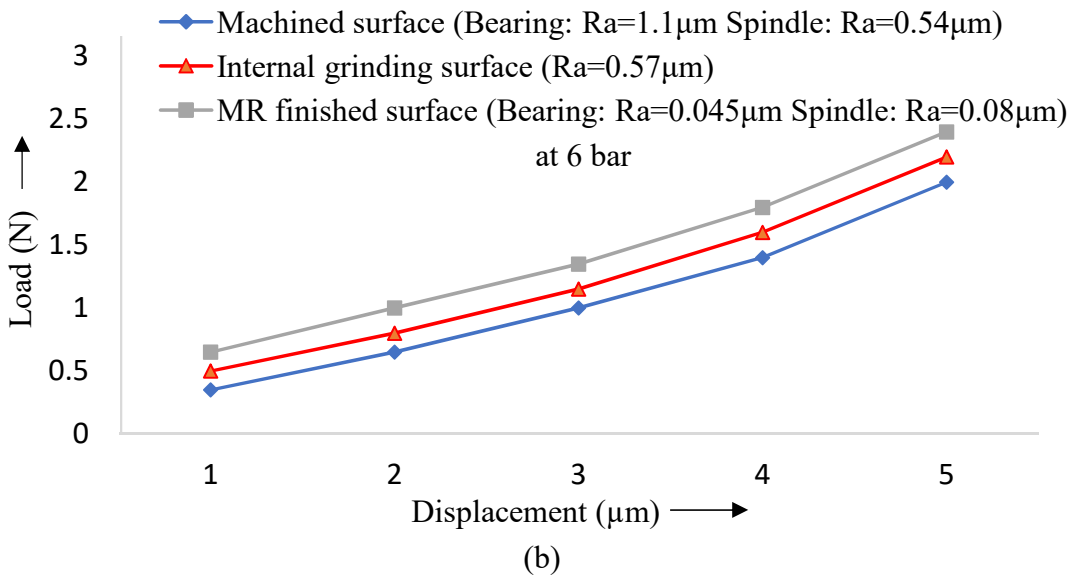

(b)

Figure 4.10 Load-displacement analysis of journal bearing at various surfaces with a supply pressure of (a) 5bar, and (b) 6bar

The comparisons for average increment in load carrying capacity due to improvement in the surface finish are shown in Figure 4.11. These values showed the effect of surface finish on the load carrying capacity of the aerostatic journal bearing.

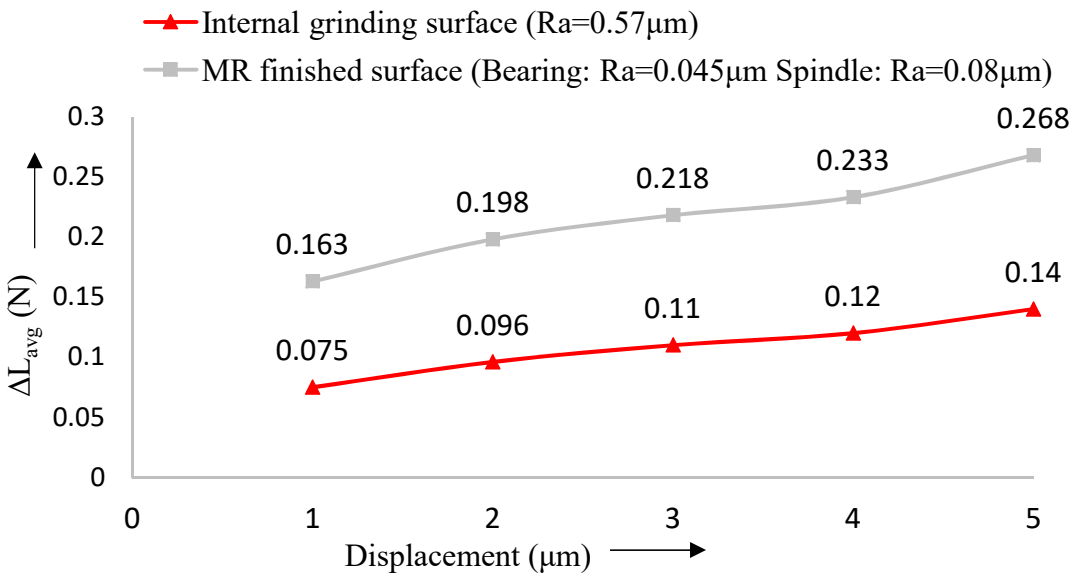

Figure 4.11 Average change in load carrying capacity of the journal bearing at internal grinding and MR finished surfaces

4.4.2 Effect of surface roughness on the thrust bearing

The testing setup for thrust bearing is the same as a journal bearing as shown in Figure 4.8(b). The initial supply pressure is 3bar which is maintained until the maximum axial load acting on the spindle at the displacement of 1µm to 5µm is being evaluated. These values of axial load are evaluated after improving surface characteristics of bearing and spindle at various supply pressure which varies from 3bar to 6bar. Based on experimental results for the initial machined surface to MR fluid finished surface, the relation between load acting on thrust bearing and displacement in the spindle is evaluated with variation in pressure is up to 6bar as shown in Figure 4.12 and Figure 4.13. The effect of surface roughness on thrust bearing is determined by the change in average load capacity (ΔL_{avg}) given in Equation (4.1) at the displacement of 1µm to 5µm. The variation in load capacity by improving surface finish by internal grinding and MR fluid finishing are compared to evaluate the average increase in load for each surface improvement technique. Firstly, the effect of internal grinding surface is evaluated by comparing axial load values with a machined surface. Based on Equation (4.1), ΔL_{avg} at the spindle displacement of 1µm is calculated as 0.825N. Similarly, for 2µm, 3µm, 4µm and 5µm of spindle displacement, the value of ΔL_{avg} is found to be 0.8N, 0.875N, 0.9N and 1.04N respectively. These values represent the average increase in axial load at different values of spindle displacement due to improvement in the average

surface finish on the internal grinding surface. Similarly, the average load variation is evaluated by the comparison of the axial load at the machined surface and MR fluid finished surface. Further improvement in the surface finish by MR polishing fluid finishing show the variation in axial load up to 2N. The values of ΔL_{avg} determined at various spindle displacement which varies from 1µm to 5µm are found to be 1.575N, 1.65N, 1.7N, 1.825N, 2.0N respectively. The average increase in axial load for both the surface finishing techniques are shown in Figure 4.14. Hence, the experimental investigation of surface roughness effect on load carrying capacity show that the improvement in surface finish increases the load carrying capacity by ΔL_{avg}.

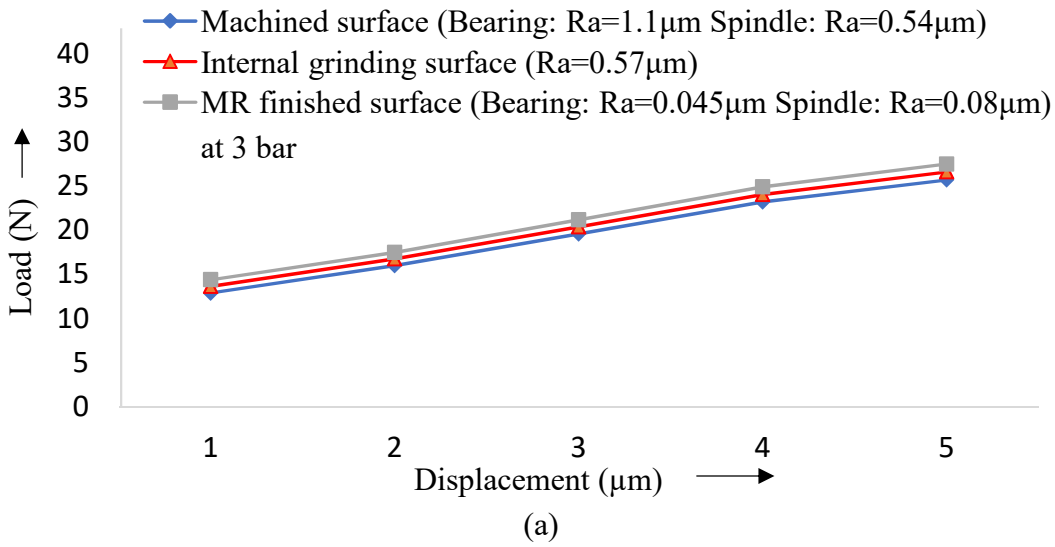

(a)

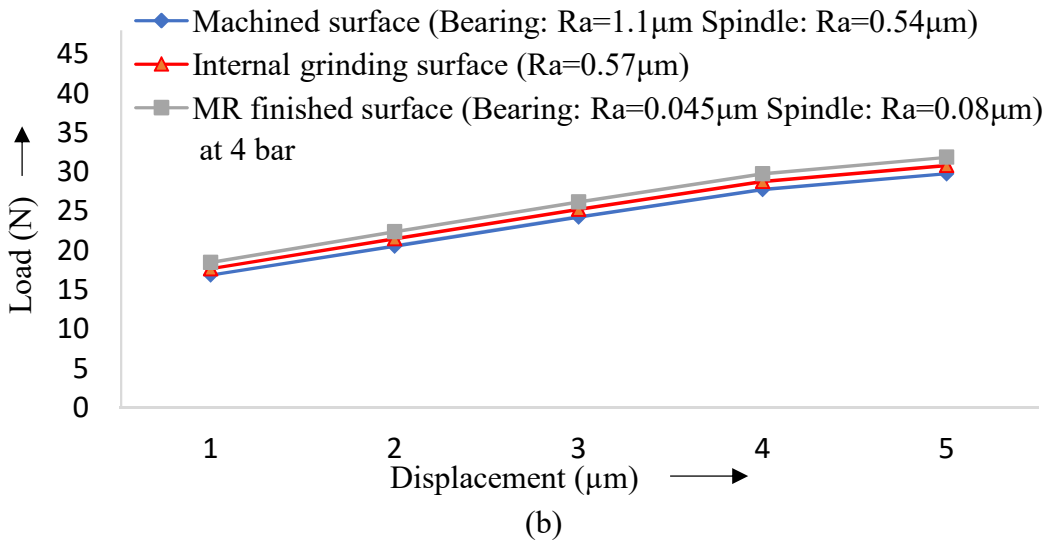

(b)

Figure 4.12 Load-displacement analysis of thrust bearing at various surfaces with a supply pressure of (a) 3bar, and (b) 4bar

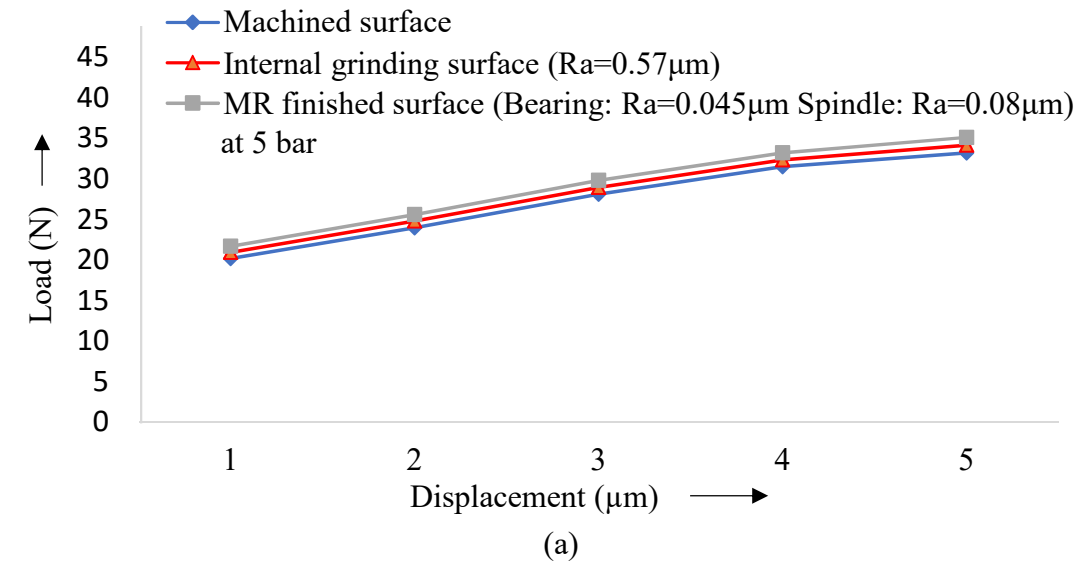

(a)

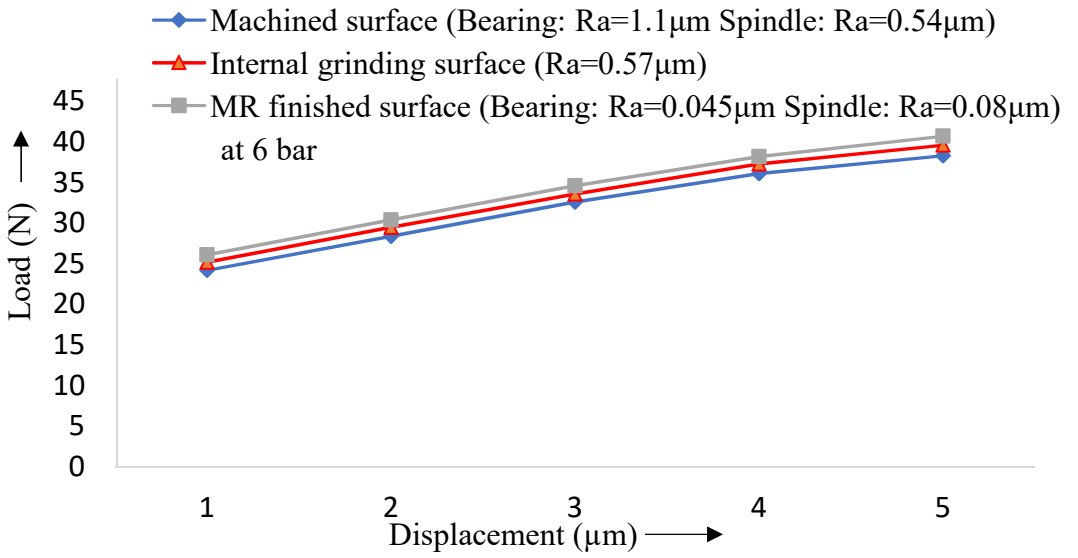

(b)

Figure 4.13 Load-displacement analysis of thrust bearing at various surfaces with a supply pressure of (a) 5bar, and (b) 6bar

The comparisons for average increment in load carrying capacity of thrust bearing due to improvement in the surface finish are shown in Figure 4.14. These values show the effect of surface finish on the load carrying capacity of the aerostatic thrust bearing.

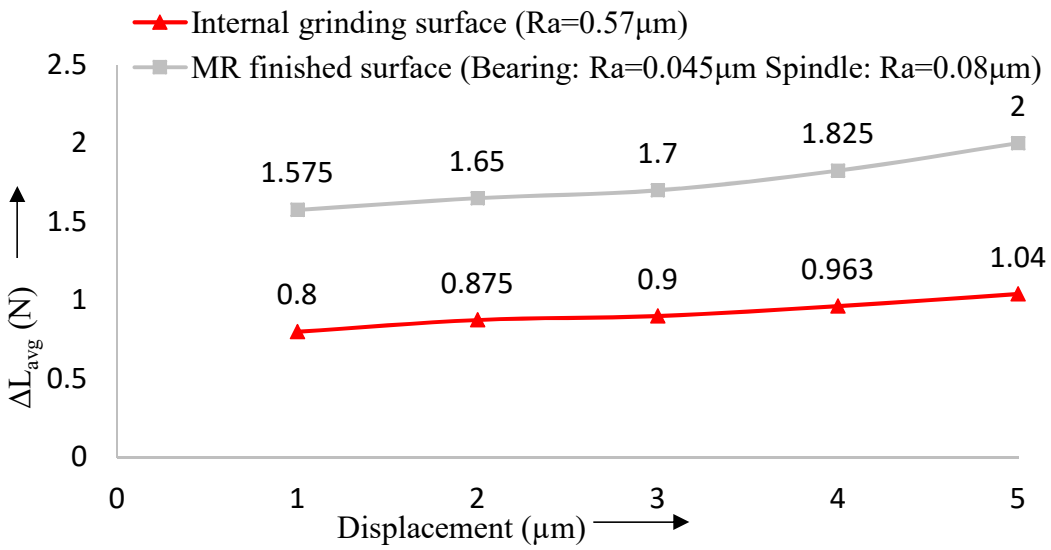

Figure 4.14 Average change in load carrying capacity of thrust bearing at internal grinding and MR finished surfaces

4.5 CONCLUSIONS

Based on the experimental analysis of the modified aerostatic bearing with the effect of surface roughness, the following conclusions are drawn.

- The experimental study of surface roughness effect on load carrying capacity showed that the improvement in performance for both journal and thrust bearings.
- The load carrying capacity of journal bearing was increased by 0.075N, 0.096N, 0.11N, 0.12N and 0.14N at the spindle displacement of 1µm to 5µm with the decreased in surface roughness value of 0.57µm at bearing surface and 0.54µm at spindle surface with internal grinding technique. Further, the surface roughness values are decreased to 0.045µm at bearing surface and 0.08µm at spindle surface with the present MR finishing technique. After reducing the roughness values up to nanometer scale, the total increment in load carrying capacity was found to be 0.163N, 0.198N, 0.218N, 0.233N and 0.68N at the spindle displacement of 1µm to 5µm.
- In thrust bearing, the effects on load capacity by reducing the average roughness value of machined surface by internal grinding technique showed the increase in load capacity by 0.8N, 0.875N, 0.9N, 0.963N and 1.04N for the variation in spindle displacement from 1µm to 5µm. The surface roughness values are further decreased to 0.045µm at bearing surface

and 0.08μm at spindle surface by MR fluid finishing enhanced the load carrying capacity by 1.575N, 1.65N, 1.7N, 1.825N and 2.0N at the spindle displacement of 1μm to 5μm.

CHAPTER 5

CONCLUSIONS AND RECOMMENDATIONS

5.1 CONCLUSIONS

The effect of surface roughness on load carrying capacity of the designed journal and thrust bearing are evaluated experimentally. On the basis of these results, the following conclusions have been drawn.

- For journal bearing, the current studies showed the improvement in pressure ratios which are in the range of 0.4 to 0.6. This range is closest to the required optimum range of pressure ratios i.e. from 0.35 to 0.6. This revealed the improvement in pressure distribution in the present journal bearing.
- For thrust bearing, the pressure distribution curve showed the enhancement in pressure within the clearance gap. By using recess at end of orifice section, the pressure distribution in the direction of radial distance was improved.
- In the present study, the region of pressure distribution was extended up to 0.06mm which thereby showed improvement in pressure at each domain within the clearance gap. But, the numerical simulation given in previous studies showed the bubble formation at the wall of spindle surface which was the major reason for high velocity and low-pressure regions when the radial distance is less than 0.05mm.
- The experimental investigation of surface roughness effect on the load carrying capacity showed the improvement in performance for both journal and thrust bearings.
- The load carrying capacity of journal bearing was increased by 0.163N, 0.198N, 0.218N, 0.233N and 0.68N at the spindle displacement of 1μm to 5μm with the decreased in surface roughness value of 0.045μm at bearing surface and 0.08μm at spindle surface with the present MR finishing technique.
- The load carrying capacity of thrust bearing was increased by 1.575N, 1.65N, 1.7N, 1.825N and 2.0N at the spindle displacement of 1μm to 5μm with the decreased in surface roughness value of 0.045μm at bearing surface and 0.08μm at spindle surface with the present MR finishing technique.

- The results determined in the improvement of load carrying capacity of the aerostatic journal and thrust bearings showed the better functional performance of the designed bearings. Thus, the present designed aerostatic bearing is effective for its precision applications in drives of production machines where the friction and surface properties are the major parameters of performance and efficiency.

5.2 RECOMMENDATIONS

This research should be aimed at manufacturing and testing of aerostatic bearing with the combination of journal and thrust bearing. The effect of surface roughness was analyzed at various surfaces achieved by manufacturing techniques. Based on the problems faced in this research work, the recommendations on modeling and manufacturing can be discussed as given below.

- The initial stage in development in the aerostatic bearing is its design methodology which is discussed in Chapter 3. The design study in the current model is only focused on the diameter of the supply orifice and a clearance gap within the spindle and bearing surface. The length of the bearing is not considered as the parameter of the restrictor model. In order to minimize the variation in pressure within the orifice and clearance, the length of the orifice can also be considered to improve the pressure distribution. The use of pocketed orifice at end of orifice section is also recommended for journal bearing as it minimizes the high-pressure peaks generated in the clearance gap of the journal bearing.
- The numerical simulation used in Chapter 4 gives an approximate solution for pressure and velocity profiles for the journal and thrust bearings. The numerical model can be further improved by obtaining a static solution by finite volume method by analyzing the flow of fluid in the orifice and clearance along with friction for compressible fluids. To minimize the computational cost in further improvement of the numerical model, the analytical model based on FEM solver may be beneficial for optimizing the solution obtained by simulation of airflow in the bearing model.
- The problems faced during manufacturing such as hole drilling and axis alignment can be eliminated by taking some measures. As stainless steel is hard material so the drilling becomes difficult when the hole size is less than 0.5mm. The literature shows that the use of inlet diameter up to 0.1mm enhances the pressure distribution and provides higher loads as compared to the larger diameter of the inlet orifice. But due to the availability of

manufacturing capability on various material, the inlet orifice of 0.5mm diameter taken into consideration in this study. In order to overcome these restrictions, the holes can be separately drilled in inserts of softer material other than stainless steel. This may reduce the cost of drilling holes and higher manufacturing capabilities are not required for processing of bearing components.

- The second major problem after manufacturing is axis alignment of all the components which is due to the surface alignment errors such as flatness and concentricity of two diameters. So, the manufacturer must be aware of these errors as they can cause problems during the assembling of all the components.
- With all these recommendations for modeling and manufacturing of aerostatic bearing, the model studied in a current research project can be further used for the analysis of performance parameters of the aerostatic bearing.

REFERENCES

[1] Powell JW, *Design of aerostatic bearing*. Brighton: Machinery Publishing, 1970.

[2] Niizeki S (2000). Ceramic bearings for special environments, *Motion & Control*, 8, 17–22.

[3] Alexander HS, *Precision machine design*. Englewood Cliffs, New Jersey: Prentice Hall, 1992.

[4] Petrov NP (1883). Friction in machines and the effect of the lubricating fluid on it, *International Engineering Journal, Saint Petersburg,* 1, 71–140.

[5] Reynolds O (1886). On the theory of lubrication and its application including an experimental determination of the viscosity of olive oil, *Philosophical Transactions of the Royal Society* [177th London, England: 1886], 157–234.

[6] Zhukovsky NE and Chaplygin SA (1883), Investigations in the history of mechanics, *Development of theoretical foundations of aviation*, 2, 183–192. (in Russian)

[7] Kingsbury A (1897). Experiments with an air lubricated journal. *Journal of American Society of Naval Engineers*, 9(2), 267–292.

[8] Harrison WJ (1913). The hydrodynamical theory of lubrication with special reference to air as a lubricant, *Transactions* of *Cambridge philosophical society*, 22(3), 39–54.

[9] Mager A, "Generalization of boundary layer momentum integral equations to three dimensional flows including those of rotating systems", National Advisory Committee for Aeronautics, Technical Report 1067.

[10] Kageyama A and Hyodo M (2006). Eulerian derivation of the coriolis force, *Geochemistry, Geophysics and Geosystem*, 7(2), 1–5.

[11] Combrinck ML, Dala LN and Lipatov II (2017). Eulerian derivation of non-inertial Navier-Stokes and boundary layer equations for incompressible flow in constant pure rotation, *European Journal of Mechanics-B/Fluids*, 65, 10–30.

[12] Morosi S and Santos IF (2011). Active lubrication applied to radial gas journal bearings - Part1: Modeling, *Tribology International* 44, 1949–1958.

[13] Dousti S, Allaire P, Dimond T and Cao J (2016). An extended Reynold equation applicable to high reduced Reynolds operation of journal bearings, *Tribology International*, 102, 182–197.

[14] Morosi S and Santos IF (2011). On the modeling of hybrid aerostatic - gas journal bearings, *Journal of Engineering Tribology*, 225, 641–653.

[15] Lin WJ, Khatait JP, Lin W and Li H (2006). Modeling of an orifice-type aerostatic thrust bearing, *International Conference on Control, Automation, Robotics and Vision* [9th: Singapore 2006] pp. 1–6.

[16] Müller C, Greco S, Kirsch B and Aurich JC (2017). A finite element analysis of air bearings applied in compact air bearing spindles, *Procedia CIRP*, 58, 607 – 612.

[17] Chen CH, Tsai TH, Yang DW, Kang Y and Chen JH (2010). The comparison in stability of rotor-aerostatic bearing system compensated by orifices and inherences, *Tribology International*, 43,1360–1373.

[18] Chen XD and He XM (2006). The effect of the recess shape on performance analysis of the gas-lubricated bearing in optical lithography, *Tribology International,* 39, 1336–1341.

[19] Aoyama T, Kakinuma Y and Kobayashi Y (2006). Numerical and Experimental Analysis for the small vibration of aerostatic guideways, *CIRP Annals*, 55, 419–422.

[20] Du J, Zhang G, Liu T and To S (2014). Improvement on load performance of externally pressurized gas journal bearings by opening pressure equalizing grooves, *Tribology International,* 73, 156–166.

[21] Kassab SZ, Noureldeen EM and Shawky MA (1997). Effects of operating conditions and supply hole diameter on the performance of a rectangular aerostatic bearing, *Tribology International*, 30, 533–545.

[22] Li Y and Ding H (2007). Influences of the geometrical parameters of aerostatic thrust bearing with pocketed orifice-type restrictor on its performance, *Tribology International,* 40, 1120–1126.

[23] Nishio U, Somaya K and Yoshimoto S (2011). Numerical calculation and experimental verification of static and dynamic characteristics of aerostatic thrust bearings with small feed holes, *Tribology International*, 44, 1790–1795.

[24] Schenk C, Buschmann S, Risse S and Tunnermann A (2008). Comparison between flat aerostatic gas-bearing pads with orifice and porous feedings at high-vacuum conditions, *Precision Engineering,* 32, 319–328.

[25] Renn JC and Hsiao CH (2004). Experimental and CFD study on the mass flow–rate characteristic of gas through orifice-type restrictor in aerostatic bearings, *Tribology International*, 37, 309–315.

[26] Neves MT, Schwarz VA and Menon GJ (2010). Discharge coefficient influence on the performance of aerostatic journal bearings, *Tribology International*, 43, 746–751.

[27] Chang SH and Chan CW (2015). Numerical analysis of discharge coefficients in aerostatic bearings with inherent orifice-type restrictors, *Tribology International*, 90, 157–163.

[28] Tawfik M and Stout KJ (1989). The design of high efficiency flat pad aerostatic bearings using laminar restrictions, *Tribology International*, 22, 273–281.

[29] Pink EG (1978). A comparison of the performance of orifice compensated and slot entry gas lubricated journal bearings. MPhil thesis, Leicester Polytechnic, England, 1978.

[30] Chen MF, Chen YP and Lin CD (2002). Research on the arc type aerostatic bearing for PCB drilling station, *Tribology International*, 35, 235–243.

[31] White JW, Raad PE, Tabrizi AH, Ketkar SP and Prabhu PP (1986). A numerical study of surface roughness effects on ultra-thin gas films, *Journal of Tribology*, 108, 171–177.

[32] Dal A and Karaçay T (2016). Effects of the surface roughness on the dynamics of a rotor supported by aerostatic bearing. Proceedings of the World Congress on Engineering [2nd London, England: 2016], 1–6.

[33] Murrenhoff H. Fundamentals of Fluid Technology Part 2: Pneumatics. Germany: Shaker Verlag, 2014.

[34] Yoshimoto S, Yamamoto M and Toda K (2007). Numerical calculations of pressure distribution in the bearing clearance of circular aerostatic thrust Bearings with a single air supply inlet, *Transactions of the ASME*, 129, 384–390.

[35] Zhou Y, Chen X, Cai Y, Chen H and Han B (2018). Measurement of gas pressure distribution in aerostatic thrust bearings using pressure-sensitive film, *Tribology International*, 120, 9–15.

[36] Li Y, Yin Y, Yang H, Liu X, Mo J and Cui H (2017). Modeling for optimization of circular flat pad aerostatic bearing with a single central orifice-type restrictor based on CFD simulation, *Tribology International*, 109, 206–216.

[37] Grover V and Singh AK (2017). A novel magnetorheological honing process for nano-finishing of variable cylindrical internal surfaces, *Mat. manuf. processes,* 32, 573–580.

[38] Singh M, Singh A and Singh AK (2018). A rotating core–based magnetorheological nano-finishing process for external cylindrical surfaces*, Mat. manuf. processes*, 33, 1160–1168.